AD-A088 364 ESL INC SUNNYVALE CA F/G 9/5
CPSK, DPSK, AND FSK DEMODULATOR PERFORMANCE UNDER NUCLEAR STRES--ETC(U)
MAR 79 R IBARAKI, R HECKMAN, L KEARNEY DNA001-78-C-0189
UNCLASSIFIED ESL-TM1083 DNA-5006F NL

1 OF 2
AD A088364

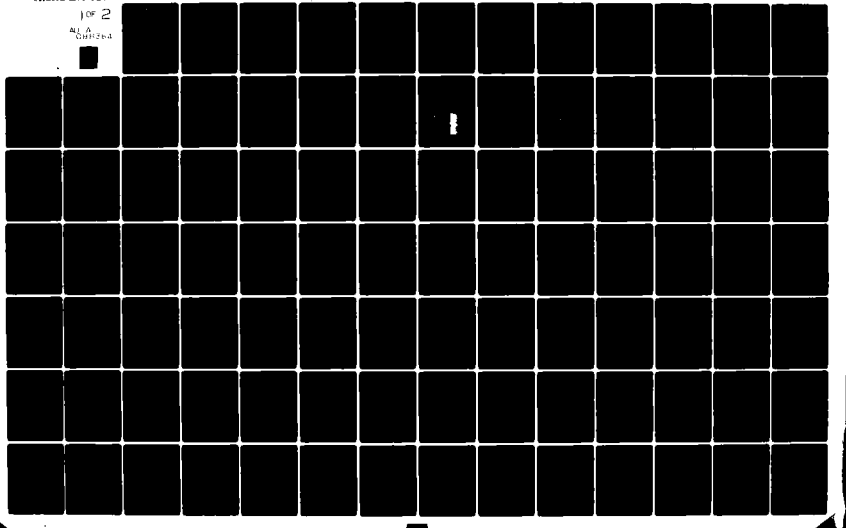

DNA 5006F

CPSK, DPSK, AND FSK DEMODULATOR PERFORMANCE UNDER NUCLEAR STRESSED CONDITIONS

ESL Incorporated
495 Java Drive
Sunnyvale, California 94086

31 March 1979

Final Report for Period 21 February 1978—31 March 1979

CONTRACT No. DNA 001-78-C-0189

APPROVED FOR PUBLIC RELEASE;
DISTRIBUTION UNLIMITED.

THIS WORK SPONSORED BY THE DEFENSE NUCLEAR AGENCY
UNDER RDT&E RMSS CODE B322078464 S99QAXHB05416 H2590D.

Prepared for
Director
DEFENSE NUCLEAR AGENCY
Washington, D. C. 20305

Destroy this report when it is no longer needed. Do not return to sender.

PLEASE NOTIFY THE DEFENSE NUCLEAR AGENCY, ATTN: STTI, WASHINGTON, D.C. 20305, IF YOUR ADDRESS IS INCORRECT, IF YOU WISH TO BE DELETED FROM THE DISTRIBUTION LIST, OR IF THE ADDRESSEE IS NO LONGER EMPLOYED BY YOUR ORGANIZATION.

UNCLASSIFIED

SECURITY CLASSIFICATION OF THIS PAGE (When Data Entered)

REPORT DOCUMENTATION PAGE

READ INSTRUCTIONS BEFORE COMPLETING FORM

1 REPORT NUMBER: DNA 5006F	2 GOVT ACCESSION NO.: AD-A088 364
3 RECIPIENT'S CATALOG NUMBER:	
4 TITLE (and Subtitle): CPSK, DPSK, AND FSK DEMODULATOR PERFORMANCE UNDER NUCLEAR STRESSED CONDITIONS	5 TYPE OF REPORT & PERIOD COVERED: Final Report for Period 21 Feb 78—31 Mar 79
	6 PERFORMING ORG. REPORT NUMBER: ESL-TM1083
7 AUTHOR(s): Ronald Ibaraki, Laurence Kearney, Randy Heckman, James Marshall	8 CONTRACT OR GRANT NUMBER(s): DNA 001-78-C-0189
9 PERFORMING ORGANIZATION NAME AND ADDRESS: ESL Incorporated, 495 Java Drive, Sunnyvale, California 94086	10 PROGRAM ELEMENT, PROJECT, TASK AREA & WORK UNIT NUMBERS: Subtask S99QAXHB054-16
11 CONTROLLING OFFICE NAME AND ADDRESS: Director, Defense Nuclear Agency, Washington D.C. 20305	12 REPORT DATE: 31 March 1979
	13 NUMBER OF PAGES: 108
14 MONITORING AGENCY NAME & ADDRESS(if different from Controlling Office)	15 SECURITY CLASS. (of this report): UNCLASSIFIED
	15a DECLASSIFICATION/DOWNGRADING SCHEDULE

16 DISTRIBUTION STATEMENT (of this Report)

Approved for public release; distribution unlimited.

17 DISTRIBUTION STATEMENT (of the abstract entered in Block 20, if different from Report)

18 SUPPLEMENTARY NOTES

This work sponsored by the Defense Nuclear Agency under RDT&E RMSS Code B322078464 S99QAXHB05416 H2590D.

19 KEY WORDS (Continue on reverse side if necessary and identify by block number)

Satellite Communication	CPSK
Nuclear Effects	DPSK
Rayleigh Fading	FSK
Scintillations	Propagation Path Effects

20 ABSTRACT (Continue on reverse side if necessary and identify by block number)

The relative performance of satellite communication links using conventional binary CPSK, DPSK, and noncoherent FSK demodulation techniques is evaluated for a range of simulated highly ionized and striation regions which may result following high attitude nuclear detonations. Performance is characterized by bit error rate estimates obtained through extensive computer simulation of satellite downlinks using various modem designs over a range of data rates and fade rates.

DD FORM 1 JAN 73 1473 EDITION OF 1 NOV 65 IS OBSOLETE

UNCLASSIFIED

SECURITY CLASSIFICATION OF THIS PAGE (When Data Entered)

20. ABSTRACT (Continued)

Phase fluctuations are shown to be an increasingly dominant performance degrading factor as fade rates increase. The interrelated effect on performance of the fade rate, data rate, carrier removal circuit noise bandwidth, and bit energy-to-noise ratio is examined in detail and a number of performance scaling relationships among these parameters are determined. Finally, a set of characteristic parameters is identified which allows the extensive simulated results obtained here to be generalized to similar modems operating at other data rates and fade rates.

TABLE OF CONTENTS

TABLE OF CONTENTS (Continued)

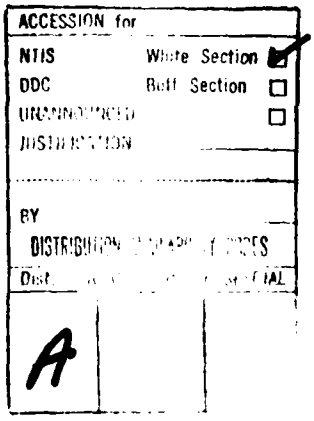

LIST OF ILLUSTRATIONS

LIST OF ILLUSTRATIONS (Continued)

LIST OF ILLUSTRATIONS (Continued)

SECTION 1
INTRODUCTION AND GENERAL SUMMARY

1.1 OVERVIEW.

There has been much concern regarding the degradation of conventional phase and frequency modulated satellite communication links following a high altitude nuclear detonation. A number of studies have examined in detail the effects of various fading environment models on specific existing or planned communication systems. These studies have indicated that if the propagation path of the signal is interdicted by the highly ionized striated plasma structure, substantial and sometimes catastrophic performance degradation may result.

The nuclear environment has been difficult for communication satellite designers to comprehend partly because its description has been very complex, and also because it is not possible to directly validate receiver performance in a nuclear channel. The development of a number of nuclear effects simulations such as the SATL, ROSCOE, and MICE/MELT computer codes have enhanced current understanding of potential nuclear environments and these codes are used to characterize the geographical and temporal extents of the nuclear striated plasma. Through the use of these codes and the development of extensive computer simulations which model the transmission, propagation, and demodulation of various digital communication signals through simulated nuclear channels, detailed performance assessments of various communication links in these disturbed signal propagation channels are now possible.

In spite of these developments, there is still much confusion about the relative importance of the channel phase fluctuations and amplitude fading as a function of the fade rate and type of modulation used. The purpose of this report is to resolve these questions as well as develop the necessary understanding of the effects of the nuclear environment on various conventional PSK and FSK satellite links.

1.2 SCOPE.

This report compares and summarizes the performance of three commonly used digital modulation techniques in simulated nuclear environments generated by the PATS Code. Performance curves of bit error rate as a function of the received bit energy-to-noise density ratio are generated for each modem over a range of potential environments and are used as the basis of performance comparison between the coherent (CPSK) and differentially coherent (DPSK) phase-shift-keyed receivers and the noncoherent (NCFSK) frequency-shift-keyed receivers.

The receiver performance curves are obtained through computer simulation of the demodulation of generic modulation waveforms which have been propagated through various fading and non-fading channel models that are representative of a wide range of nuclear environments which may be encountered. Through comparison of these curves at different data rates and for different modem designs a number of performance scaling relationships are developed and a set of basic environmental and link design parameters which characterize bit error rate performance for each of the three modems is identified.

A description of the fading environments used for this analysis is given in Section 2. The signal envelope decorrelation time associated with the fading environment is shown to be a basic parameter in characterizing link performance. An equation which relates decorrelation time to the rms phase deviation and relative cloud velocity is given.

The theoretical equations for the probability of bit error as a function of bit energy-to-noise density ratio are given for ideal CPSK, DPSK, and NCFSK receivers in additive, white Gaussian noise alone and in concert with slow Rayleigh fading. Simulation results are also given which show the additional degradation introduced by nonideal doppler removal circuits.

Results of extensive simulations of each of the three receivers over a range of fading environments are given in Section 4. The performance of each receiver for several fade rates, data rates, and noise levels is presented and various performance scaling relationships are discussed. Finally for each receiver a set of three parameters which can adequately specify its performance over a range of potential nuclear environments is given.

Additional supporting material used in the formulation of the scaling relations and performance characterization of the various receivers is given in Appendices A, B, and C.

1.3 GENERAL SUMMARY.

Results of this study show that phase fluctuations of the nuclear channel can be a significant source of bit error rate performance degradation for binary CPSK, DPSK, and NCFSK satellite links. In noise-only or very slow fading environments the CPSK modem is the best and the NCFSK modem is the worst. However, in faster fading

environments where the phase fluctuations are the dominant source of performance degradation, the NCFSK modem is degraded least, followed by the DPSK modem, and the CPSK modem is the worst of the three. (See Figure 1-1.)

The fade rate at which the phase fluctuations become significant are a function of the data rate, the received bit energy to-noise density ratio, the modulation type, and the particular modem design used. Simulation results show that phase fluctuations become significant for CPSK before either DPSK or NCFSK at values of T_D/T_S ratios of approximately 40-150. Phase degradation for DPSK become significant at T_D/T_S ratios around 20-40, and for NCFSK (NSPACE = 1) at a value of about 10.

The severity of a nuclear striated channel which exhibits Rayleigh statistics (usually having rms phase deviations in excess of 1000 degrees at 7.3 GHz) to digital satellite communication links can be adquately characterized by the signal envelope decorrelation time which is approximately inversely proportional to both the rms phase deviation and the relative cloud velocity of the environment. For such environments, the bit error performance of CPSK, DPSK, or NCFSK modem can be characterized by a set of three characteristic parameters. For CPSK and DPSK demodulators, the characteristic parameter set consists of the bit energy-to-noise density ratio, the ratio of fading decorrelation time to the bit period, and the ratio of the loop noise bandwidth to the data rate. The first two characteristic ratios are the same for the NCFSK modem, but the third parameter is the ratio of the tone spacing to the data rate.

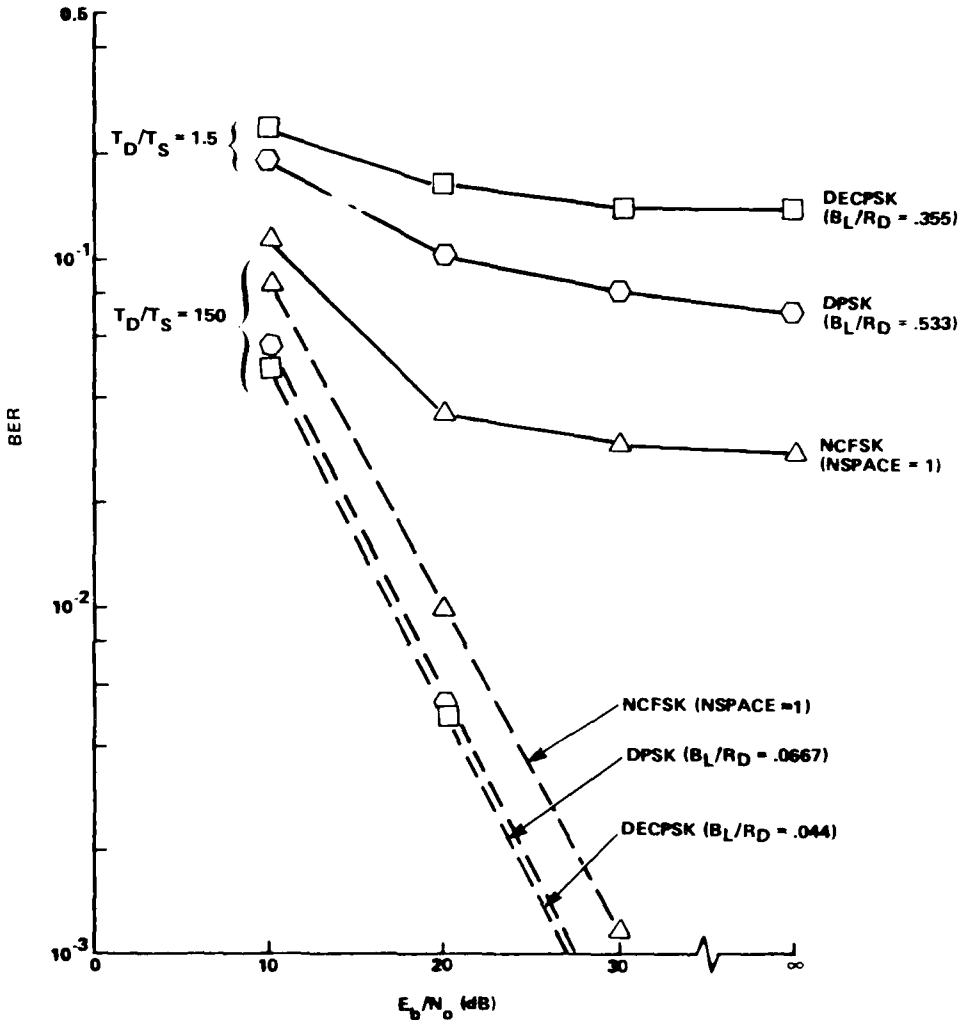

Figure 1-1. BER performance comparison of CPSK, DPSK, and NCFSK modem

Through simulated performance studies, the relative importance of the channel phase fluctuations and amplitude fading has been quantified as a function of the modulation type and fade rate. Parametric curves of bit error rate performance as a function of the bit energy-to-noise density ratio and parametric in the decorrelation time of the striated nuclear environment are presented for various PSK and FSK receiver designs. The performance scaling relationships which were determined in this study enable link designers to use the performance curves obtained here to estimate performance degradation for other similar modem designs at other data rates.

SECTION 2
ENVIRONMENT DESCRIPTION

Simulation of the nuclear environment has been the subject of several large-scale computer software codes developed by DNA and AFWL. Generally, these codes indicate that it is possible to have significant and persisting levels (5000 degrees) of rms phase fluctuation at X-band (integrated electron content spatial variation). The ionized plume associated with high altitude bursts is primarily responsible for the high persisting level of ionization associated with these striations.

The disruptive amplitude and phase effects on communication signals propagating through the ionized structure of the nuclear plasma has been modeled by PATS, a diffraction simulation computer code. The striated portions of the fireball are modeled by a series of thin phase screens with an integrated electron content spatial variation described by an inverse cubed power law PSD of the form, k^{-3}, where $k = \frac{2}{\lambda}$ and λ is the spacial wavelength. The PATS code provides spacially dependent amplitude and phase perturbation data for signals propagating through striation regions and the numerical outputs of this code are readily used as the disruptive nuclear channel in simulations of satellite communication links.

2.1 ENVIRONMENT CHARACTERIZATION.

A number of PATS code fading records were generated for a range of rms phase deviations to form a reference set of environments at X-band for this study. Although the rms phase deviation is a basic parameter in describing the fading channel, the decorrelation time (or spectral bandwidth) of the fading in comparison to the receiver filter bandwidths and the link data rate is a more characteristic parameters

in describing the severity of the fading to a digital communication link. Figure 2-1 shows a plot of decorrelation time (left-hand scale) and rms spectral bandwidth (right-hand scale) as a function of the rms phase deviation, parametric in the striation velocity component normal to the striation axis relative to the signal path. These approximate curves which estimate the decorrelation times of the PATS code fading records at various velocities are plotted on log-log scales and show that decorrelation time (T_D) is inversely proportional to the relative velocity (v) and inversely proportional to the rms phase deviation (σ) raised to an exponent slightly larger than unity and is given by

$$T_D \approx \frac{1.08 \times 10^5}{v\ \sigma^{1.095}} \text{ (seconds)} \qquad (2\text{-}1)$$

where σ is in degrees and v is in meters per second. The received signal envelope spectral bandwidth (B_{sp}) is inversely proportional to the decorrelation time and is given by

$$B_{sp} = \frac{0.225}{T_D} \qquad (2\text{-}2)$$

2.2 REPRESENTATIVE ENVIRONMENTS.

In order to characterize link performance over a wide range of decorrelation times, a set of four environments (denoted by circles in Figure 2-1) with decorrelation times of approximately 1.0, 0.1, .01, and .001 seconds were selected to be representative

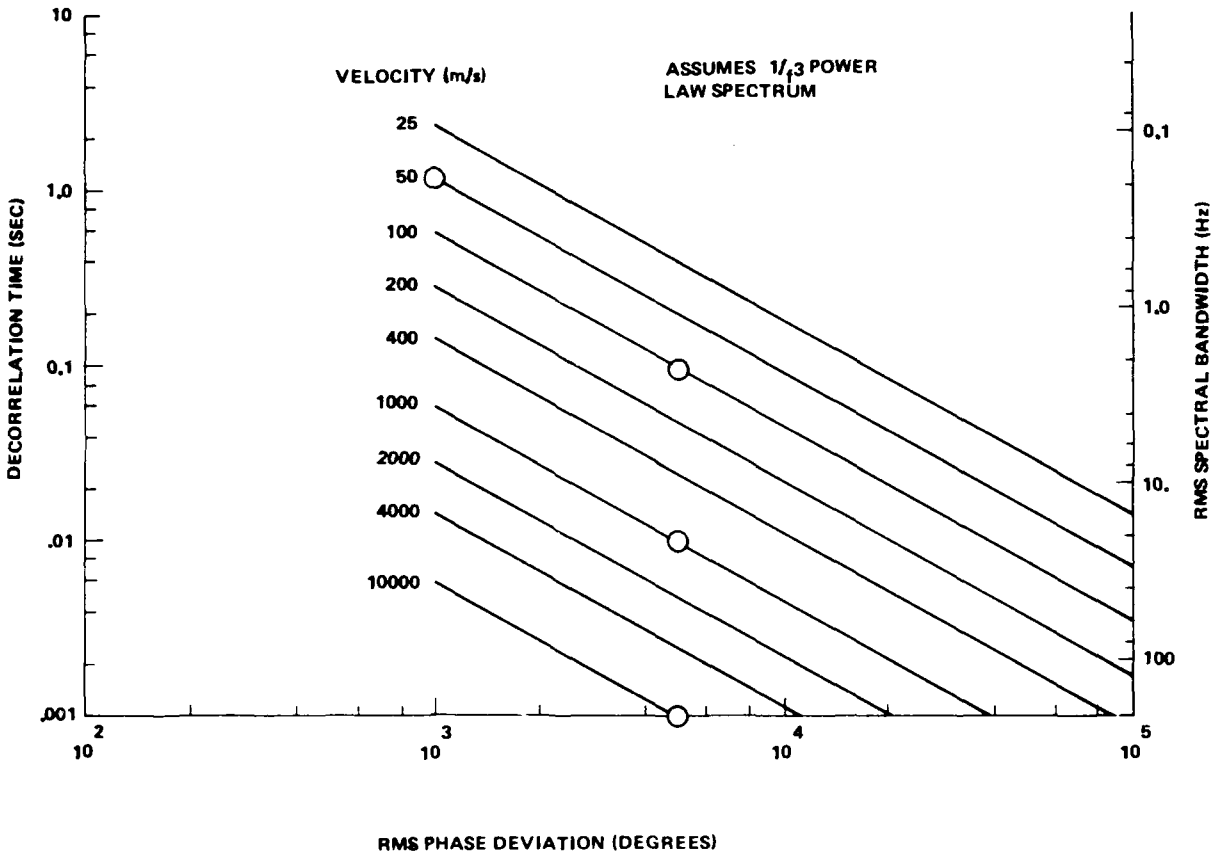

Figure 2-1. Fading decorrelation time as a function of relative velocity and RMS phase deviation

of a slow, moderate, fast, and very fast fading environments, respectively. The rms phase deviation and velocities for these environments are given below in Table 2-1.

Table 2-1. Representative environments

T_D(sec.)	σ	v	Comment
1.0	1000°	50 m/sec	slow
0.1	5000°	100 m/sec	moderate
0.01	5000°	1000 m/sec	fast
0.001	5000°	10 km/sec	very fast

Plots of the amplitude and phase records of these fading environments are shown in Figure 2-2. These PATS code generated records represent the received signal at the ground of a unity amplitude, zero-phase transmitted signal which propagates through a striated 5-layer stochastic cloud model that is 960 kilometers thick and centered 1520 kilometers from the receiver.

The rms envelopes of the FFT coefficients at various frequency separations from a transmitted tone are shown in Figure 2-3, and demonstrate the degree of rms spectral spreading of a tone which propagates through these representative environments. The FFT coefficients were obtained by taking 64-point FFT's of the simulated received signal at .02 second intervals over the 20 kilometer cloud. The plot shows that spectral spreading is negligible for the T_D = 1.0 second environment, but becomes significant for the faster fading environments where the 10 dB down bandwidth reaches several hundred Hz at T_D = .001 second. This plot shows the severity of the faster fading environments and the problems created for channel phase tracking loops with PSK and intersymbol interference with FSK demodulation.

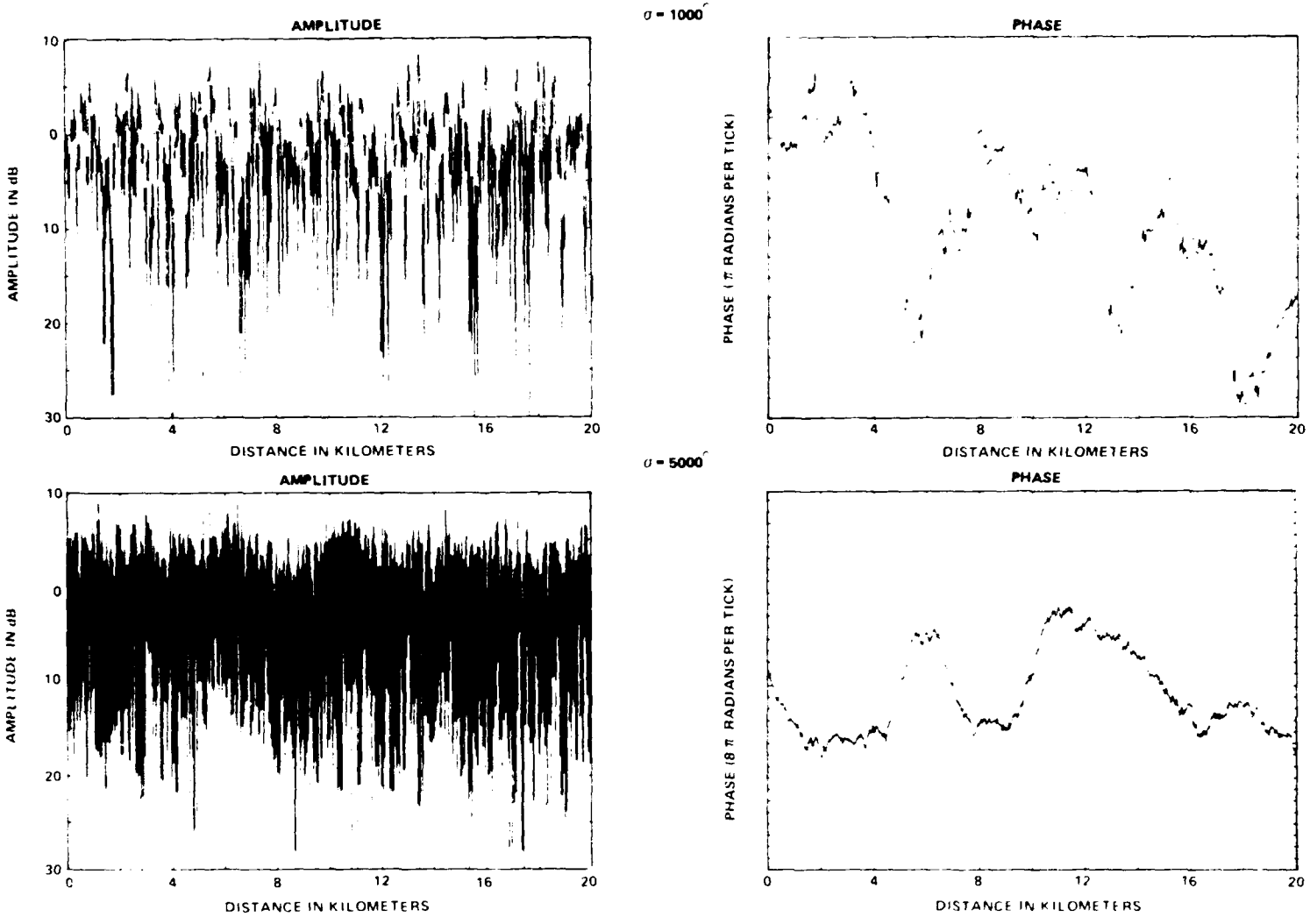

Figure 2-2. Received envelope and phase records of PATS code simulated nuclear environments

2.3 TEMPORAL EFFECTS.

The signal envelope decorrelation time may span four order of magnitude following a nuclear burst. A typical plot of the decorrelation time as a function of time after burst is given in Figure 2-4 (nominal environment). Also shown are possible variations believed to be representative of strongly and weakly striated plasmas. The nominal environment is shown to drop rapidly to T_D = 0.01 second in the first few minutes after detonation then gradually increase to a moderate rate of approximately T_D = 0.1 second after 20 minutes or so. The weaker and stronger fading environments also plotted on this figure provide a feel for the potential range of uncertainty in severity of fading. The dashed lines at the bottom of the figure indicate the estimated lower limits on the fading decorrelation times for several dish antenna diameters. The narrow beamwidths of high gain antennas spatially filter the energy incident on the receiver from large angular deviations at the situations. As a result some phase interference fading is eliminated giving rise to slower fading.

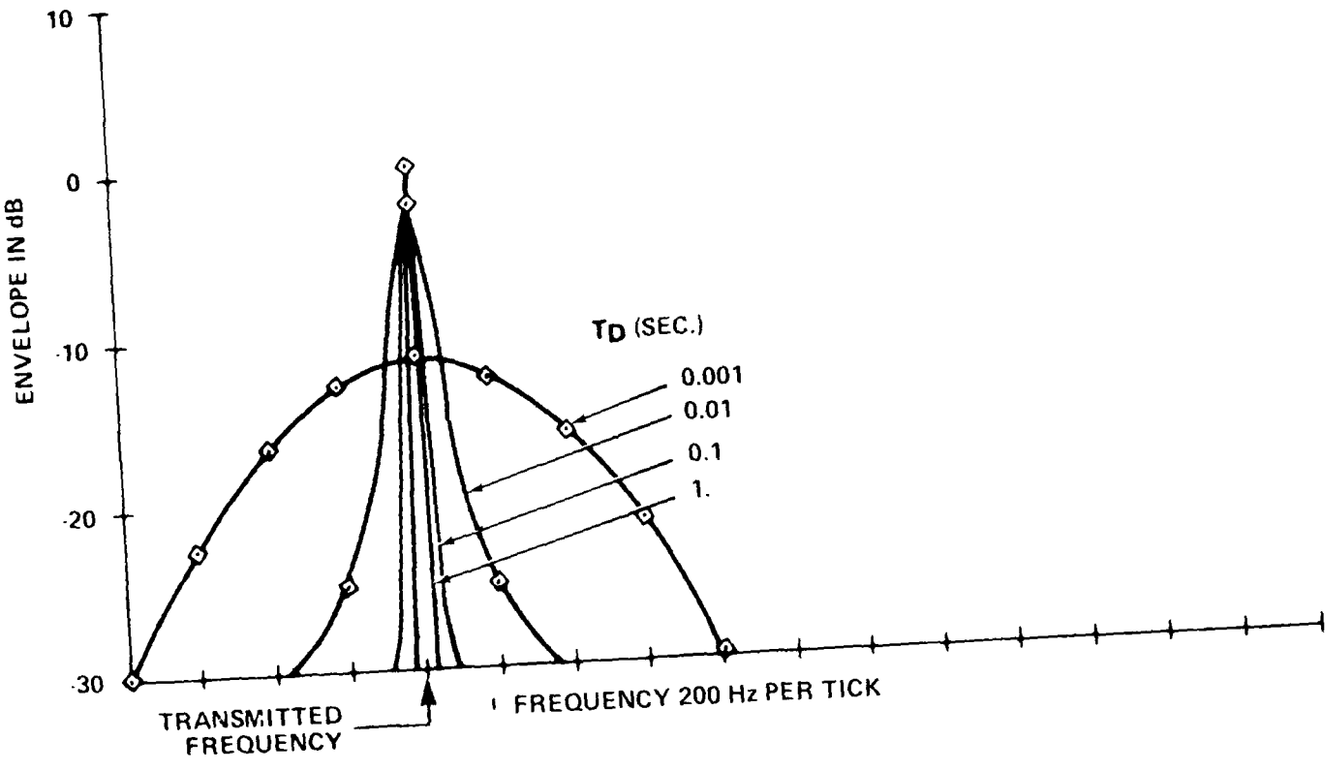

Figure 2-3. RMS spectral spreading of representative environments

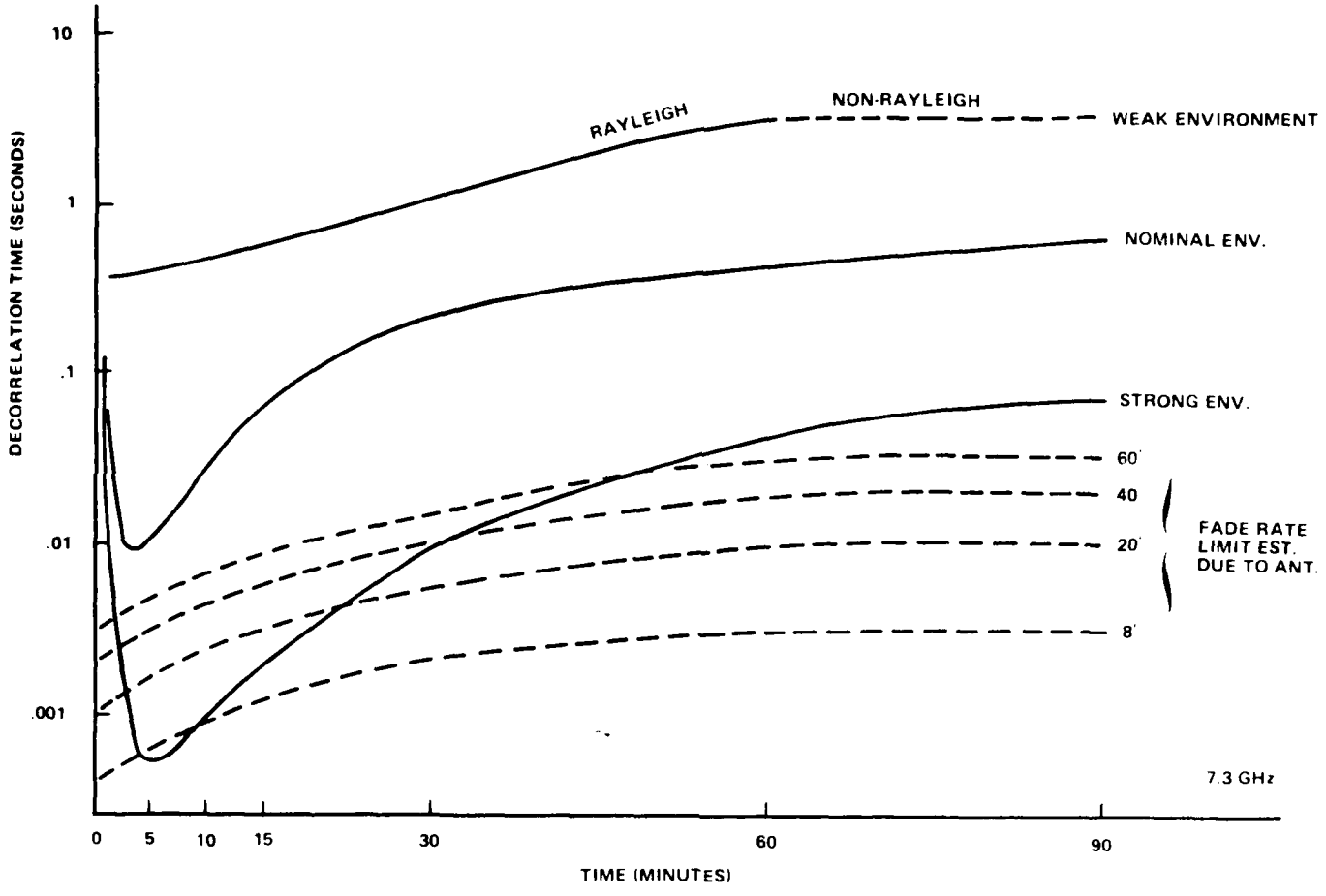

Figure 2-4. Typical envelope decorrelation times

SECTION 3
PERFORMANCE COMPARISON IN AWGN AND SLOW RAYLEIGH FADING

The bit error rate (BER) performance of DECPSK, DPSK, and NCFSK modem is examined in detail in the following sections. Theoretical equations and performance curves are presented for ideal demodulation for each demodulator type in additive Gaussian noise (AWGN) only and in concert with slow Rayleigh fading (SRF). Using a software simulation of typical receiver implementations of each modulation type, comparable BER performance curves are obtained. The simulated results in AWGN show the additional performance losses resulting from nonideal phase and frequency doppler correction circuits for the CPSK and DPSK modem. No additional degradation over ideal performance is shown by the NCFSK modem simulation for which doppler correction circuits are not modeled.

Block diagrams and descriptions of the simulator models used for each modem and the simulated communication link are given in Appendix B.

3.1 THEORETICAL PERFORMANCE.

3.1.1 Performance in AWGN.

The well known equations[1] which describe the probability of bit error (or bit error rate) for ideal CPSK, DPSK, and NCFSK are given by

$$P_{CPSK} = \frac{1}{2} \operatorname{erfc} \left(\sqrt{E_b/N_o}\right) , \qquad (3\text{-}1)$$

$$P_{DPSK} = \frac{1}{2} \exp(-E_b/N_o) \quad , \tag{3-2}$$

$$P_{NCFSK} = \frac{1}{2} \exp(-\frac{1}{2} E_b/N_o) \quad . \tag{3-3}$$

where E_b/N_o is the bit energy-to-noise density ratio of the decision variable. Differential encoding and decoding of the data is normally used to resolve the radians phase ambiguity of CPSK demodulator and the bit error rate for differentially encoded CPSK is given by

$$P_{DECPSK} = 2 P_{CPSK} (1-P_{CPSK}) \quad . \tag{3-4}$$

These BER performance curves are plotted for comparison in Figure 3-1 as a function of E_b/N_o and show that the BER performance of DECPSK is slightly better than DPSK and NCFSK performance is some 3 dB worse than DPSK performance.

3.1.2 Performance in Slow, Nonselective Rayleigh Fading (SRF).

The theoretical performance of these modulation types in slow nonselective Rayleigh fading is also a well known result which is obtained by averaging the conditional BER's given by Equations (3-2), (3-3), and (3-4) over the Rayleigh PDF as given by

$$P_X^{SRF} = \int_0^\infty P_X(E_b/N_o \cdot a^2)\, p(a)\, da \tag{3-5}$$

where p(a) is given by

$$p(a) = 2\, a \exp(-a^2). \tag{3-6}$$

Closed form expressions for DPSK and NCFSK are given in Reference 8 as

$$P_{DPSK}^{SRF} = \frac{1}{2 + 2\ E_b/N_o} \quad , \text{ and} \tag{3-7,}$$

$$P_{NCFSK}^{SRF} = \frac{1}{2 + E_b/N_o} \ . \tag{3-8}$$

Plots of these expressions are also shown in Figure 3-1 along with the DECPSK result which was obtained by numerical integration. These curves still show DPSK has a 3 dB advantage over NCFSK and DECPSK has increased its advantage over DPSK by more than 2 dB at lower BER's.

3.2 SIMULATION PERFORMANCE IN AWGN.

3.2.1 DECPSK Performance.

A modified Costas loop demodulator was simulated in an AWGN environment and Figure 3-2 shows simulation results of BER on an expanded E_b/N_o scale for first, second (a'=1/2) and third-order loops (a'=1/2, b'=1/8). Two curves for each loop order are presented which correspond to typical values of the B_L/R_D ratio which is defined as the ratio of the loop noise bandwidth B_L to the data rate R_D . At the lower value of B_L/R_D = .044 which can represent a 6.66 Hz bandwidth with a 150 bps data rate or 53.3 Hz bandwidth with a 1200 bps data rate, all three loops perform essentially the same in noise in fairly good agreement with ideal theoretical DECPSK. At a value of B_L/R_D eight times larger, however, the resulting increase in phase error variance degrades performance. The first and second order loops still perform similarly, but the third order loop shows somewhat worse performance as a result of its instability at low E_b/N_o .

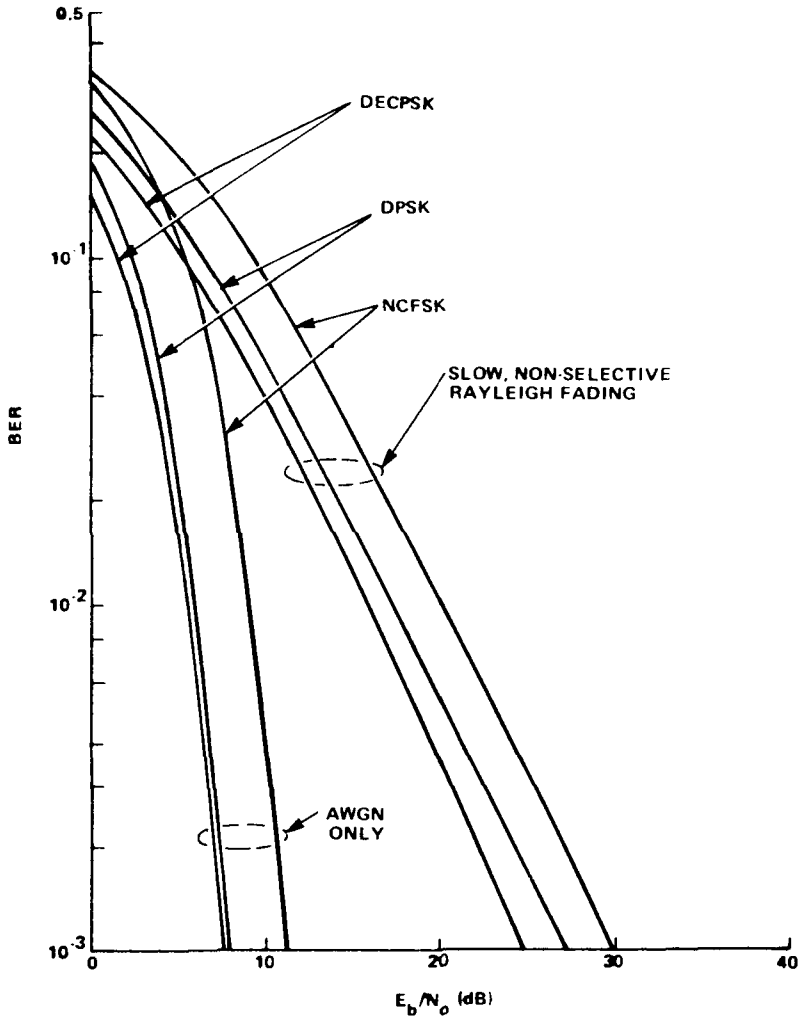

Figure 3-1. Theoretical performance curves in AWGN and slow Rayleigh fading

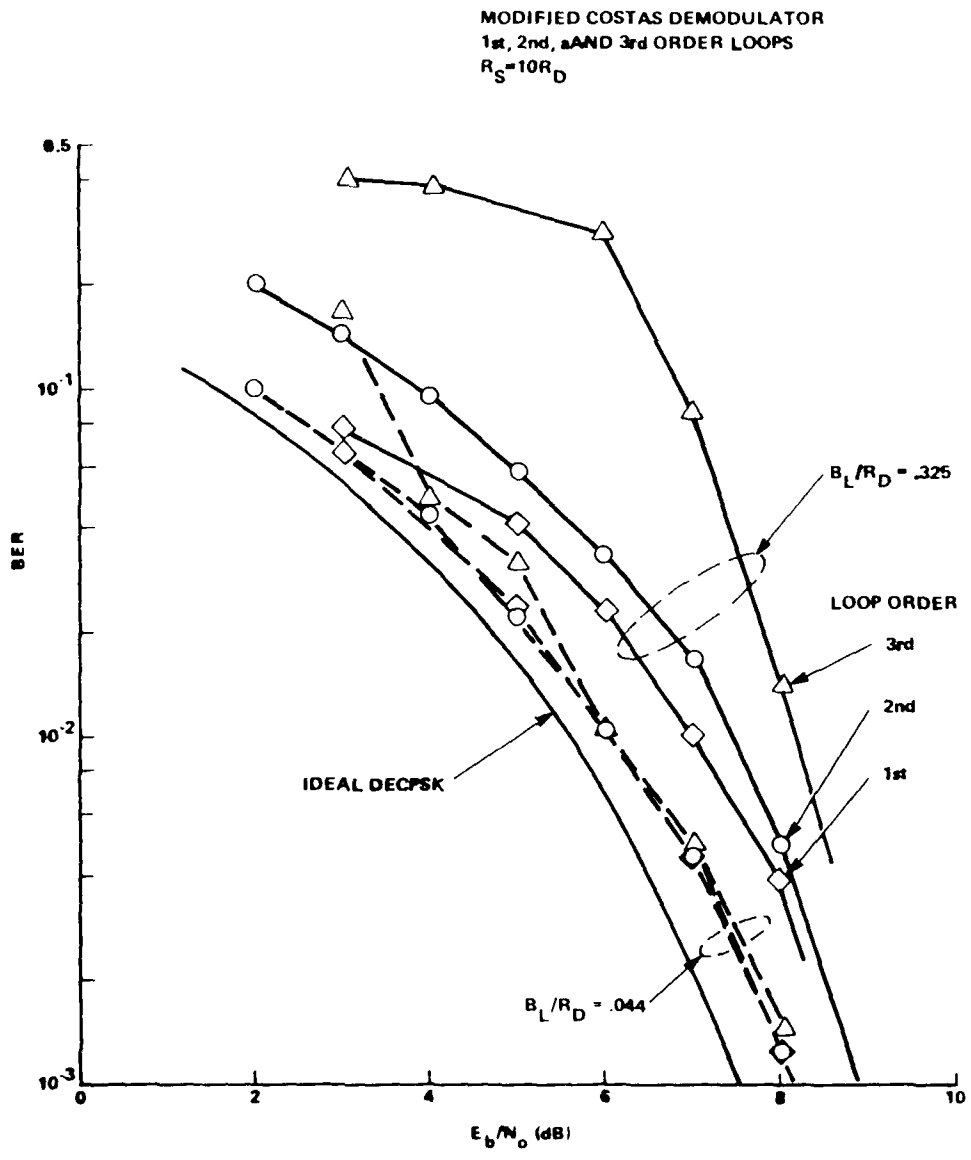

Figure 3-2. Simulated DECPSK performance in AWGN

The dependence of demodulator performance on the B_L/R_D ratio, independent of the individual R_D and B_L values, has been verified via simulation and is shown by the expression for the phase error variance due to noise given in Reference 2 as

$$\sigma_\phi^2 = \frac{B_L}{R_D} \frac{4}{E_b/N_o} \text{erf}^{-2}\left(\sqrt{E_b/N_o}\right) \quad (3\text{-}9)$$

The resulting BER is a function of effective E_b/N_o which is reduced by the cosine of the demodulator phase error whose distribution shape is approximated by the Tikhonov probability density which only depends on the variance σ_ϕ^2 .

Values of B_L/R_D larger than 30 percent are not very common. For larger B_L/R_D values the phase tracking loops are likely to begin tracking the data phase transition as shown in earlier studies.

3.2.2 DPSK Performance.

Performance curves for a simulated DPSK demodulator in AWGN are shown in Figures 3-3 and 3-4. Like the DECPSK curves these figures show performance parametric in B_L/R_D since the same scaling relation holds. With first-order modified Costas loop aiding (Figure 3-3) and B_L/R_D = .0667 the simulation result show about a 1 dB loss over ideal DPSK performance and increasing B_L/R_D by a factor of eight resulted in an additional 1 dB loss. With

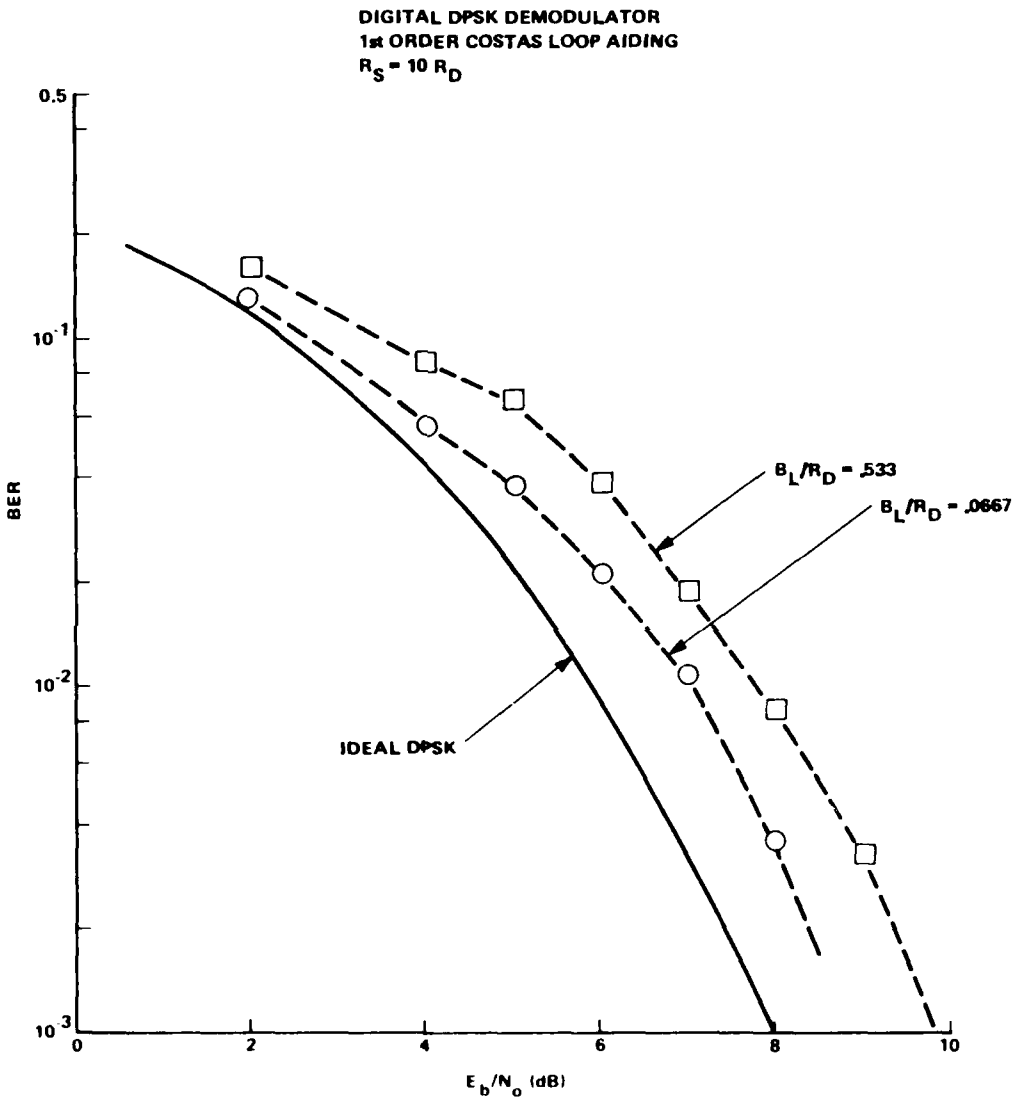

Figure 3-3. Simulated DPSK performance in AWGN, Costas aiding

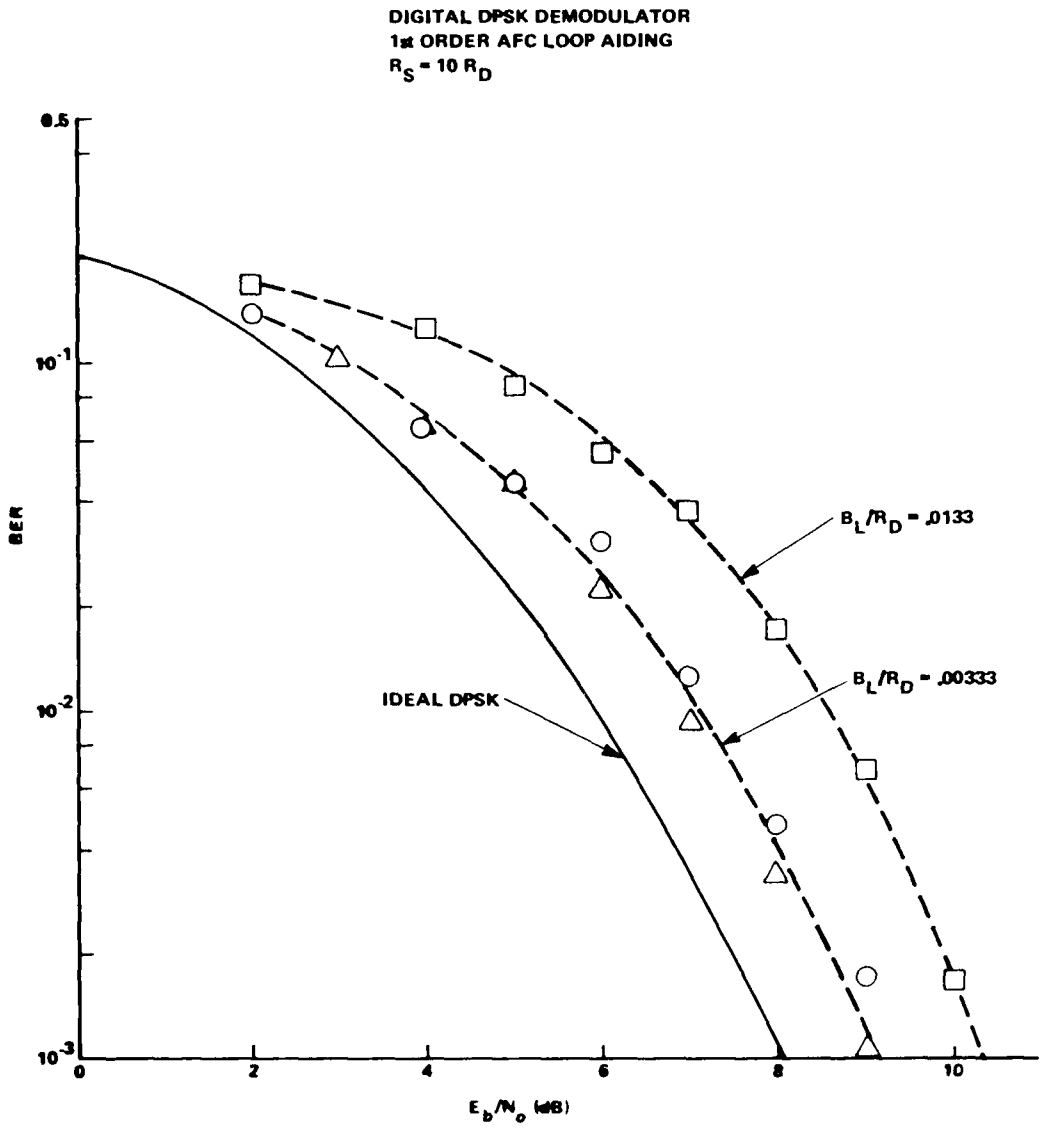

Figure 3-4. Simulated DPSK performance in AWGN, AFC aiding

first-order automatic frequency control (AFC) aiding (Appendix B) and a value of B_L/R_D of .00333 simulation results show a 1.5 dB loss over ideal DPSK and an increase in B_L/R_D by a factor of four results in another 1 dB loss.

3.2.3 NCFSK Performance.

As opposed to the PSK demodulators whose performance depended on the doppler tracking loop performance, the FSK demodulator simulator was not modeled with a doppler tracking circuit. This assumption is good so long as the actual doppler error variations with a frequency tracking loop are negligible in comparison to the data rate. Thus, simulated noise performance was essentially that of ideal noncoherent FSK as shown in Figure 3-5. In general, we expect some loss due to a widening of the tone filters to accomodate frequency tracking errors.

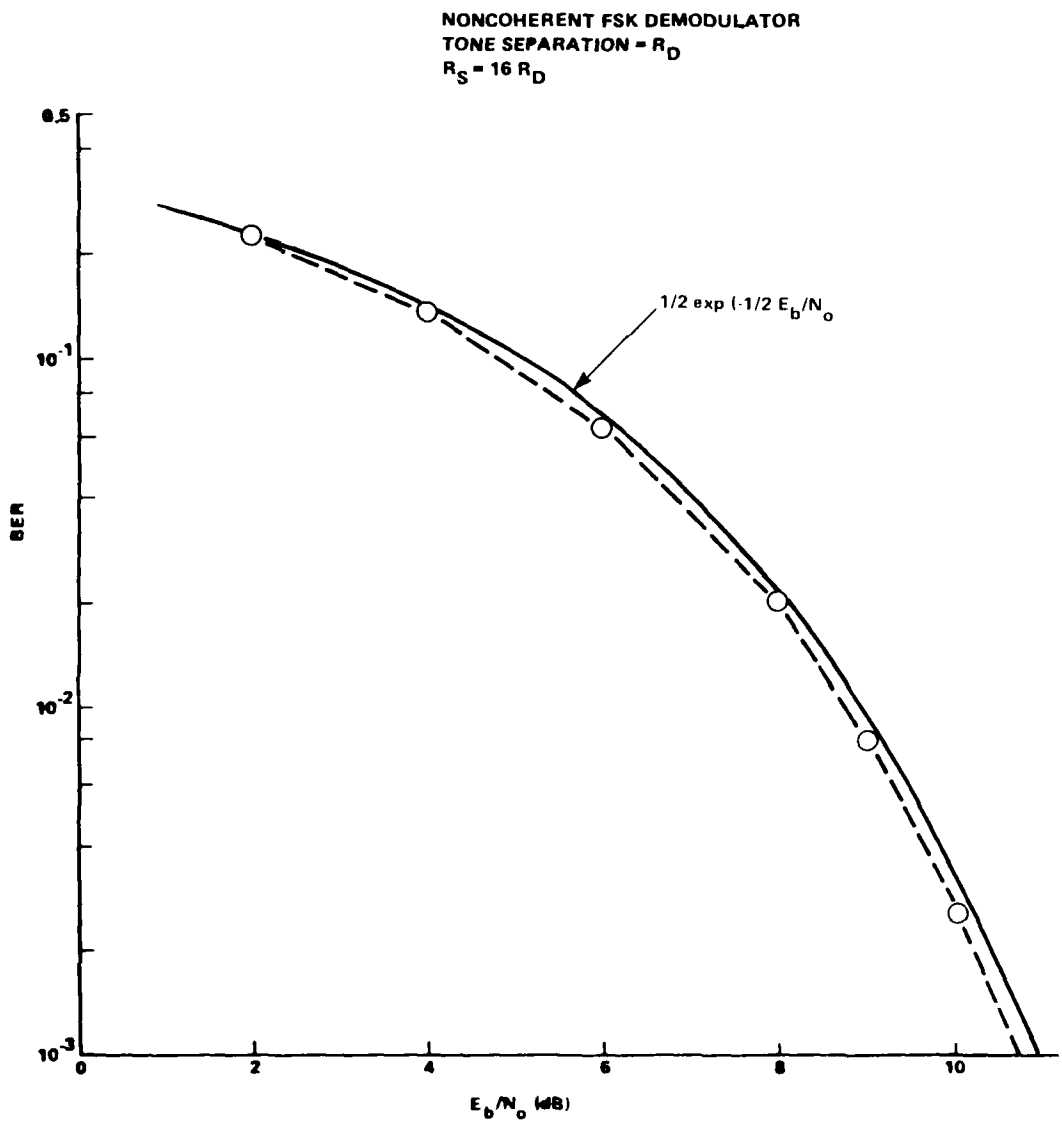

Figure 3-5. Simulated NCFSK performance in AWGN

SECTION 4
SIMULATED PERFORMANCE IN THE FADING ENVIRONMENT

The BER performance of DECPSK, DPSK and NCFSK demodulators in noise only environments and in concert with slow Rayleigh amplitude fading (SRF) environments can be adequately described from theoretically derived equations for the probability of bit error. The actual implementations of these demodulators are usually between 1-2 dB worse than theory due to losses resulting from narrowband IF filtering, doppler and phase tracking circuits, and bit sync circuits.

The SRF curves approximate BER performance of the demodulators in the PATS code modeled nuclear environments relatively well, but as the fade rate increases this approximation fails. Performance gets considerably worse as errors due to phase fluctuations become a significant source of degradation. Phase glitches destroy the phase coherence of the channel over bit period intervals on which PSK demodulators depend and introduce significant amounts of spectral spreading which translates energy outside the transmitted FSK signal bandwidths. The expressions for BER in SRF no longer apply and analytical expressions for BER in these faster fading environments are difficult to derive.

At this time, simulation of demodulators in representative fading environments appears to be the only feasible way to accurately estimate BER performance in the potential nuclear fading environment. Results from simulation of DECPSK, DPSK and NCFSK demodulators are presented in this section. It is determined that PSK demodulator performance can be adequately specified by the three parameters:

bit energy to noise density ratio (E_b/N_o), loop noise bandwidth, B_L , to the data rate, R_D, ratio (B_L/R_D), and decorrelation time, T_D , to symbol period, T_S , ratio (T_D/T_S). Similarly, the performance of NCFSK demodulators can be adequately specified by the three parameters: (E_b/N_o) , tone spacing, Δf, to data rate, R_D , ratio, ($\Delta f/R_D$) , and (T_D/T_S) . Finally, a set of curves is presented which shows BER performance parametrically in these parameters which can be used to estimate performance over a wide range E_b/N_o , designs, data rates and fading environments.

4.1 DECPSK PERFORMANCE.

4.1.1 E_b/N_o and B_L Dependence.

Figures 4-1 and 4-2 show simulated BER performance curves as a function of E_b/N_o in PATS code modeled fading environments for two modified Costas loop demodulator designs (B_L/R_D = .044, .355) at a 150 bps data rate. Each set of curves plotted parametrically in the fading environment decorrelation time shows that performance degrades steadily from a few dB off the slow Rayleigh fading curve for a 1-second T_D to very poor BER's of greater than 0.1 even for infinite E_b/N_o for a .01 second decorrelation time fading environment. At very slow fade rates ($T_D/T_S >> 1$), the Costas phase tracking loop tracks the slow, time varying phase of fading channel and performance degradation is primarily due to noise and amplitude fading which reduces the effective tracking loop SNR and the effective E_b/N_o on which demodulator decisions are based. The 1-second T_D curve is, however, a few dB worse than the ideal SRF curve - a loss partly attributable to the non-ideal phase tracking loops and partly due to a statistical departure of the simulated 1000° environment from an ideal Rayleigh distribution. (The 6400 bits simulated to estimate BER represent only 2.1 kilometers of the 20 kilometer cloud model shown in Figure 2-1 or approximately 43 decorrelation times of the fading channel at the 50 meter per second velocity.)

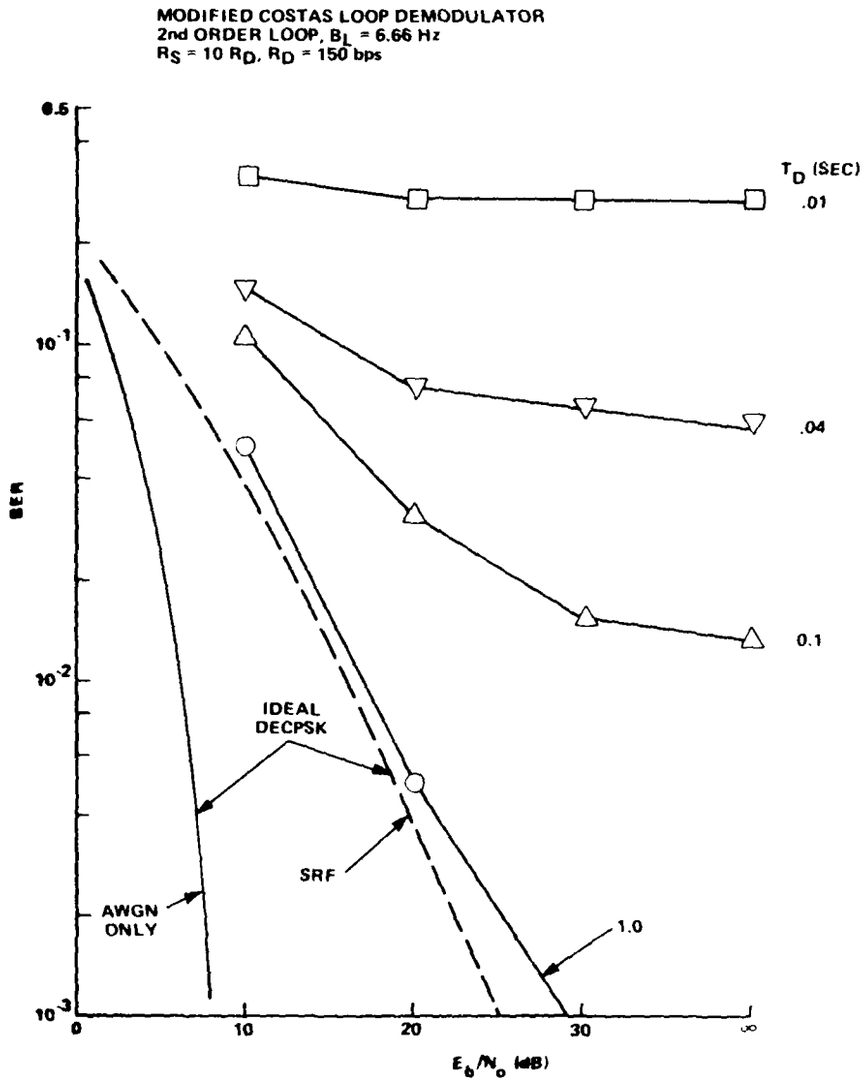

Figure 4-1. DECPSK BER Performance for B_L = 6.66 Hz, R_D = 150 bps

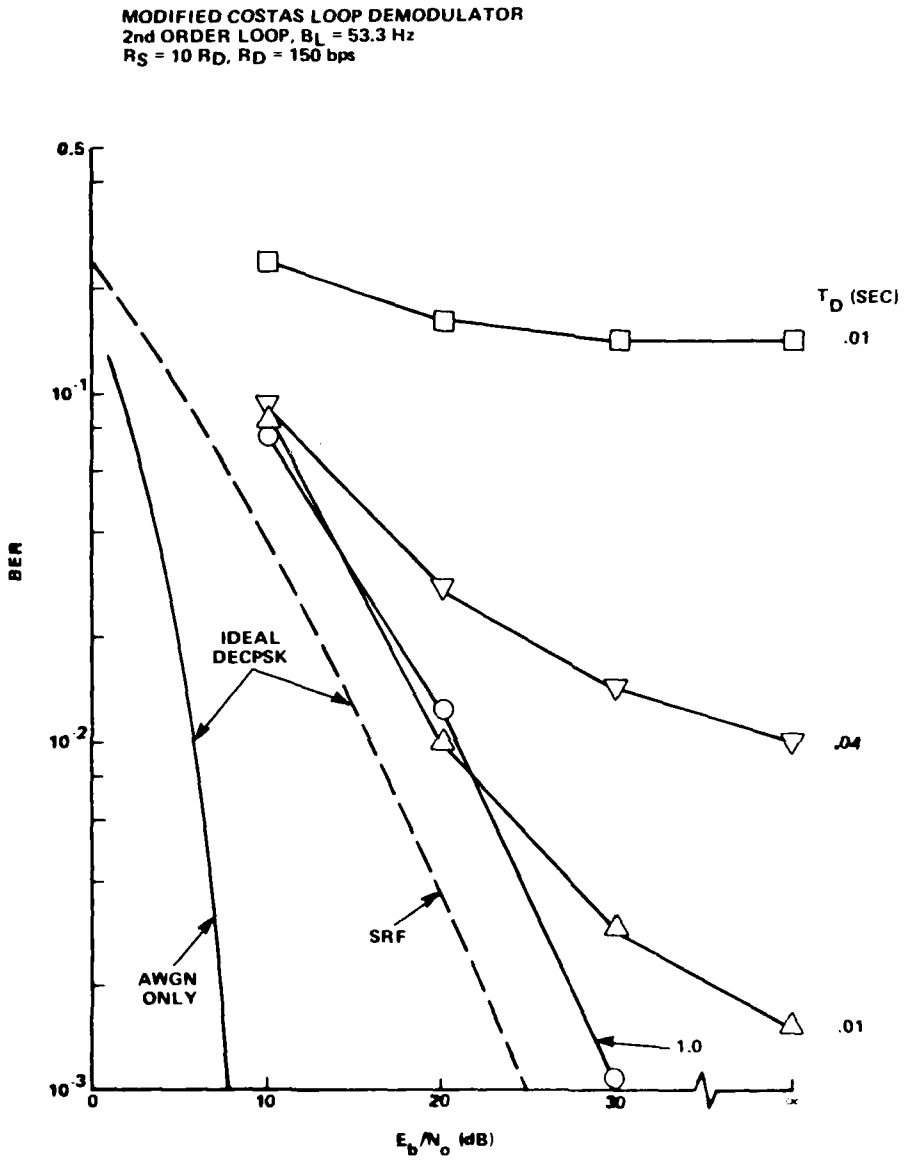

Figure 4-2. DECPSK BER performance, B_L = 53.3 Hz, R_D = 150 bps

As the fade rate increases, the channel phase variations quicken and performance gets progressively worse as phase tracking errors become a dominant source of degradation. Simulation results show nonzero error rates even for a noiseless fading environment. These errors are caused by rapid changes in signal phase (or phase glitches) which cannot be tracked by the fixed bandwidth Costas loops and which result in an error after differential decoding due to a slipped cycle between the loop's reference phase and the received signal phase. The figures also show that performance is improved for the larger (B_L = 53.3 Hz) loop bandwidths in the low noise, fast fading environments. Although noise performance is degraded, the wider more responsive bandwidth loop enables it to track a portion of the slower phase glitches which were untrackable by the smaller bandwidth loop and elimination of these potential errors more than compensates for additional errors resulting from the reduced loop SNR at low noise levels. The potential performance improvement which can be achieved by increasing loop bandwidth (or B_L/R_D ratio) is limited, however, by the bandwidth (or BT product) of the received PSK signal. As shown in Reference 1 as B_L approaches the signal bandwidth, the additional potential phase glitch errors avoided are offset by errors introduced as the loop tracks data encoded phase transitions.

At higher data rates the degradation due to phase fluctuations does not become a dominant source of errors until smaller decorrelation times as shown by Figures 4-3 and 4-4. These figures show BER performance at a 1200 bps data rate for the same noisy fading environments for data rate equivalent modified Costas loop demodulator designs with the same B_L/R_D (= .044, .355) ratios. The 1200 bps performance curves show the same characteristic shapes as a function of E_b/N_o as the 150 bps curves and it appears that each curve may be adequately characterized by its BER at 30 dB E_b/N_o . It is believed that knowing this BER, the reader should

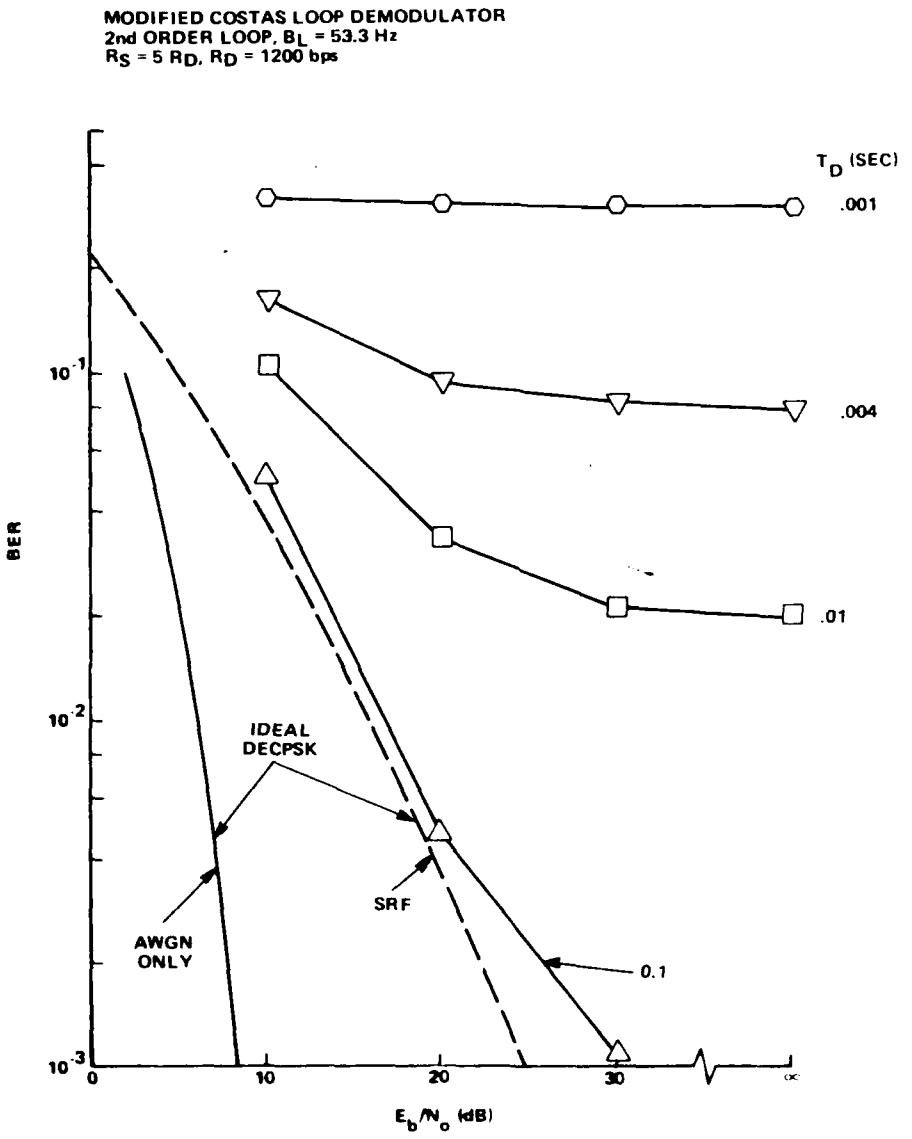

Figure 4-3. DECPSK BER performance, B_L = 53.3 Hz, R_D = 1200 bps

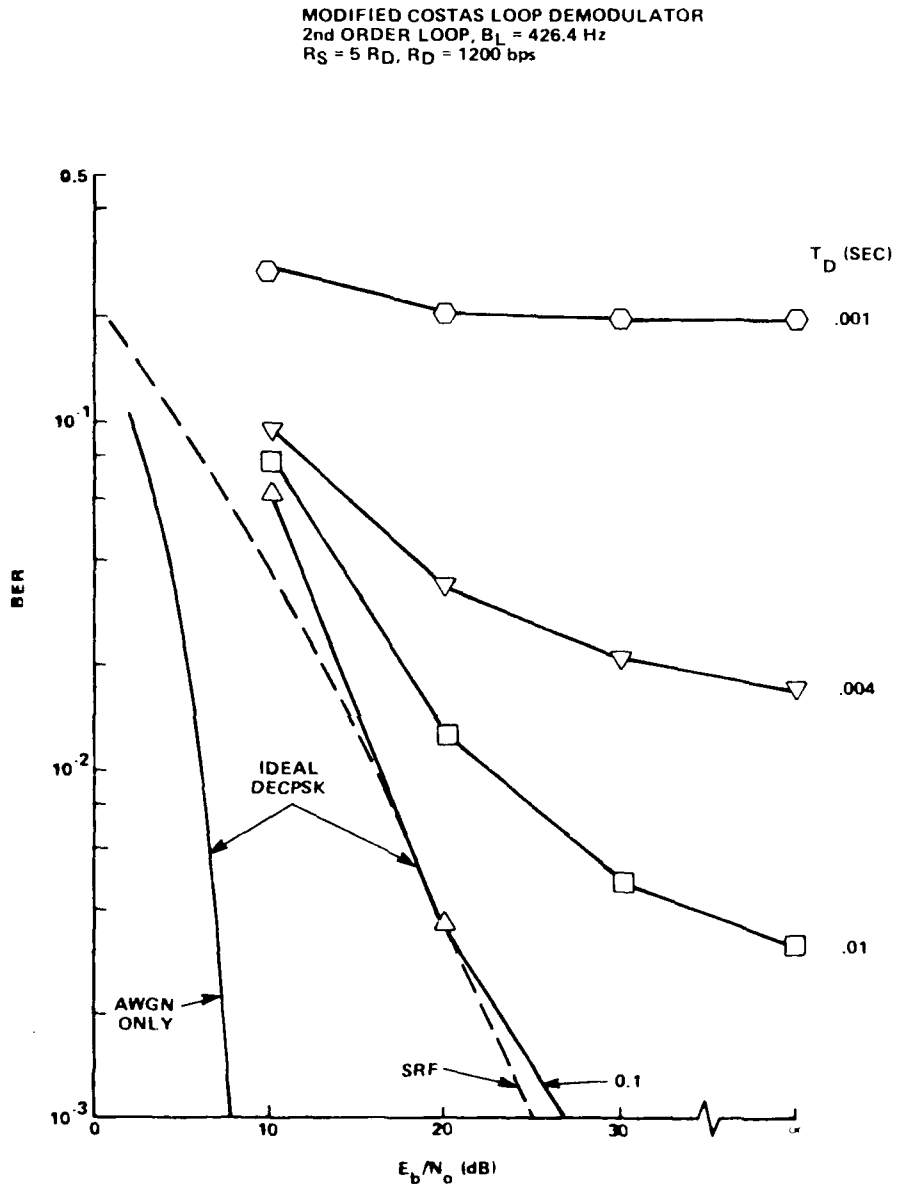

Figure 4-4. DECPSK BER performance, B_L = 426.4 Hz, R_D = 1200 bps

be able to determine BER's at other values of E_b/N_o to within a reasonable degree of accuracy from the shapes of the curves presented in these figures. This convention of representing a curve by a single point was primarily adopted to conserve substantial amounts of computer time which would have been required if the BER's at several E_b/N_o values were computed. It also provides a succinct performance measure by which different simulated links may be compared. The same convention will be shown to be appropriate for both DPSK and NCFSK demodulators in the sections that follow.

4.1.2 Data Rate Dependence.

A comparison of Figures 4-2 and 4-3 shows that for the same tracking loop noise bandwidth (B_L = 53.3 Hz) the higher data rate link has a significantly lower BER for the same faster fading environments where phase glitches are the dominant source of bit errors. These results are summarized in Figures 4-5 and 4-6 which show BER at 30 dB for the .01 second decorrelation time environment as a function of data rate, parametric in loop bandwidth for first, second, and third order loops. All loop orders and bandwidths show consistent performance improvement with increasing data rates. The performance of the first and second order loops are nearly identical and show a performance improvement for larger loop noise bandwidths at all data rates. Similar improvements are shown by the third order loop, but the overall BER is slightly greater than for first or second order loops with the same bandwidth. Again the instability of the third order loop is the cause of this performance degradation.

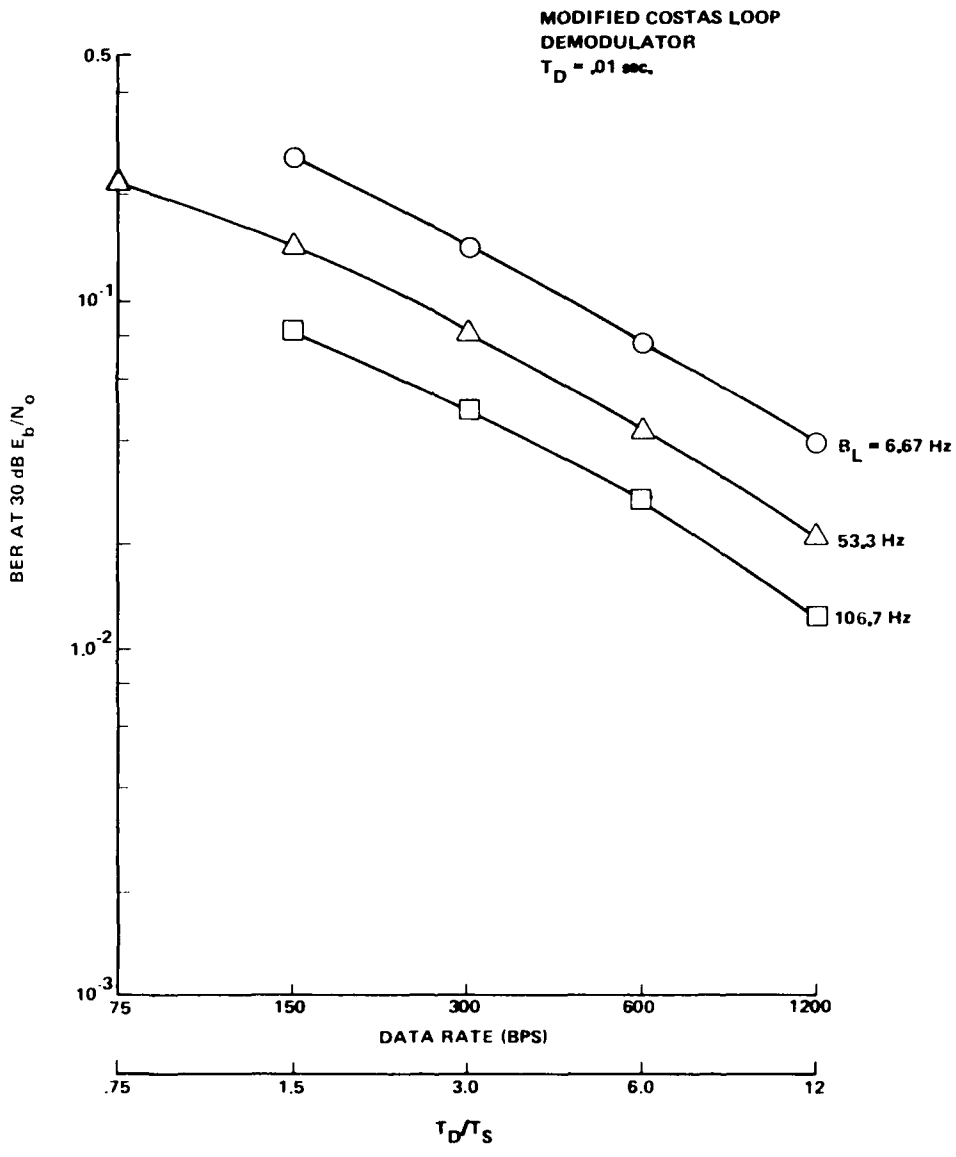

Figure 4-5. DECPSK performance versus data rate, 2nd order loop

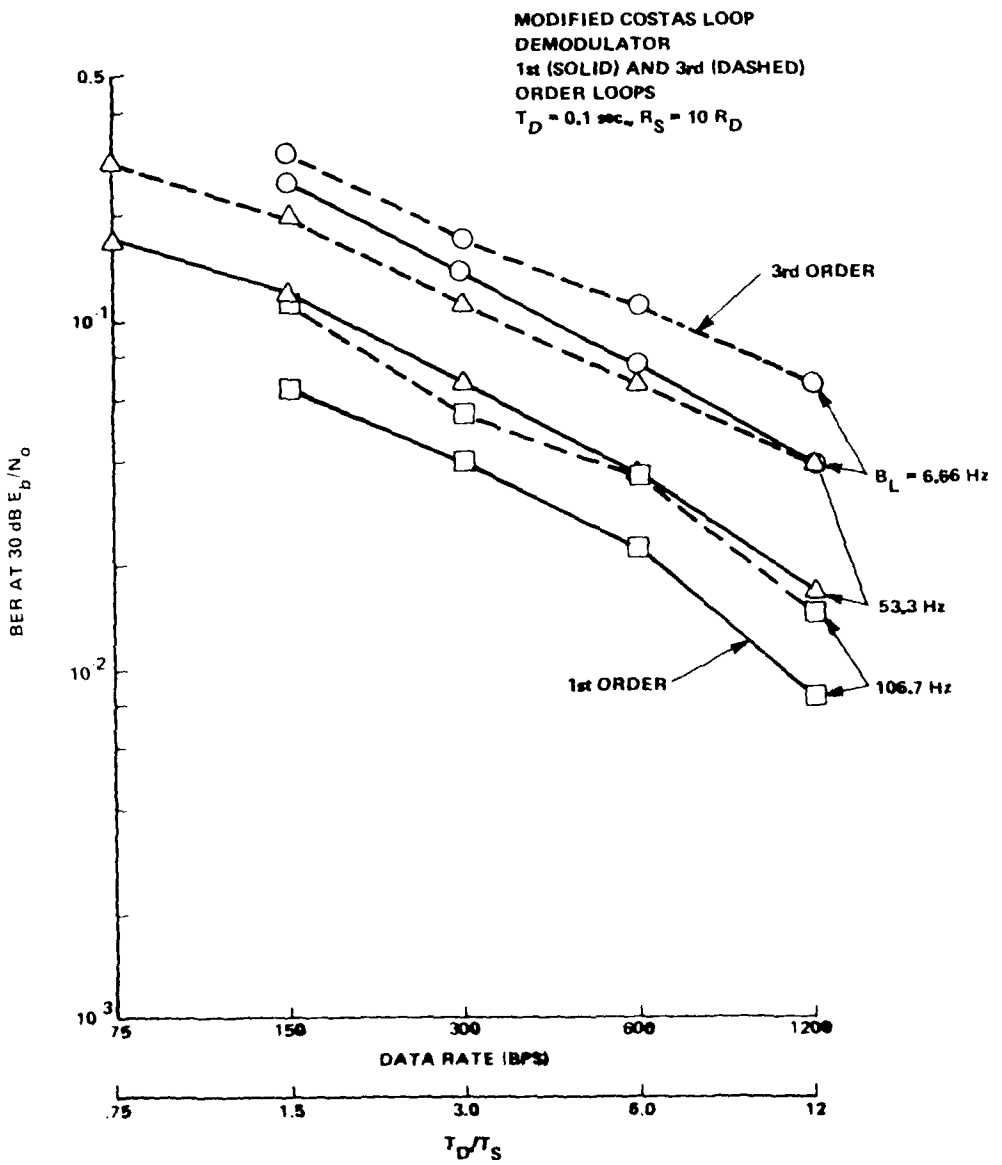

Figure 4-6. DECPSK performance versus data rate, 1st and 3rd order loops

4.1.3 DECPSK Performance Characterization.

Although not entirely obvious from Figure 4-1 through 4-4, there appears to be an apparent similarity between the curves at the two data rates (which differ by a factor of 8) for decorrelation times which differ by approximately the reciprocal ratio. A more definitive study of this apparent performance scaling relation is presented in Appendix A where it is concluded that PSK demodulator performance can be adequately specified by the three parameters: E_b/N_o , B_L/R_D , and T_D/T_S .

As a consequence of this result, Figures 4-1 through 4-4 can be condensed into two curves (one for each B_L/R_D) of BER performance as a function of E_b/N_o and parameteric in T_D/T_S . These curves, shown in Figures 4-7 and 4-8, are a more general result which can be used to estimate DECPSK receiver BER performance over a wide range of fade rates and data rates for two second-order modified Costas loop demodulator designs (B_L/R_D = .044 and .355). Performance curves for first and third order loops are not presented since their performance is quite similar to that of the second order loop.

On the other hand, BER performance may change significantly for different loop designs. The two values of B_L/R_D selected for presentation were chosen as typical values which represent a range of potential demodulator designs currently in use. One additional curve, Figure 4-9, is presented to show the variation of BER performance at 30 dB as a function of B_L/R_D . The reader can use this curve to interpolate a BER performance curve for loop designs other than for the B_L/R_D values presented. For very small values of B_L/R_D (B_L · 0) the curves appear to be asymptoting to a limiting BER value for each T_D/T_S value. For B_L/R_D values near 0.5, BER performance appears to be improving, but it should be noted here that performance will be reaching a minimum value soon depending on the BT product of the received signal bandwidth as the data transition tracking errors become significant.

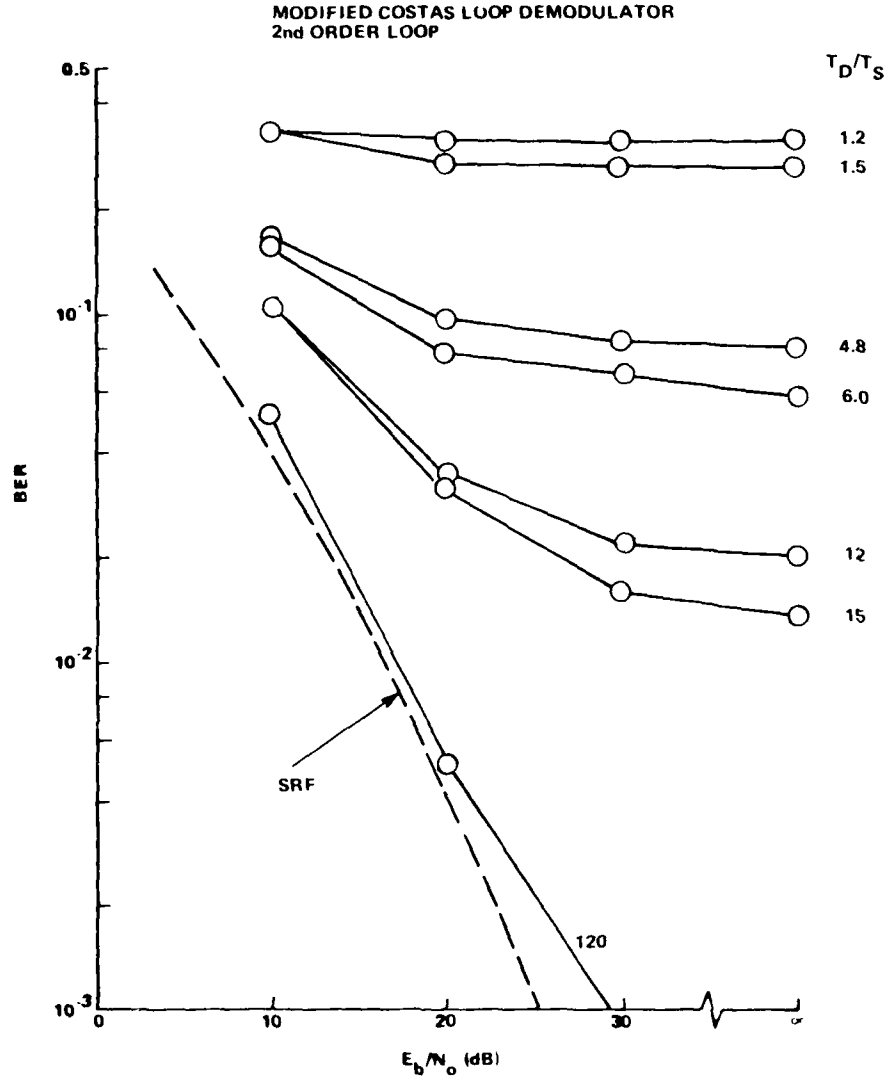

Figure 4-7. DECPSK performance B_L/R_D = .044

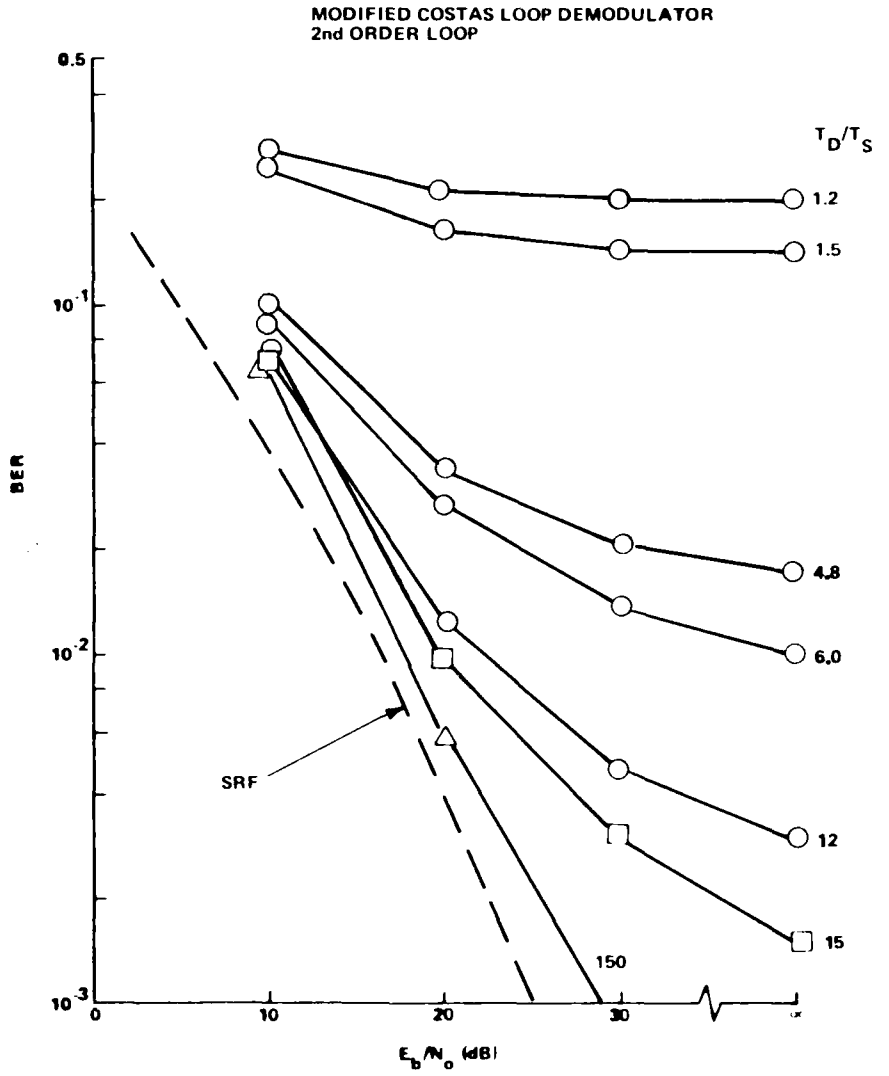

Figure 4-8. DECPSK performance B_L/R_D = .355

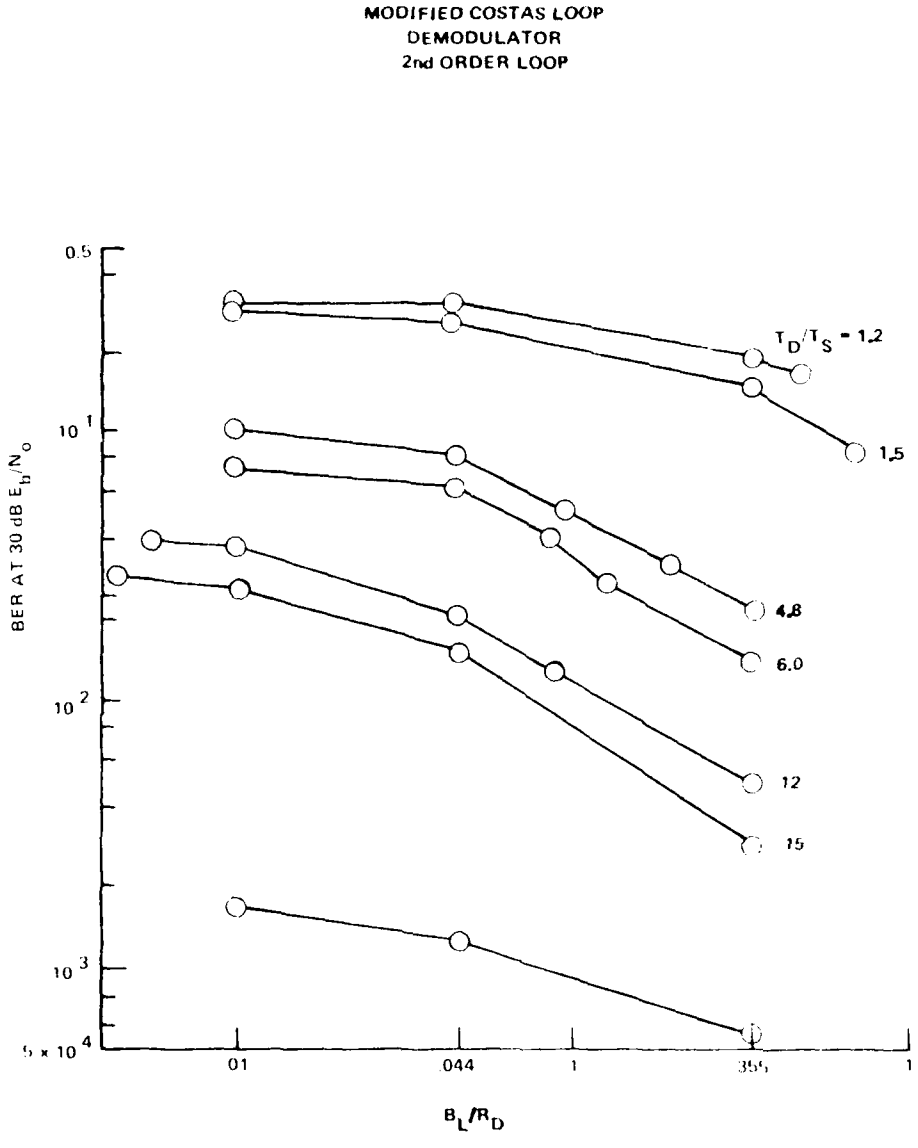

Figure 4-9. DECPSK performance versus B_L/R_D

4.2 DPSK PERFORMANCE.

4.2.1 E_b/N_o and B_L Dependence.

The BER performance of a DPSK demodulator with modified Costas loop aiding in noisy fading channels is shown in Figures 4-10 through 4-13. These figures like the DECPSK results show simulated BER as a function of E_b/N_o, parametric in the fading channel decorrelation time for two aiding loop bandwidths at 150 bps and 1200 bps data rates. The DPSK demodulator performance shows much the same trend as is shown by the CPSK demodulator in Figures 4-1 through 4-4, except that DPSK performance appears to be slightly better at faster fade rates and not as strongly dependent on the loop noise bandwidth as CPSK appears to be. Loop phase tracking performance of the first order aiding loop is presumed to be similar to the CPSK phase reference loop although the simulated bandwidths are [illegible] times larger. Amplitude fading and noise are the dominant sources of degradation at low fade rates and E_b/N_o, thus DPSK performance is slightly worse since bit decisions are dependent on both inphase and quadrature noise components as opposed to CPSK [illegible] which depend only on the inphase noise component.

As fade rate increases, DPSK performance gets progressively [illegible] but does not degrade as rapidly as [illegible]. DPSK results also show [illegible] improvement at the faster fade rates. [illegible]

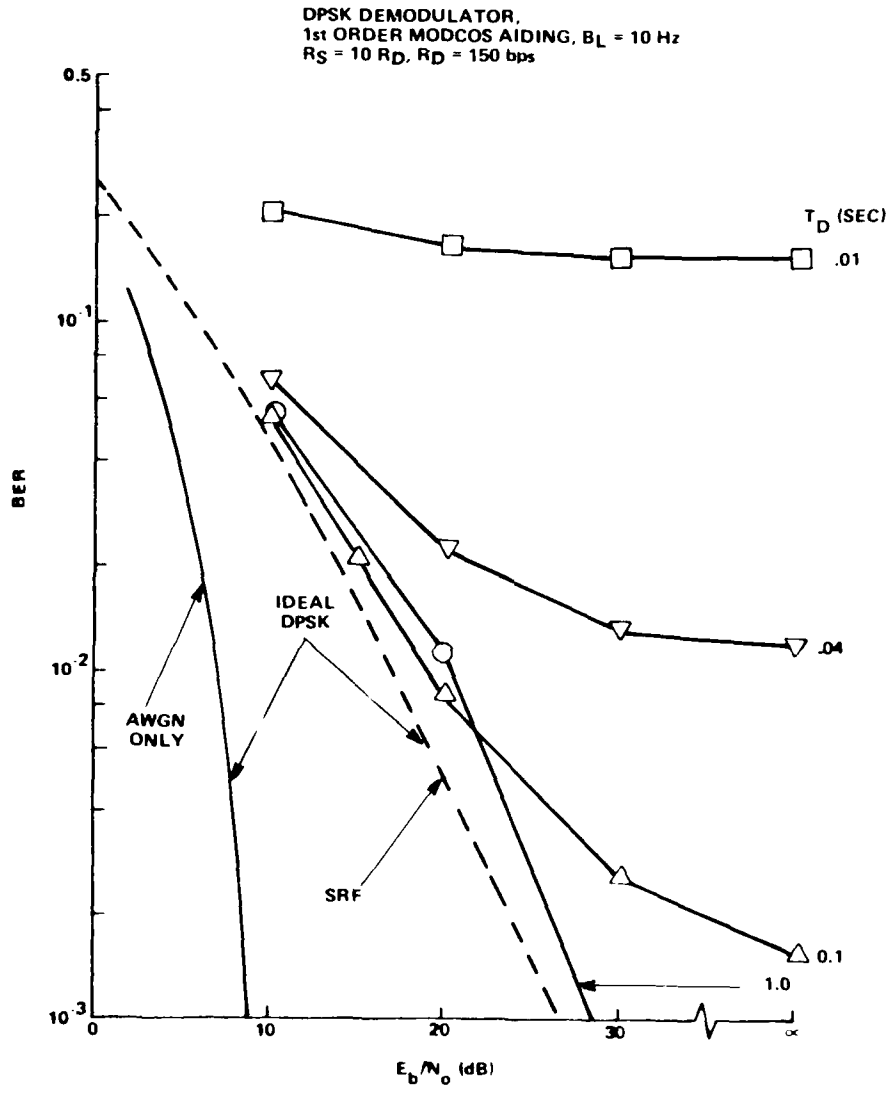

Figure 4-10. DPSK BER performance for B_L = 10 Hz and R_D = 150 bps

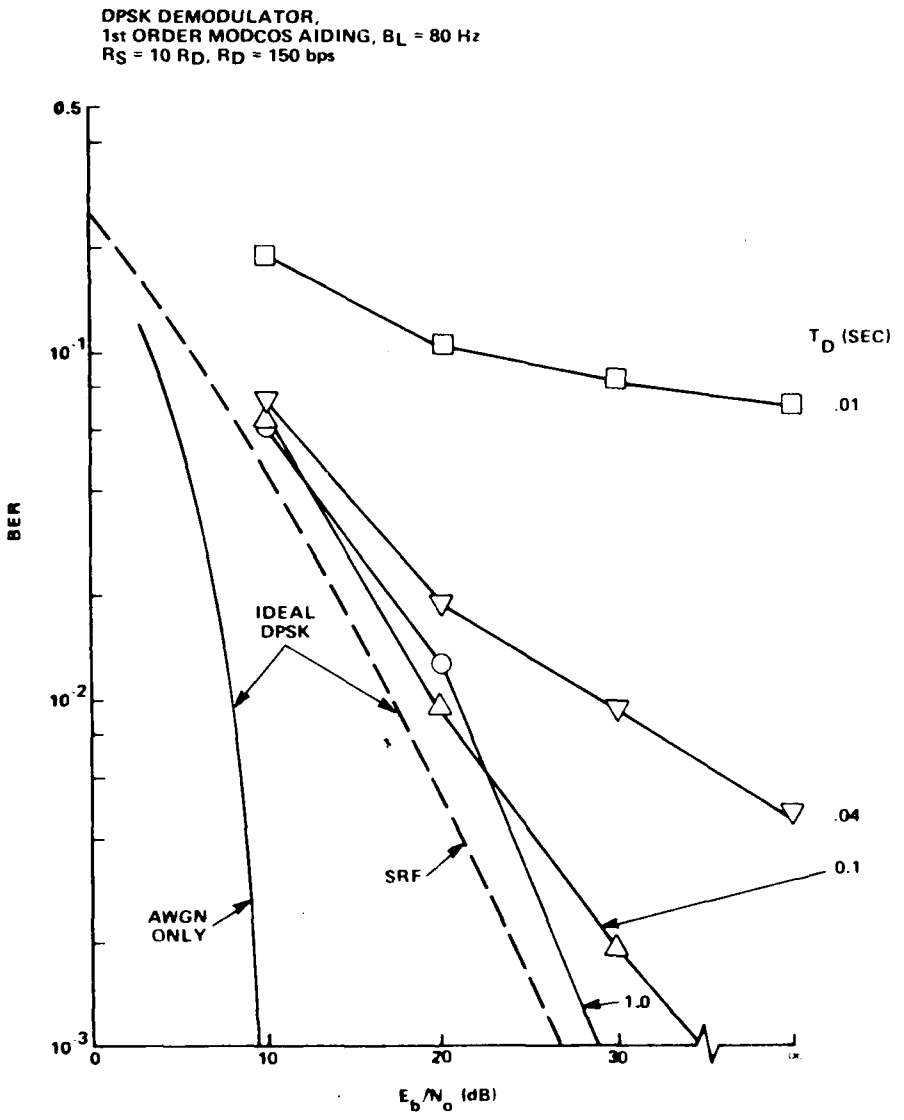

Figure 4-11. DPSK BER performance for B_L = 80 Hz and R_D = 150 bps

DPSK DEMODULATOR,
1st ORDER MODCOS AIDING, B_L = 80 Hz
R_S = 5 R_D, R_D = 1200 bps

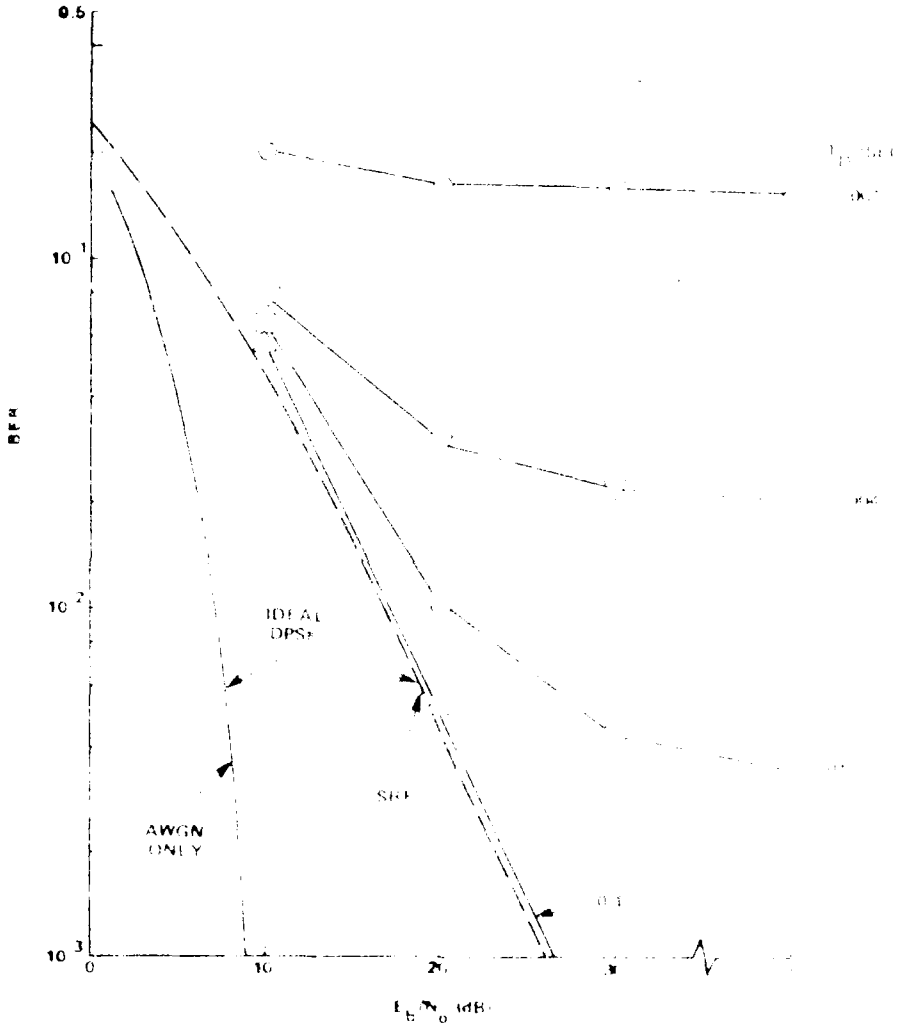

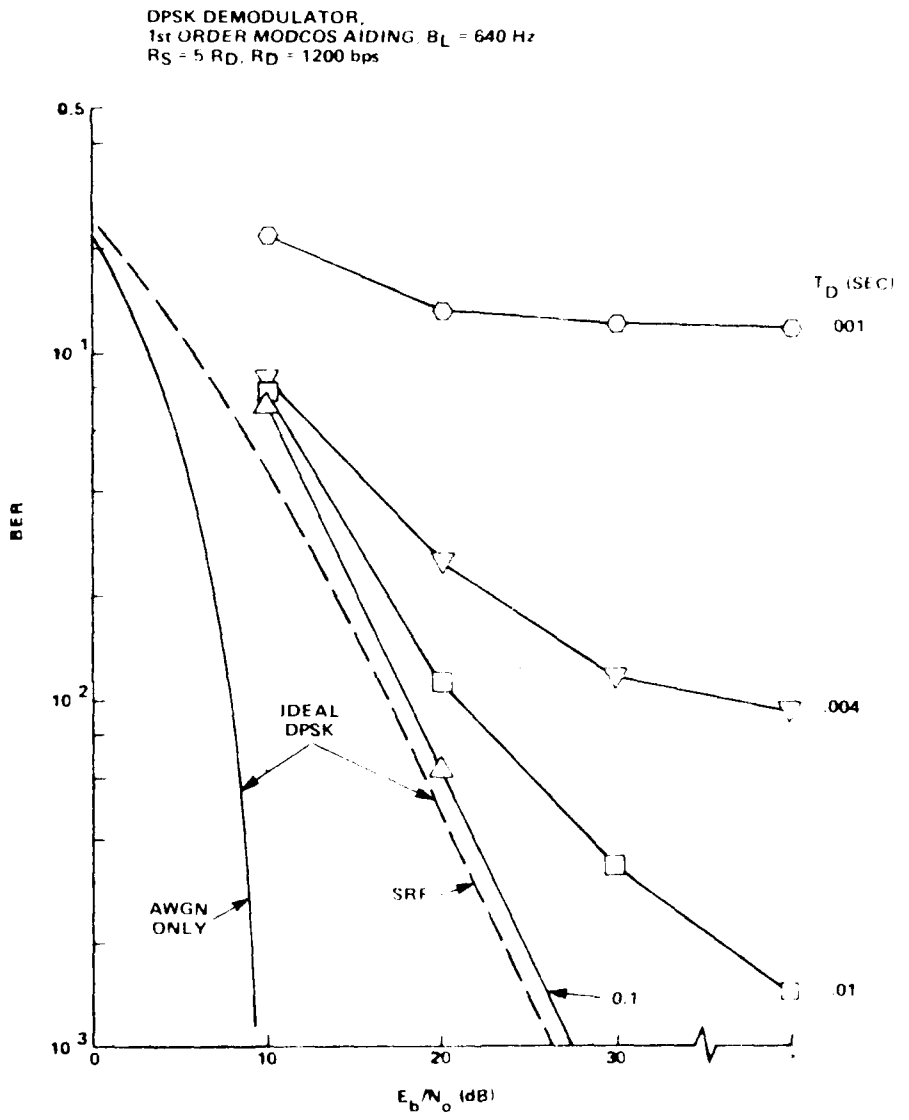

Figure 4-13. DPSK BER performance for B_L = 640 Hz and R_D = 1200 bps

correctly demodulate a few more "phase glitched" data bits which result in cycle slip caused errors for the CPSK demodulator. Like CPSK, DPSK BER also improves with larger loop bandwidths but is not as strongly dependent on loop bandwidth as CPSK performance - a result which is also attributable to the bit decision criteria being independent of cycle slipping for DPSK.

4.2.2 Data Rate Dependence.

Since DPSK bit decisions are based on the absence or presence of phase changes between data bit periods, shorter bit periods (high data rates) result in better demodulator performance. For a given residual phase glitch after aiding the phase comparison interval is shorter at higher data rates and thus reduces the potential phase change within that reduced comparison interval. A comparison of Figures 4-11 and 4-12 shows that BER performance of a DPSK demodulator can improve by more than an order of magnitude as data rate increases from 150 to 1200 bps at high E_b/N_o in the T_D = .01 second fading environment. Figure 4-14 shows BER performance for DPSK is more strongly dependent on data rate than CPSK (Figures 4-5 and 4-6) in the fast fading environment as indicated by the steeper slope of these lines. In contrast to CPSK performance this figure shows that at low data rates, DPSK BER is also strongly dependent on the aiding loop noise bandwidth, but at higher data rates this dependence decreases as BER performance for three different bandwidths converge to the same line. At these high data rates the change in the VCO phase over a bit period is small and has a negligible effect on demodulator performance.

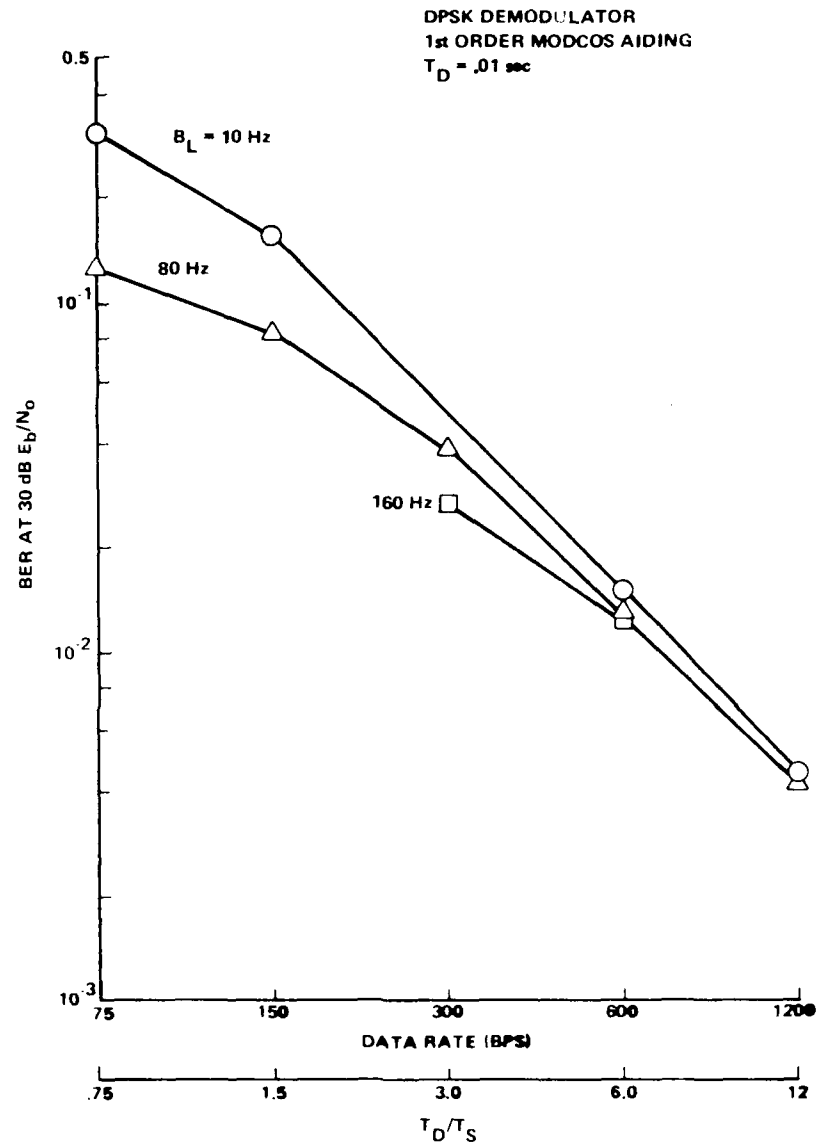

Figure 4-14. DPSK performance versus data rate

4.2.3 DPSK Performance Characteristics.

DPSK performance has also been found to scale, like DECPSK performance, with the ratio of decorrelation time and bit period, T_D/T_S . As shown in Appendix A, DPSK demodulator performance in the noisy fading environment can be adequately specified by the three parameters: E_b/N_o , B_L/R_D , and T_D/T_S . As a consequence of this result, Figures 4-10 through 4-13 have been condensed into two curves (one for each B_L/R_D) of BER as a function of E_b/N_o , parametric in T_D/T_S and is shown in Figures 4-15 and 4-16. These curves are a more general result which can be used to estimate BER performance over a wide range of fade rates and data rates for a DPSK demodulator with first-order modified Costas loop aiding designed with B_L/R_D = .067 and .533. It is believed that performance for second and third order aiding loops would be similar to the first order loop results presented here and adequate performance estimates could be obtained from them.

Although the weak dependence of BER performance on the aiding loop bandwidth for the T_D = .01 fading environment is shown in Figure 4-14, a more general result which verifies this fact is shown in Figure 4-17. This figure shows DPSK BER performance at 30 dB E_b/N_o is primarily dependent on the T_D/T_S ratio of the environment and has very little dependence on aiding loop bandwidth as indicated by the B_L/R_D ratio. In comparison to CPSK performance (Figure 4-9) DPSK performance in fast fading environment appears to be somewhat better. However, this advantage diminishes at slower fade rates and lower E_b/N_o values where amplitude fading and noise become the dominant source of degradation.

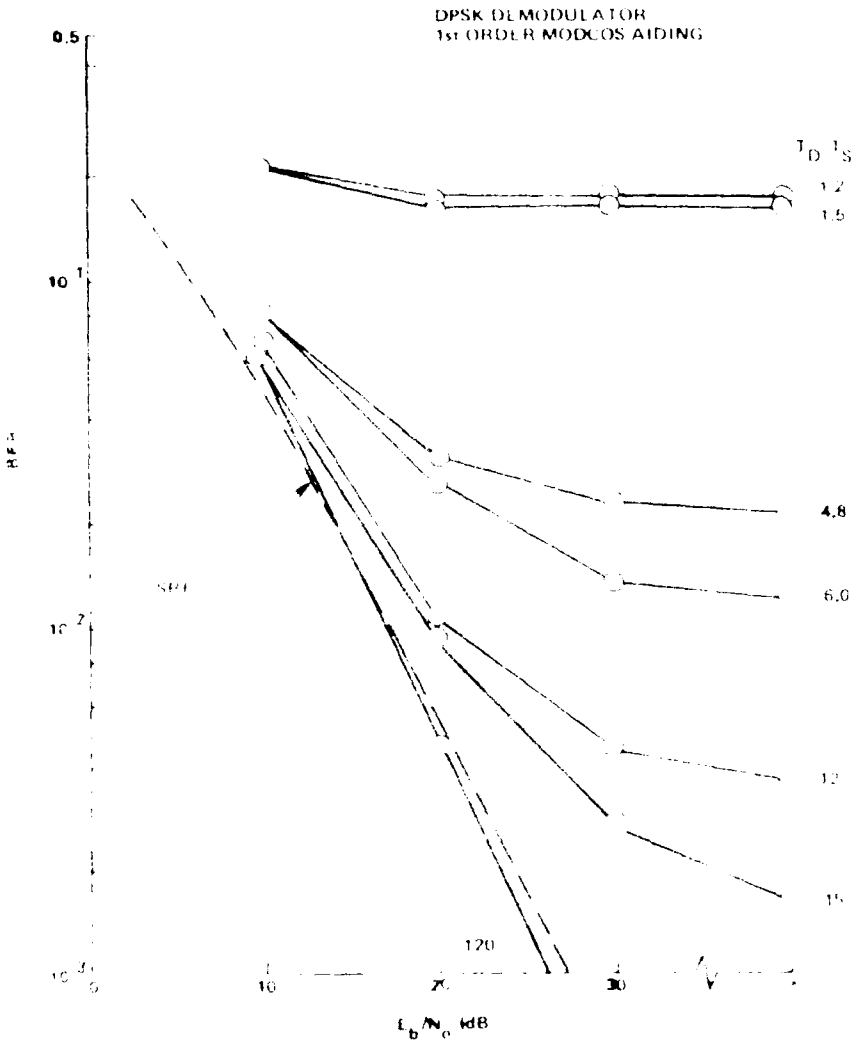

DPSK performance T_D/T_S

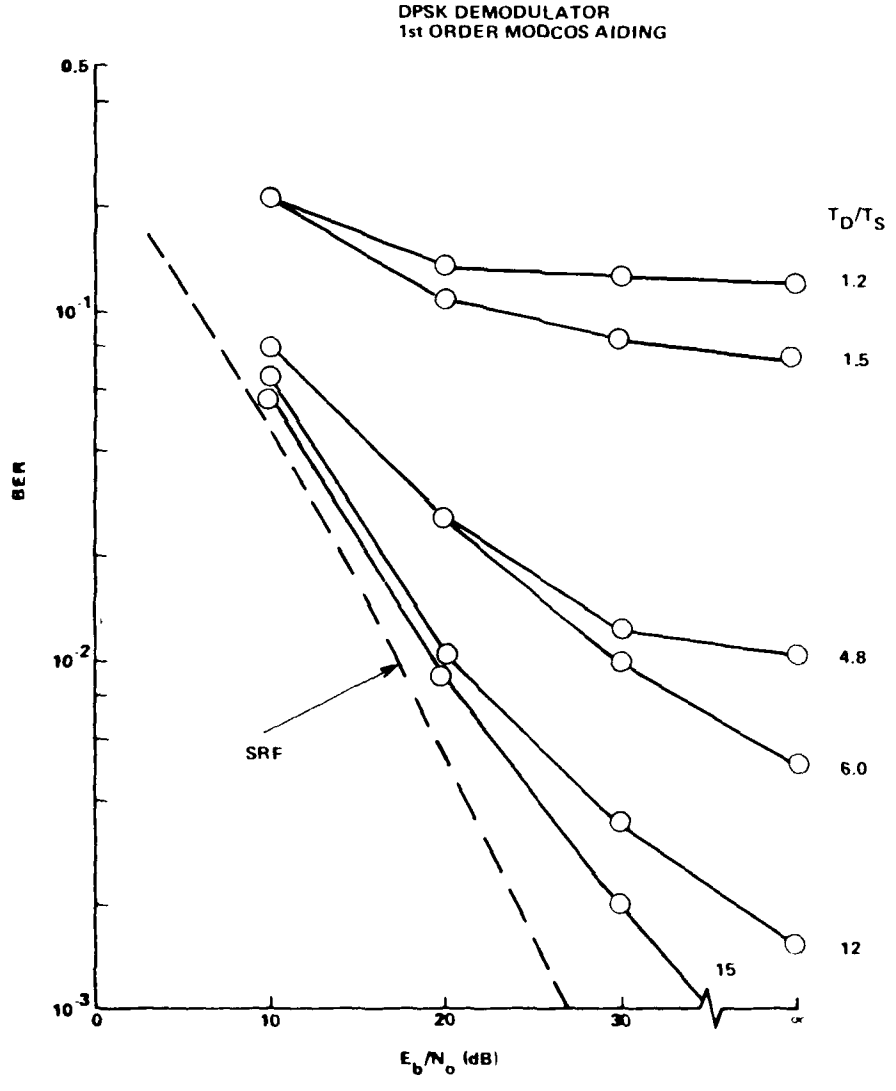

Figure 4-16. DPSK performance, B_L/R_D = .533

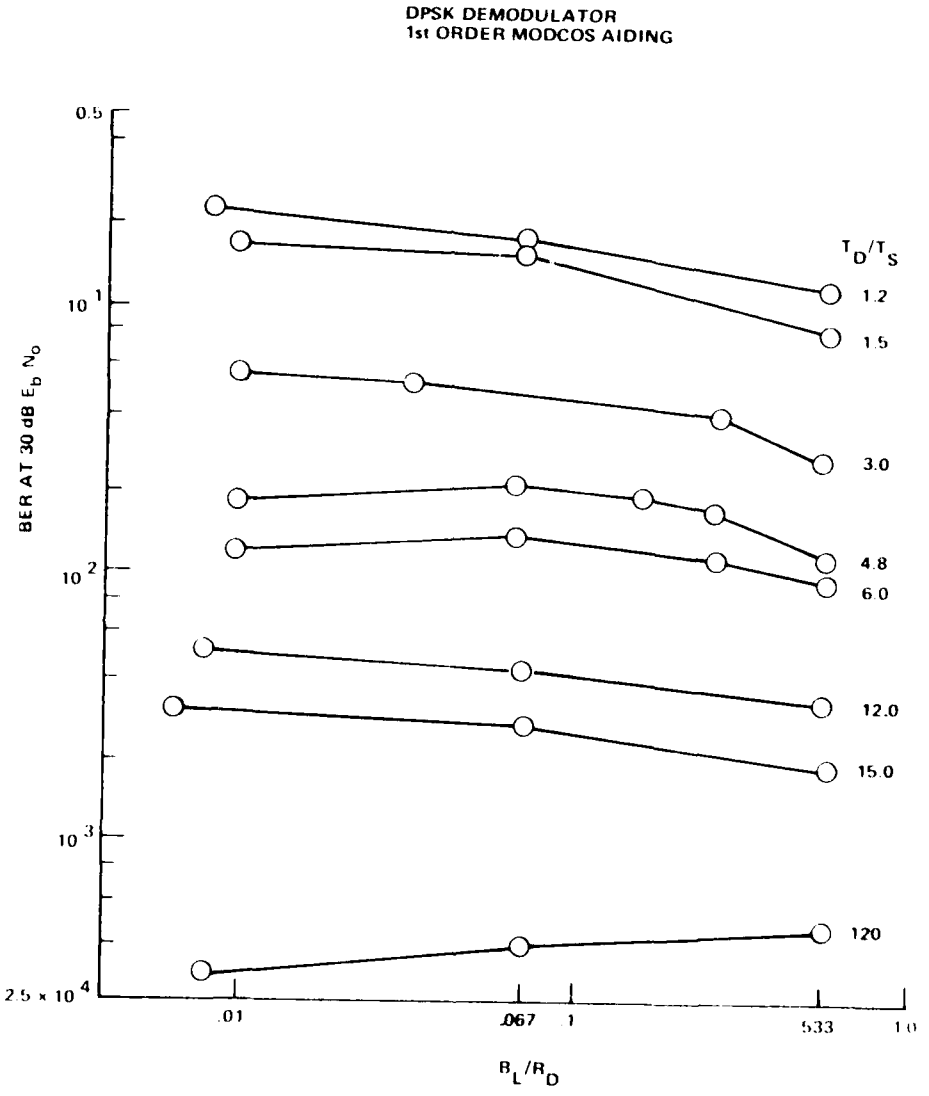

Figure 4-17. DPSK performance versus B_L/R_D

4.3 NCFSK PERFORMANCE.

4.3.1 E_b/N_o and $\Delta f/R_D$ Dependence.

Although the modulation format of NCFSK signaling is somewhat different than that of PSK modulation, the general shape and characteristics of the curves for the NCFSK modem is quite similar to those of PSK modulation presented in the previous section. Figures 4-18 and 4-19 show BER performance as a function of E_b/N_o for a number of 150 bps demodulator designs ($\Delta f/R_D$ = 1,2,4 and 8) for two fading enviornments with 0.1 and .004 second decorrelation times, respectively. The parameter $\Delta f/R_D$ is defined as the ratio of the tone separation in Hz, Δf, divided by the data rate R_D. At the 0.1 second decorrelation time, receiver performance is essentially that of slow Rayleigh fading for all tone separations. These results, as discussed in Appendix [illegible] are typical of performance which results for NCFSK demodulation with large [illegible] ratios. Amplitude fading and noise are the predominant sources of degradation in these environments which only [illegible] small amount of spectral spreading. On the other hand, the [illegible] .004 second environment does produce significant amounts of spectral spreading as shown in Figure 2-5, which results [illegible] noiseless fading environments. [illegible] of this severe spectral spreading [illegible] results in increasing [illegible] of intersymbol interference and corresponding BER degradation as the separation between binary signaling frequencies [illegible] is reduced. Performance is further [illegible] E_b/N_o is increased and the curves appear to [illegible] asymptote toward the [illegible] curves.

Results [illegible] with the preceding [illegible] were obtained for other [illegible] presented here. Instead Figure 4-[illegible] is presented which [illegible] performance [illegible]

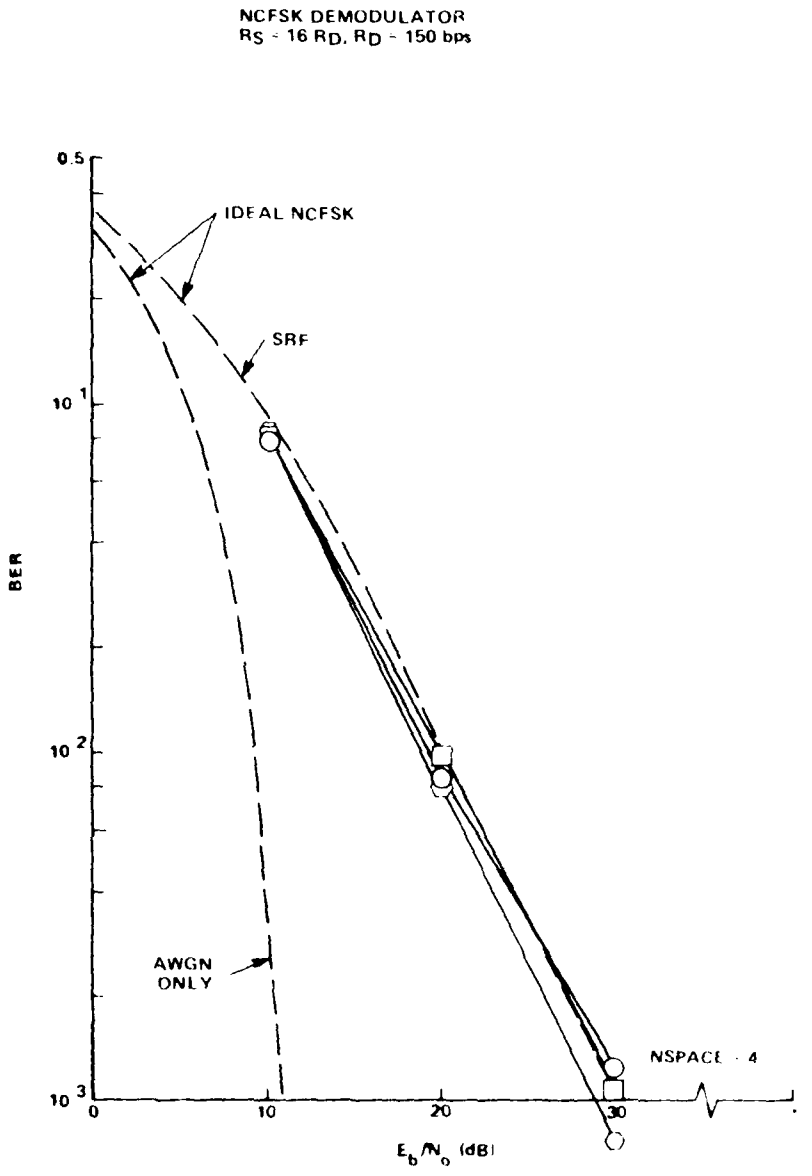

Figure 4-18. NCFSK BER performance at T_D = 0.1 sec

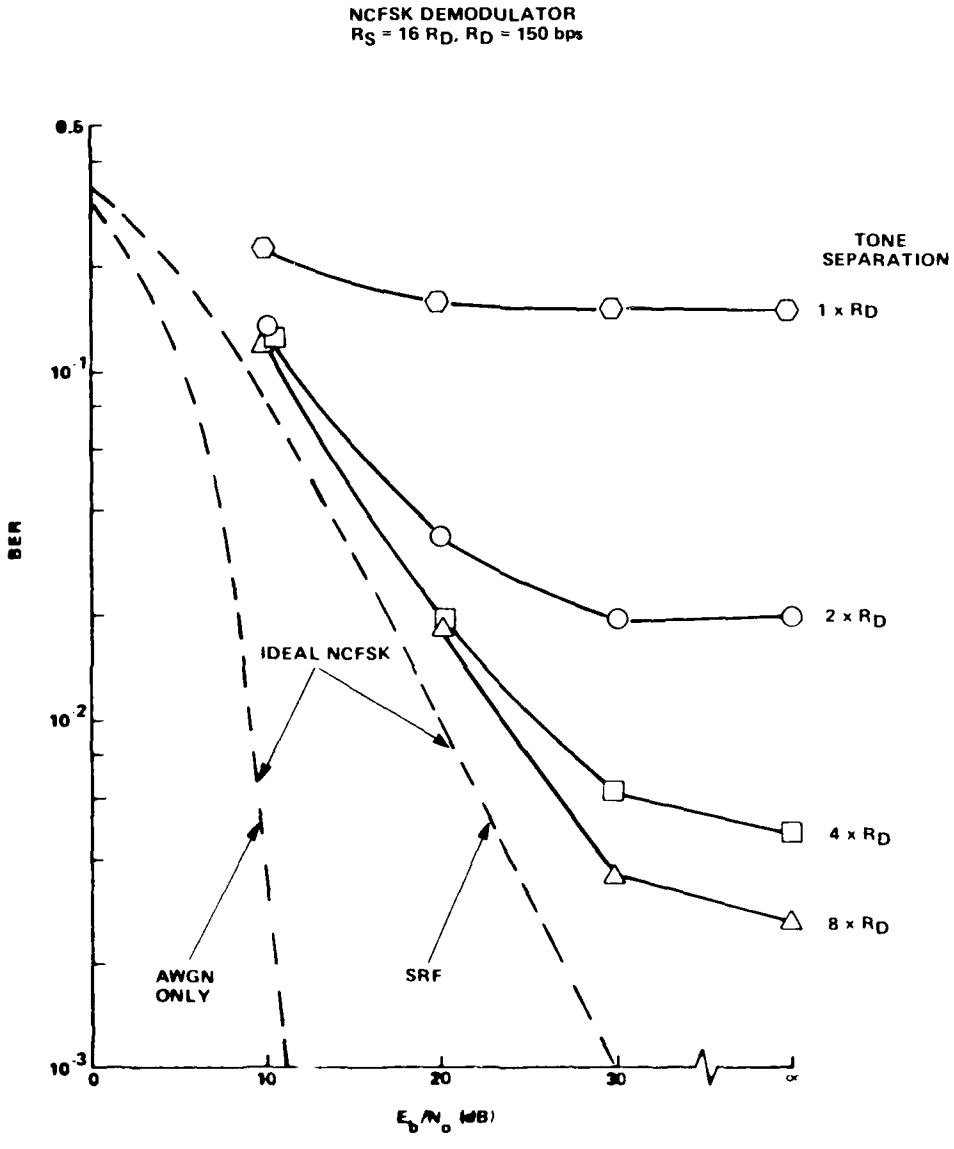

Figure 4-19. NCFSK BER performance at T_D = .004 sec

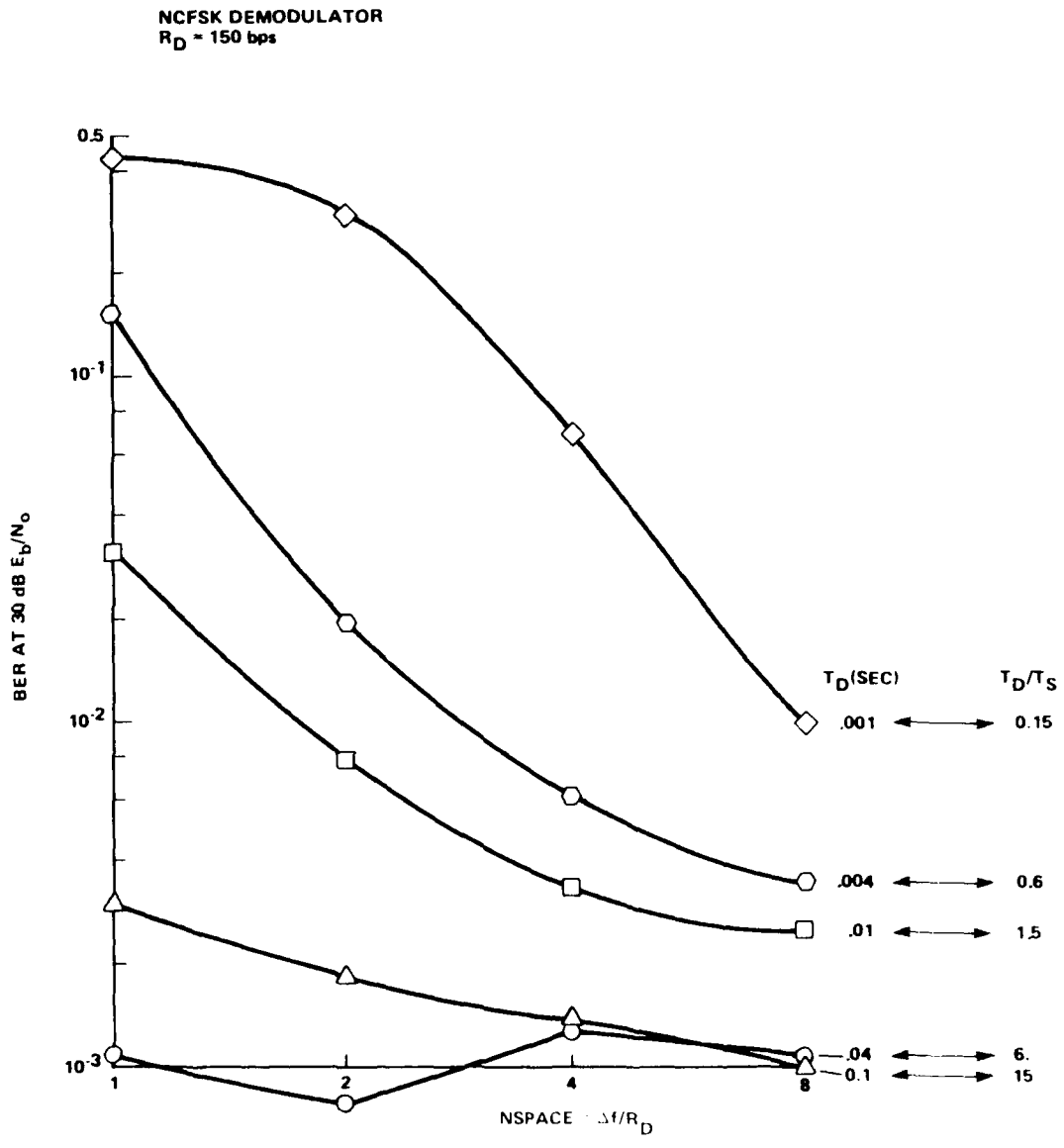

Figure 4-20. NCFSK BER performance parametric in environment

separation and parametric in the environment decorrelation time. The figure shows that NCFSK BER performance can be catastrophically degraded for small tone separations ($\Delta f/R_D = 1$) in fast fading environments. By increasing tone separation, however, the degradation due to intersymbol interference is reduced and substantial performance improvement can be achieved in fast fading environments. Even with the widest tone seperation, however, some of the signal energy is still lost outside the symbol bandwidth at the demodulator which has the effect of reducing the total bit energy to noise density ratio at the demodulator. This effect is clearly shown in Figure 2-3 at decorrelation times of 10 ms or less.

4.3.2 Data Rate and Tone Separation Dependence.

Both DECPSK and DPSK demodulators showed consistent BER performance improvement at higher data rates. In contrast, FSK demodulator performance remains relatively constant over a range of data rates, as shown in Figure 4-21 for a fixed tone separation. The figure does show, however, that BER performance at 30 dB E_b/N_o does improve for wider tone separations in the 0.01 second fading environment. Unlike differentially encoded PSK modulation whose signaling spectrum is contained in a narrow bandwidth at the carrier frequency, FSK modulation utilizes a wider spectral bandwidth specified by the tone separates. Phase glitches which often result in differential decoded PSK demodulation errors appear as sudden frequency translations of the received modulated carrier. FSK bit decisions based on the rate of change of received signal phase (rather than the amount of phase change per bit period like PSK) are not significantly affected by the bit duration. However, by increasing the frequency difference between complementary bits, frequency translations due to the fading channel are less likely to be confused with translations due to the data and account for the improved performance at the wider tone separations.

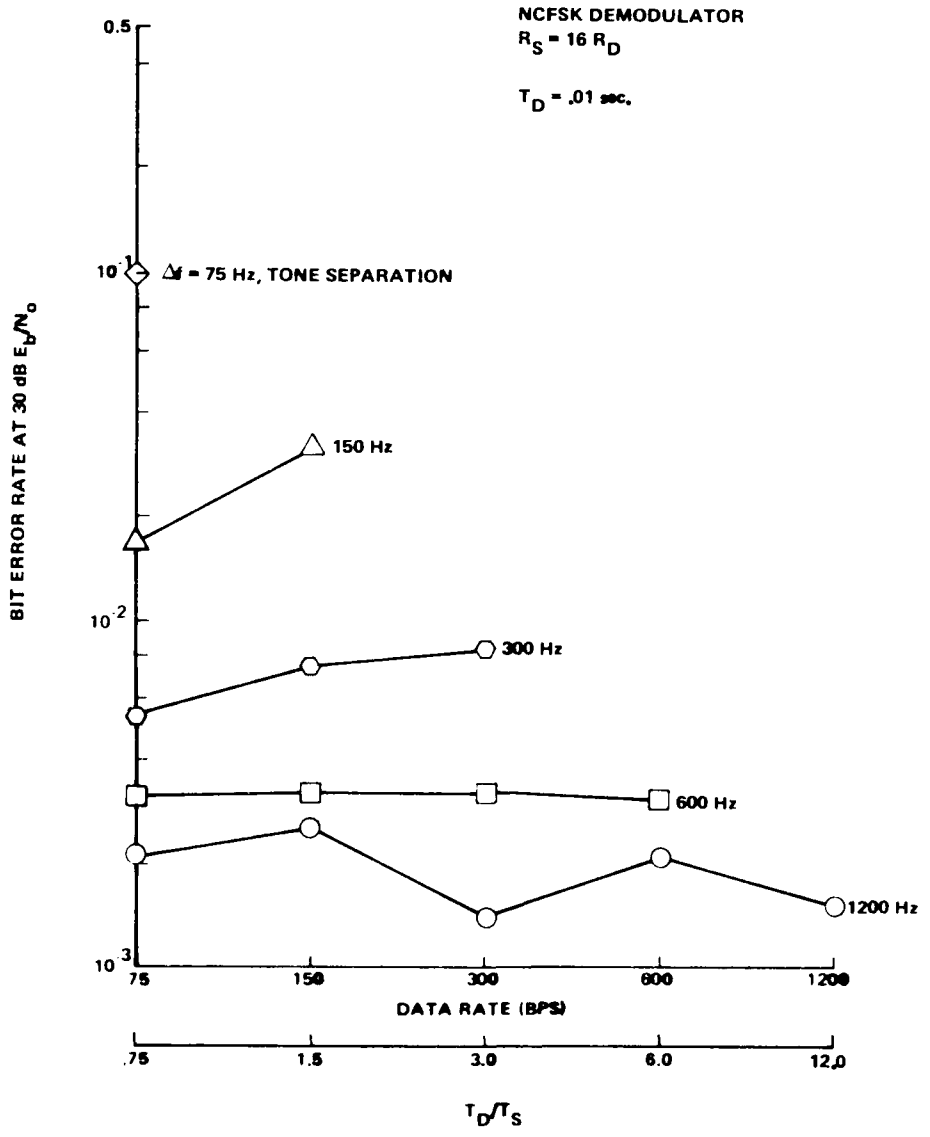

Figure 4-21. NCFSK BER performance parametric in tone separation

4.3.3 NCFSK Performance Characterization.

Much like the PSK demodulation results shown in Section 4.1 and 4.2, NCFSK modem performance in the noisy fading environments can be adequately specified by the three parameters: E_b/N_o , $\Delta f/R_D$, and T_D/T_S as discussed in Appendix B. As a result of this performance scaling, extensive amounts of BER performance data f r wide ranges of data rate, tone separation, and fading decorrelation time can be condensed into a set of performance curves, parametric in these characteristic scaling parameters. Figures 4-22 through 4-25 show BER performance as a function of E_b/N_o , parametric in T_D/T_S ratio for $\Delta f/R_D$ of 1,2, 4, and 8, respectively. Although these results were obtained for a 150 bps data rate, simulation results have shown that essentially the same performance curves are obtained at other data rates provided the tone separation, environment decorrelation time, and signal power are appropriately scaled to maintain the same values for the characteristic parameters, E_b/N_o , $\Delta f/R_D$, and T_D/T_S . Using these figures, it is believed that the reader could estimate BER performance for many NCFSK demodulators in a range of fading environments to within a reasonable degree of accuracy.

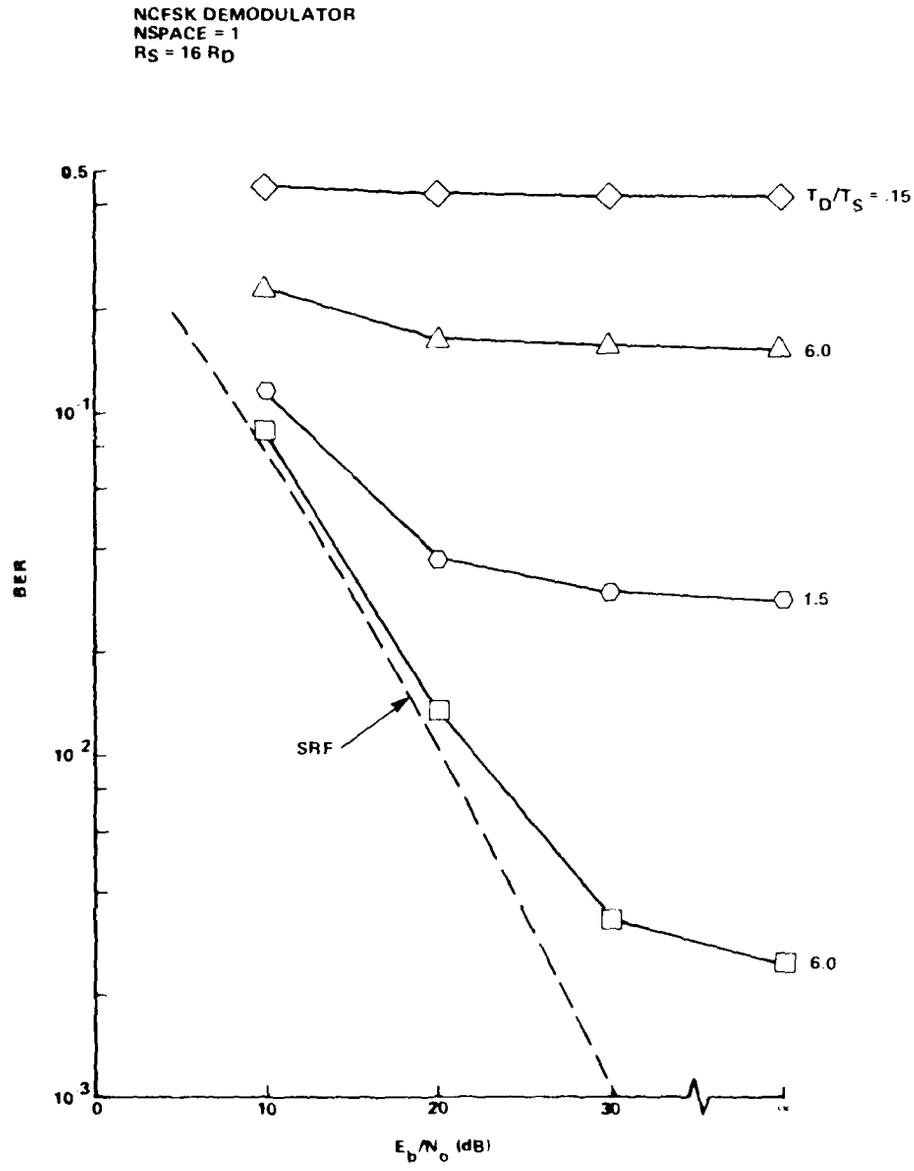

Figure 4-22. NCFSK performance, $\Delta f/R_D = 1$

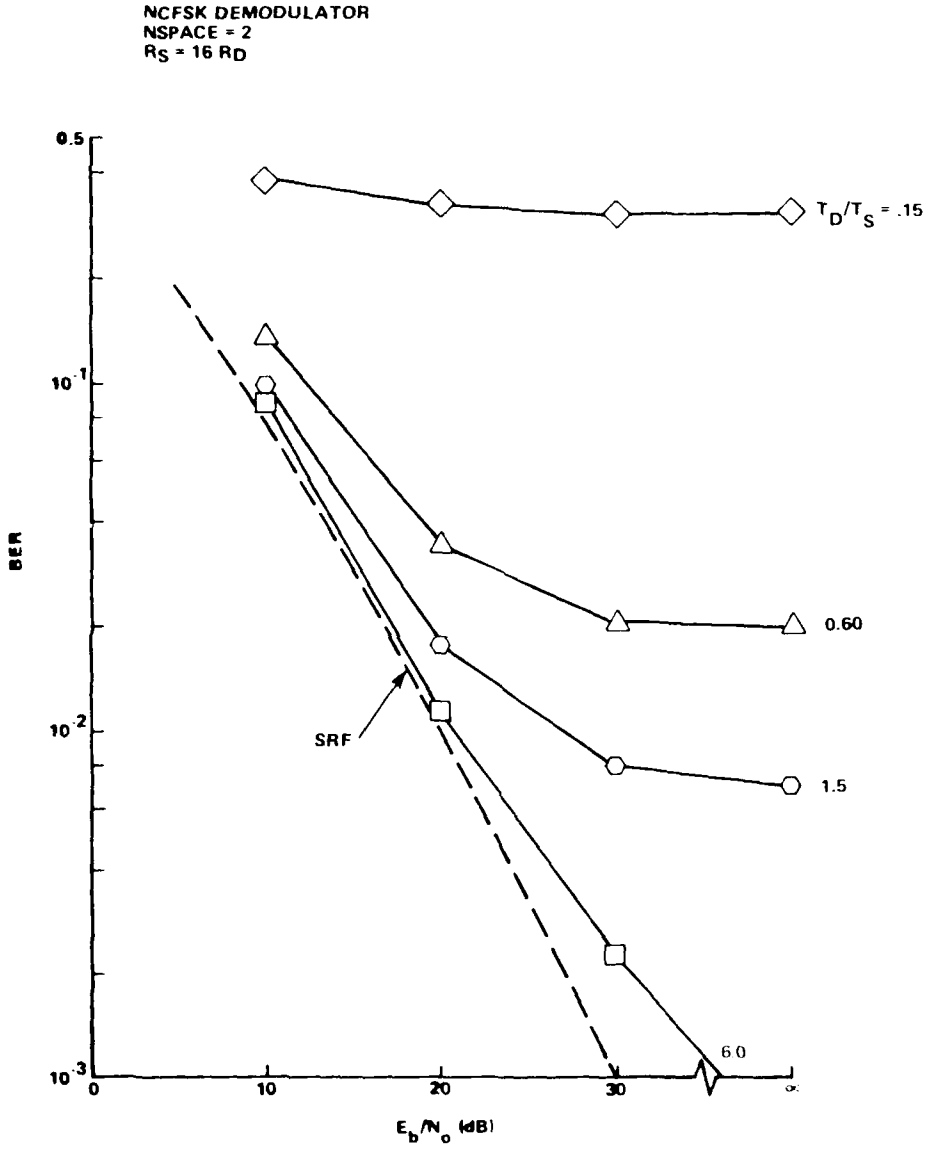

Figure 4-23. NCFSK performance, $\Delta f/R_D = 2$

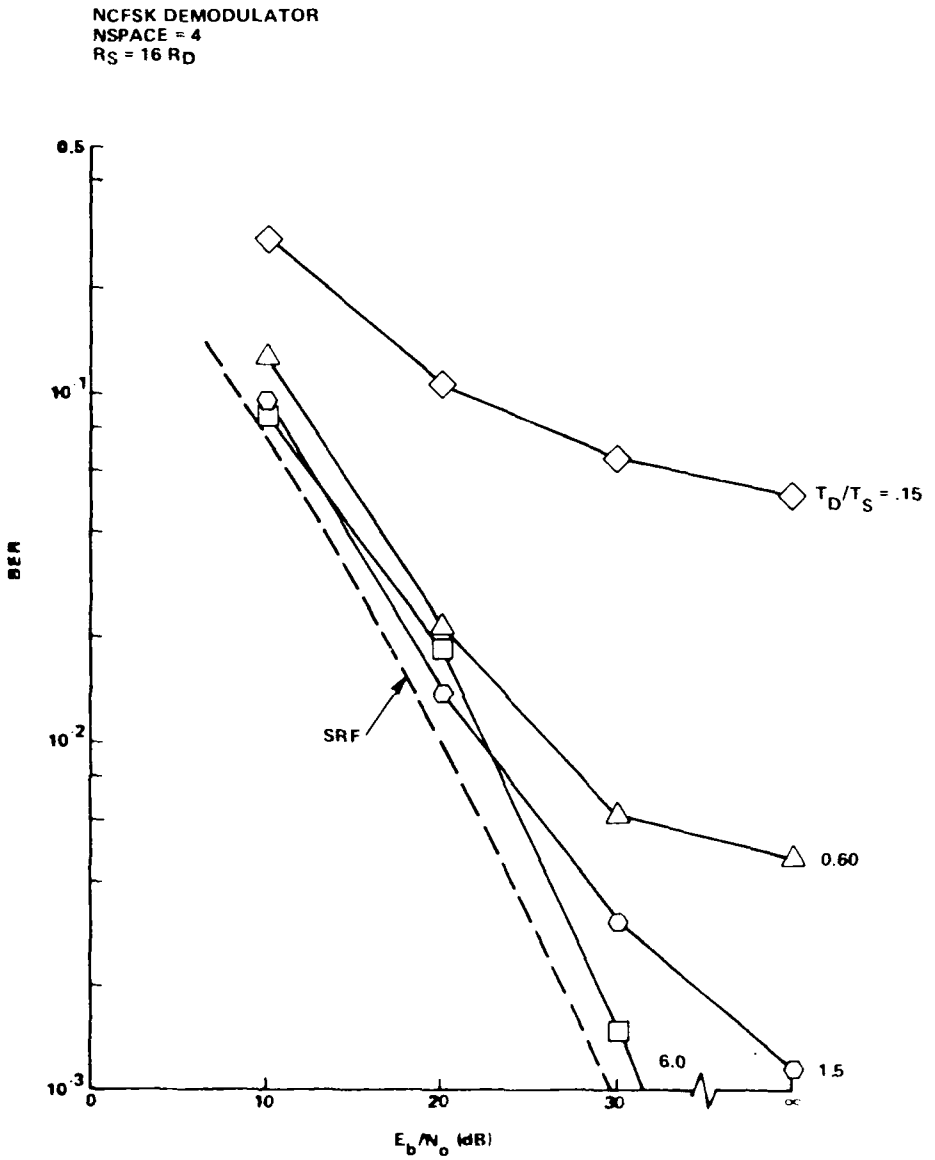

Figure 4-24. NCFSK performance, $\Delta f/R_D = 4$

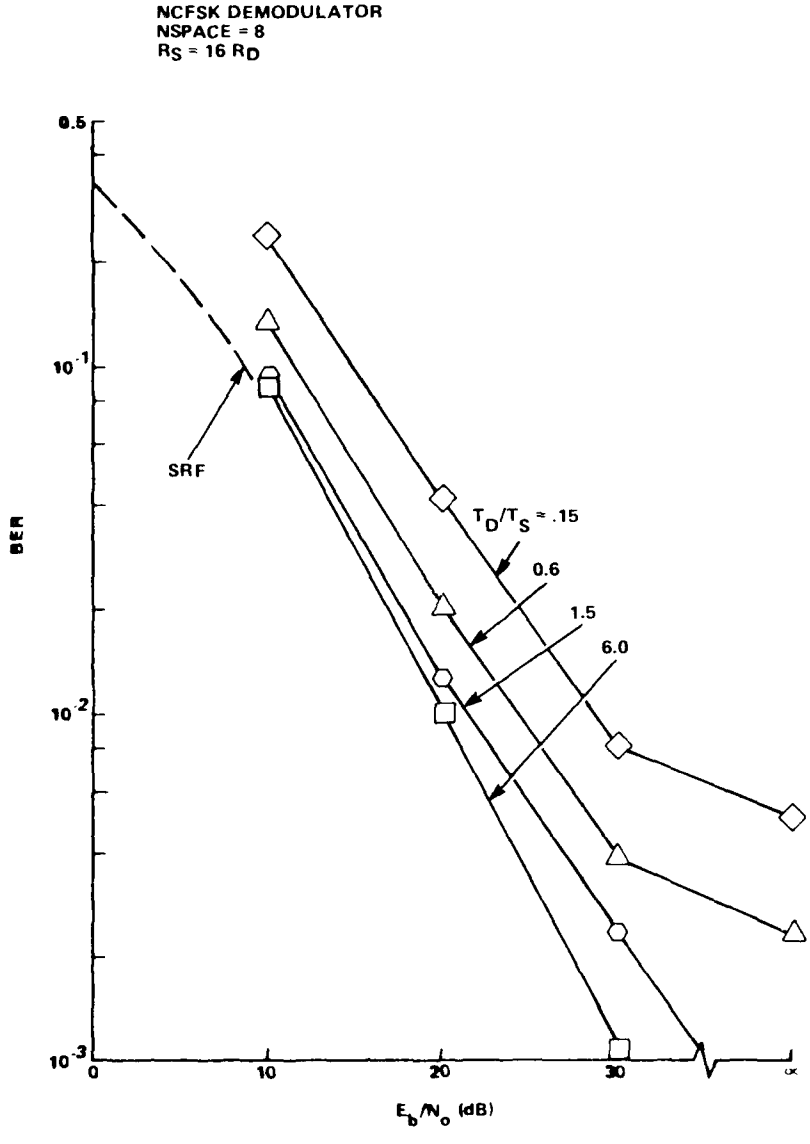

Figure 4-25. NCFSK performance, $\Delta f/R_D = 8$

REFERENCES

1. M. Schwartz, W. Bennett, and S. Stein, Communication Systems and Techniques, McGraw-Hill Inc., New York, 1966.

2. M.K. Simon, "Tracking Performance of Costas Loops with Hard-Limited In-Phase Channel," I.E.E.E. Transactions on Communications, Vol. COM-26, No. 4, April 1978, pp. 420-432

3. C.R. Cahn, D.K. Leiner, C.L. Marsh, F.J. Huntowski, G.L. Larue, "Software Implementation of a PN Spread Spectrum Receiver to Accommodate Dynamics," I.E.E.E. Transactions on Communications, Vol. COM-25, No. 8, August 1977, pp. 832-840.

APPENDIX A
ENVIRONMENT CHARACTERIZATION

In previous studies of demodulator performance in various PATS code fading environments, the fading has been described by its RMS phase deviation (σ) and the relative user-cloud velocity (v). In an earlier study, it was determined that for a given σ, PSK demodulator performance at a particular E_b/N_o and B_L/R_D ratio would scale with the ratio R_D/v , where E_b/N_o is the bit energy-to-noise density ratio, B_L is the loop noise bandwidth of a phase tracking loop R_D is the link data rate, and where v and σ are the characteristic fading parameters.

It is believed that the severity of PATS code modeled Rayleigh fading channel to the performance of digital communication links could be characterized by a more basic parameter related to the spectral content of the fading channel rather than σ and v. The signal envelope decorrelation time (T_D) of the fading environment is such a parameter and an approximate expression showing its relation to σ and v is given by[9]

$$T_D \approx \frac{1.08 \times 10^5}{v\ \sigma^{1.095}} \text{ seconds} \qquad \text{(A-1)}$$

where the units of v are in meters per second and the units of σ are in RMS degrees. This expression was derived for a CW tone phase modulated by plasma striations with a $1/f^3$ phase power spectrum and is valid whether or not the signal is in the far field of the plasma phase screen. Its application to the scaling relations developed herein assume Rayleigh amplitude statistics which occur in the far field. Rayleigh statistics generally occur at X-band for values of σ greater than 1000 degrees.

The inverse velocity dependence of the decorrelation time suggests that demodulator performance can now be characterized by only three parameters, E_b/N_o , B_L/R_D , and T_D/T_S ($=T_D \cdot R_D$). The last parameter T_D/T_S incorporates the spectral content or rate of fading relative to the data rate independent of the individual values of v and σ. Since performance scaling has already been established for the ratio of R_D/v in earlier studies, only the scaling of $(R_D/v)/\sigma^{1.1}$ must be verified to justify the characteristic performance scaling parameter T_D/T_S as given by

$$T_D/T_S = T_D \cdot R_D \propto \frac{R_D}{v\,\sigma^{1.095}} \quad . \qquad \text{(A-2)}$$

In order to establish the accuracy of using the T_D/T_S ratio to characterize receiver performance in the fading environments, a number of simulation results were obtained for the three demodulators for a range of σ, v, and R_D's. A subset of these results, shown in Figures A-1 through A-4, show bit error rates at 30 dB E_b/N_o as a function of σ's ranging from 1000 to 8000 degrees and parametric in velocities ranging from 50 to 3200 meters per second. Using the value of σ=2000 degrees as a reference, lines of constant T_D are also indicated by dashed lines on each figure.

A.1 PERFORMANCE SCALING WITH T_D/T_S FOR DPSK.

Figure A-1 shows BER performance at 30 dB E_b/N_o for an unaided DPSK demodulator as a function of rms phase deviation for several user-cloud velocities. Although these results were obtained for a 150 bps data rate, the performance scaling for constant R_D/v ratios make these results applicable at other data rates with the same R_D/v ratio. An unaided demodulator was chosen for this comparison to isolate the DPSK demodulation process by

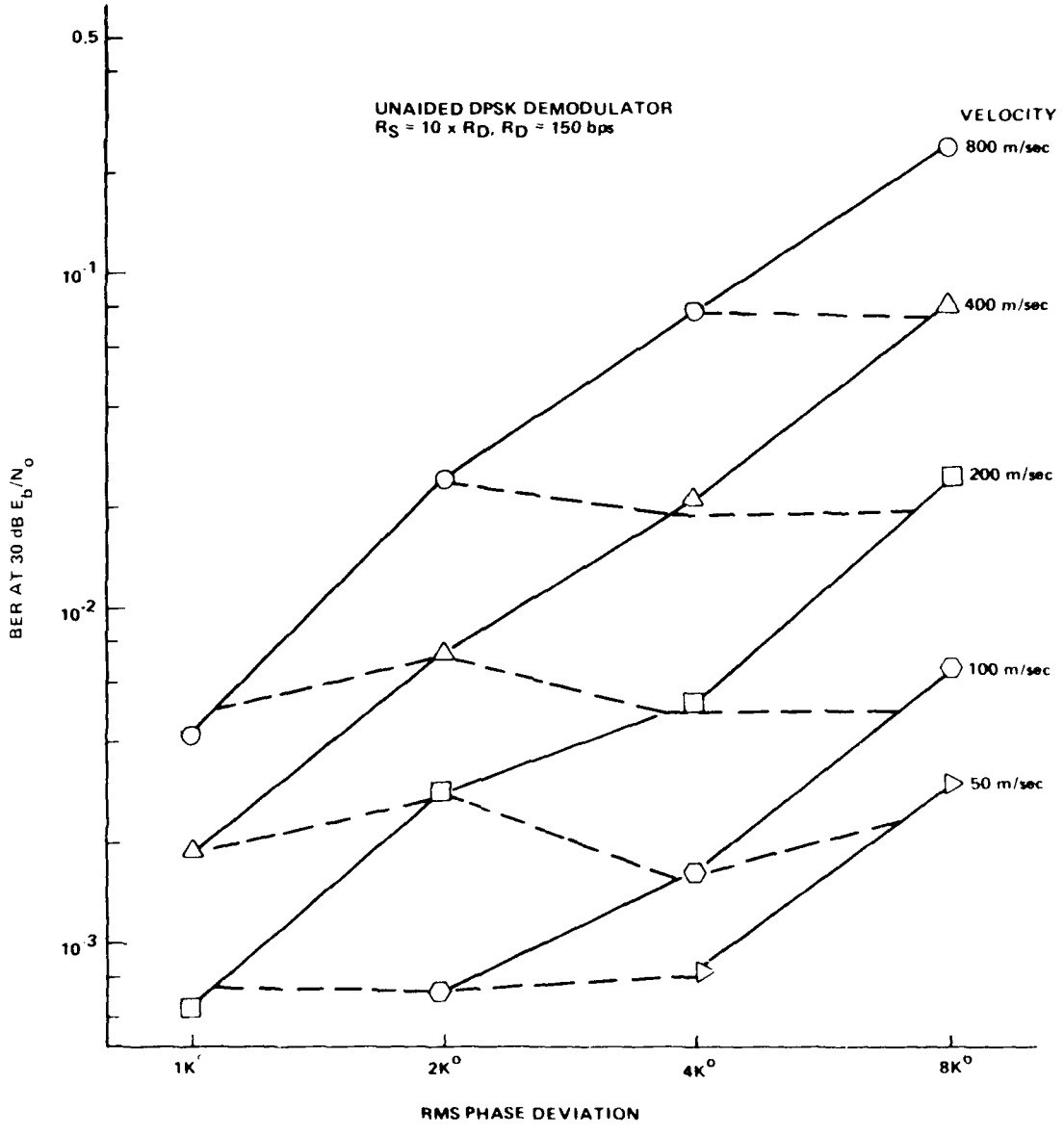

Figure A-1. Performance scaling with T_D, unaided DPSK, 150 bps

removing any losses due to the aiding loop performance, however, since performance is not strongly dependent on loop performance these results also hold for aided DPSK demodulators. The dashed lines of constant T_D show that DPSK performance can be adequately characterized by T_D (within a reasonable degree of accuracy) over a range σ and R_D/v values and this justifies the use the T_D/T_S ratio as a parameter in characterizing DPSK performance in the fading environment.

A.2 PERFORMANCE SCALING WITH T_D/T_S for DECPSK.

Similar curves showing BER performance for two DECPSK demodulator designs (B_L/R_D = .044, .355) are shown in Figures A-2 and A-3. Dashed lines of constant T_D in these figures also indicate that for given E_b/N_o and B_L/R_D ratios, DECPSK receiver performance for fixed T_D is relatively constant over a range of σ values and velocities. These results coupled with the fact that performance scales with the same R_D/v ratio verify that DECPSK receiver performance in the fading environment can be characterized by the three parameters: E_b/N_o , B_L/R_D , and T_D/T_S .

A.3 PERFORMANCE SCALING WITH T_D/T_S FOR NCFSK.

An equivalent set of parameters which characterize the performance of an NCFSK demodulator in PATS code modeled Rayleigh fading consists of E_b/N_o , $\Delta f/R_D$ (=NSPACE), and T_D/T_S . The E_b/N_o characterizes the performance degradation due to noise where the latter two parameters characterize the spectral spreading of the fading environment relative to the tone separation and the relative decorrelation of the received faded signal over the bit integration interval.

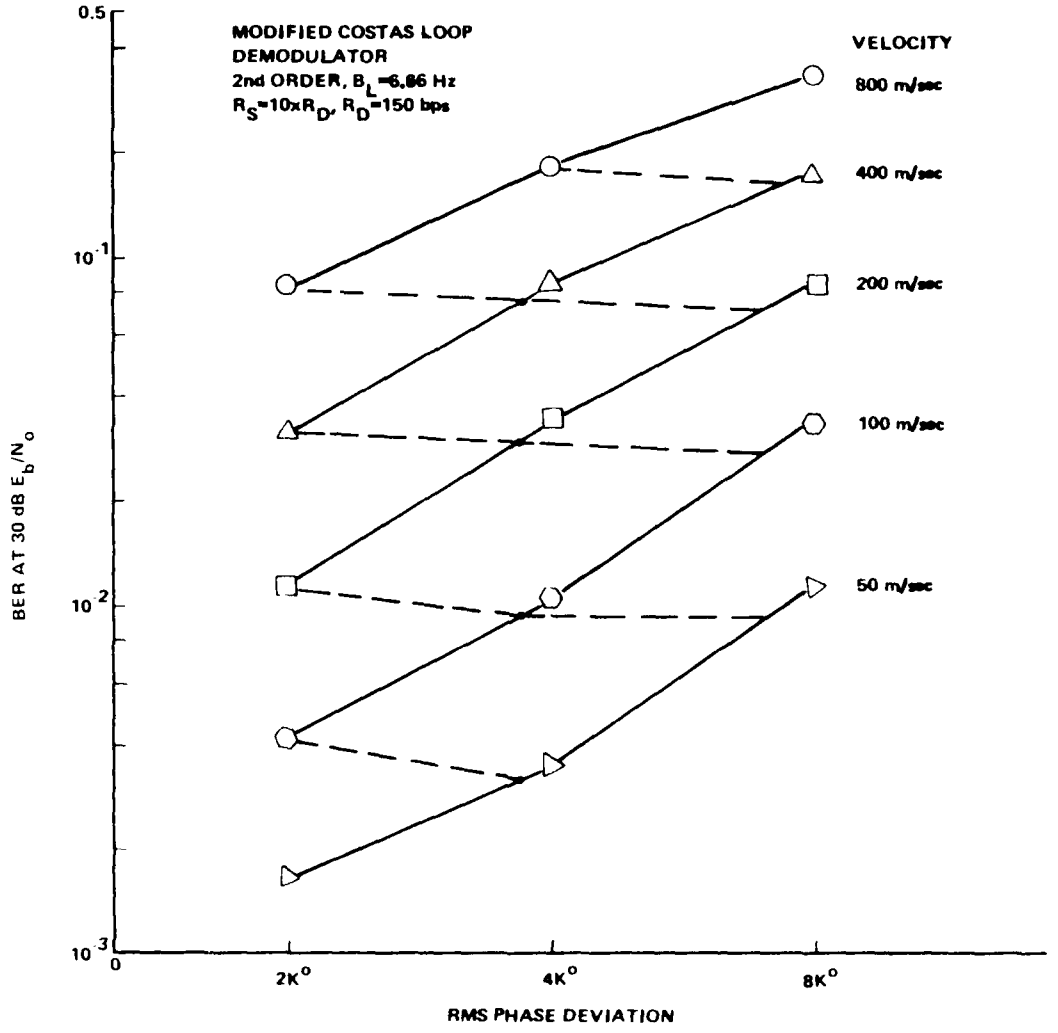

Figure A-2. Performance scaling with T_D, Costas DECPSK, B_L/R_D = .044

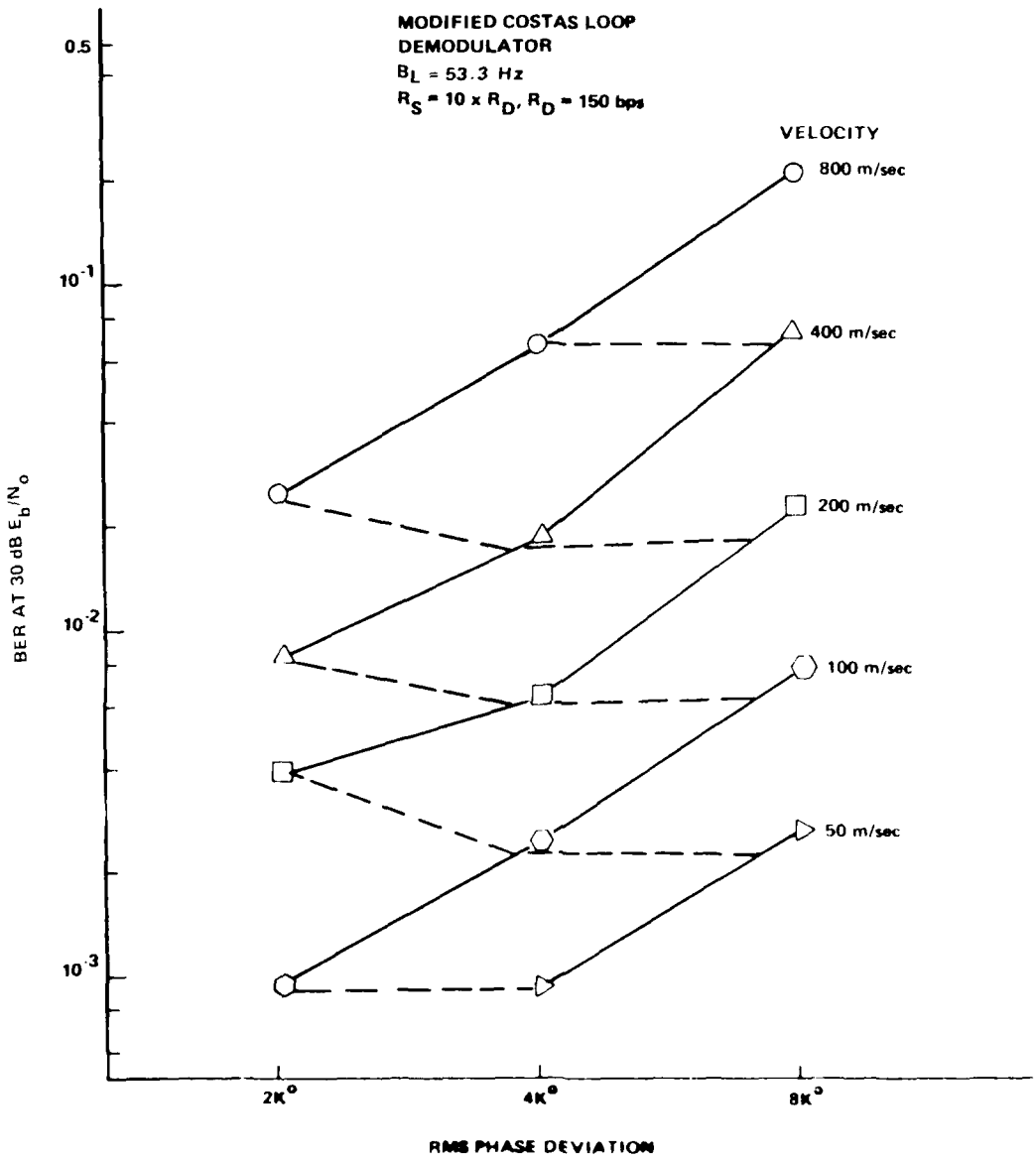

Figure A-3. Performance scaling with T_D, Costas DECPSK, B_I/R_D = .355

Figure A-4 shows BER performance at 30 dB for a NCFSK demodualtor with $\Delta f/R_D$ in several fading environments parametrically described by their respective σ and v values. These results show that for a given E_b/N_o and $\Delta f/R_D$, NCFSK performance remains relatively constant for fixed values of T_D (given by Equation (A-1)) over a range of σ and v values. Other simulation results have verified that the same BER performance will result when both data rate and velocity are proportionately scaled (keeping T_D/T_S constant) for fixed E_b/N_o and $\Delta f/R_D$ values. Thus the combination of these results verifies that NCFSK performance can be adequately characterized by the parameters E_b/N_o , $\Delta f/R_D$, and T_D/T_S .

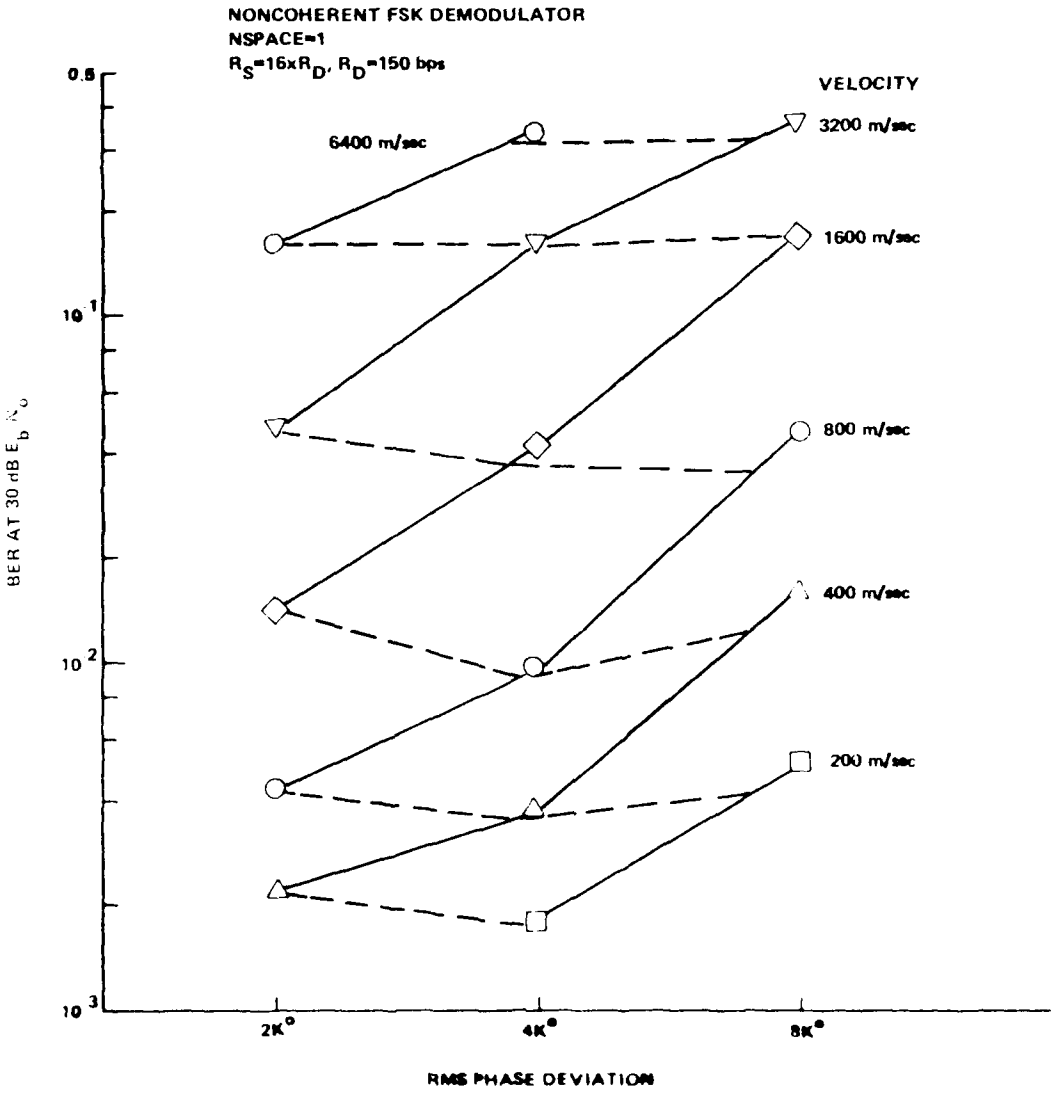

Figure A-4. Performance scaling with T_D , NCFSK, $\Delta f/R_D = 1$

APPENDIX B

PSK AND FSK LINK SIMULATOR

B.1 GENERAL SIMULATOR MODEL.

The interconnections between the basic units that model the transmission of a differentially encoded BPSK signal or a noncoherent FSK signal through a noisy channel with PATS code simulated amplitude and phase scintillations are shown in Figure B-1.

For PSK modulation the binary data, d(t), is differentially encoded and used to modulate the phase of a sinusoidal carrier with 180 degree phase shifts at the data rate R_D . The transmitted baseband signal is represented by the complex phasor given by

$$s(t) = Ae^{j\theta_c(t)} \qquad \text{(B-1)}$$

where

$$\theta_c(t) = \theta_{c_0} + m(t) \qquad \text{(B-2)}$$

and m(t) can take values 0 or 1 and is the differentially encoded bit stream of the binary data.

For FSK modulation, d(t) is used directly to frequency modulate the carrier. The transmitted baseband signal for FSK is represented by the same complex phasor given in Equation B-1 but where $\theta_c(t)$ is given by

$$\theta_c(t) = 2\,\Delta f t \cdot d(t) + \theta_0 \qquad \text{(B-3)}$$

where d(t) is the binary 0,1 data and $\Delta f (= \text{NSPACE} \cdot R_D)$ is the tone separation in Hz and is chosen to be an integer multiple of the data rate. The data rate multiple tone separation makes the binary signals an orthogonal signaling set.

The channel consists of PATS code generated signal fading and additive, white Gaussian noise. The propagation of the signal through the simulated striated environment is incorporated by converting the distance dependent faded signal vector record to a function of time via the relative screen velocity and treating it as a complex amplifier gain, $A_f(t)e^{j\theta_f(t)}$, operating on the transmitted signal. White Gaussian noise $n(t)e^{j\theta_n(t)}$ of the proper variance is added to simulate the nominal link carrier-to-noise ratio. The resulting received signal vector is given by:

$$r(t) = s(t)\, A_f(t)e^{j\theta_f(t)} + n(t)\, e^{j\theta_n(t)} \,. \qquad \text{(B-4)}$$

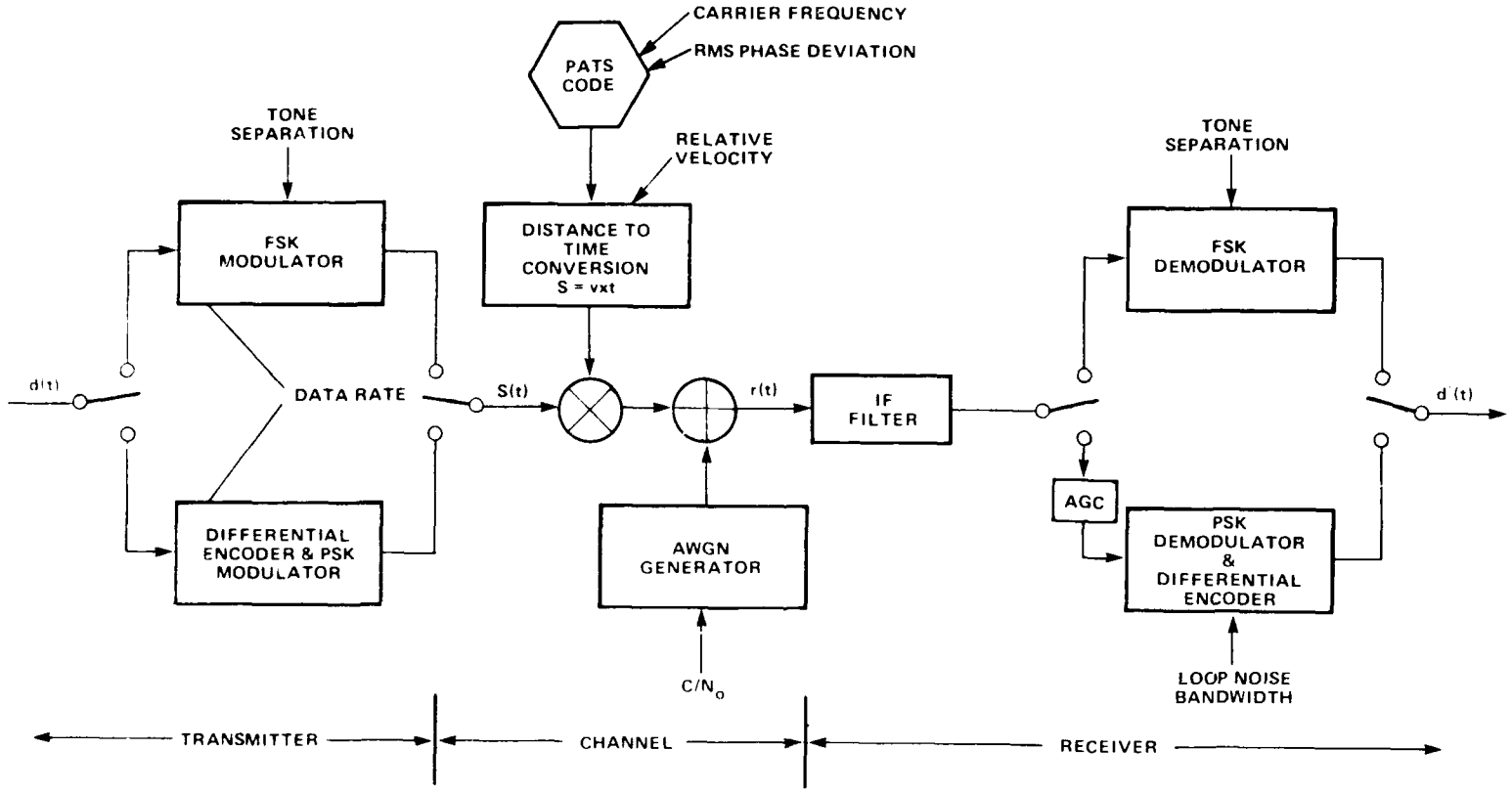

Figure B-1. Simulated FSK and PSK digital data link

It is assumed that the received signal is passed through a bandpass IF filter with a flat frequency response and whose bandwidth is large enough so that intersymbol interference can be neglected. Thus the IF filter was not simulated here as in the simulation of Reference 1 to obtain faster simulation running times. Noise samples of the received signal were independent and were generated with a variance appropriate for the Nyquist rate (which was usually 10 times the data rate).

B.2 PSK DEMODULATOR MODELS.

Demodulation of the differentially encoded PSK signal is performed by either a coherent modified Costas loop demodulator followed by a differential decoder or by a noncoherent DPSK demodulator. Both demodulator designs were modeled after [illegible] designs similar to that described Reference 3. The DPSK demodulator uses a modified Costas loop (see Figure B-2a) to track the carrier phase reference and mix the modulated PSK signal [illegible]. The digital DPSK demodulator can also use the Costas loop to track the carrier and doppler, or it could also use a frequency tracking loop for this purpose (see Figure B-2b). Since the response of the loops to a given phase or frequency error is a function of the input signal level, a signal automatic gain control (AGC) which maintains constant loop gain is modeled immediately preceding the carrier removal circuits. This AGC stabilizes the loop bandwidth by removing any amplitude fluctuations on the received signal and also stabilizes the damping ratio for higher order loops.

For the various performance curves presented in this report the loop bandwidths and damping ratios are preset at the specified values at each E_b/N_o ratio and are maintained at that specified level

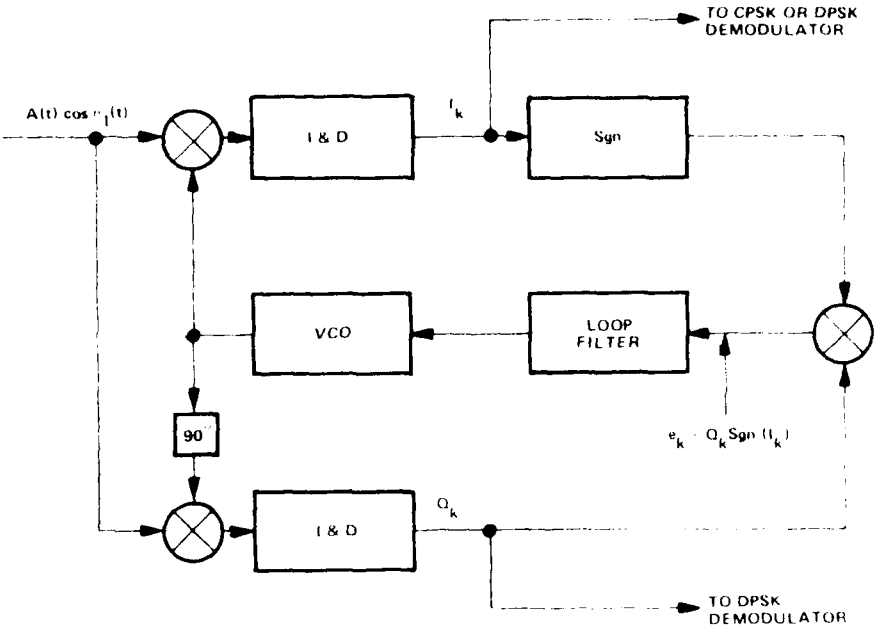

(a) MODIFIED COSTAS LOOP

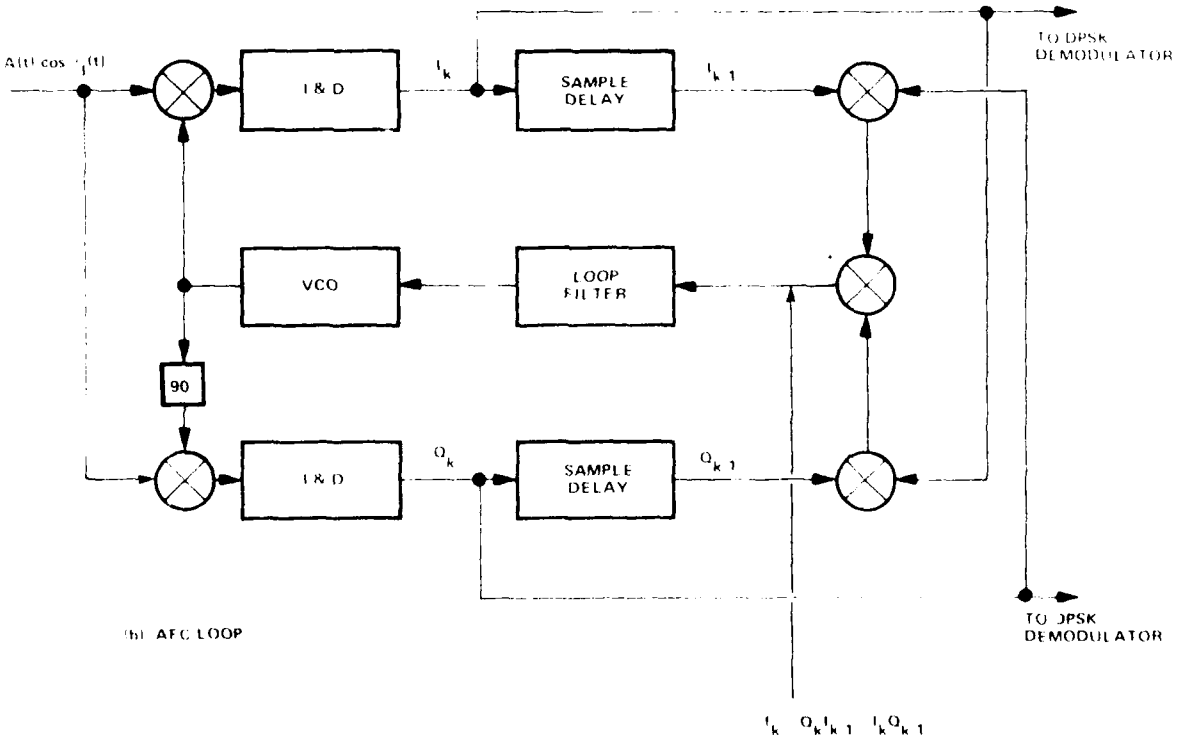

(b) AFC LOOP

Figure B-2. Phase and frequency tracking loops

even through signal fading by the AGC. If no signal AGC is used, the effective loop bandwidth and damping ratio would change as a function of received signal level and for such a situation noise only performance at high SNR could be estimated by interpolating between results for different loop bandwidths. In a fading channel, however, the loop gain would change with the fading received signal level and corresponding changes would occur in the instantaneous loop bandwidth and damping ratio. The probable net result is to worsen BER performance in fading since the loop bandwidth would narrow as the signal level fades - a time at which phase fluctuations become more rapid.

B.2.1 Modified Costas I-Q Loop.

After the AGC, the received signal $A(t)e^{j\theta_I(t)}$ is mixed with the sinusoidal VCO reference signals in phase quadrature. The products are low pass filtered by integrated-and-dump circuits whose output samples are inphase (I) and quadrature (Q) samples of the baseband signal. Let k denote the index of the current time sample, t_k , then the I and Q samples are defined as

$$\begin{aligned} I_k &\triangleq A(t_k) \cos \phi_k \\ Q_k &\triangleq A(t_k) \sin \phi_k \end{aligned} \qquad \text{(B-5)}$$

where

$$\phi_k \triangleq \theta_I(t_k) - \theta(t_k)$$

is defined as the phase error at t_k and is the difference between the input signal phase $\theta_I(t_k)$ and the VCO phase estimate $\theta(t_k)$. The restoring error signal e_k is given by

$$e_k = Q_k \operatorname{sgn}(I_k) \qquad \text{(B-6)}$$

and input to the recursive digital loop filter equations

$$\ddot{\theta}_{k+1} = \ddot{\theta}_k + T\, b'\, AK^3\, e_k$$

$$\dot{\theta}_{k+1} = \dot{\theta}_k + T\, \ddot{\theta}_{k+1} + T\, a'\, AK^2\, e_k$$

$$\theta_{k+1} = \theta_k + T\, \dot{\theta}_{k+1} + T\, AK\, e_k \qquad \text{(B-7)}$$

where

θ_k , $\dot{\theta}_k$, and $\ddot{\theta}_k$ are the phase, frequency, and rate estimates of the received signal, respectively,

T is the sampling interval,

AK is the loop gain, and

a' and b' are the normalized 2nd and 3rd order loop integrator coefficients whose values are chosen to be a' = 1/2 and b' = 1/8 for a .707 damping ratio.

B.2.2 AFC Loop.

Using the I and Q samples obtained in a manner identical to the Costas loop, the AFC loop forms a restoring error signal, f_k , which is proportional to the frequency error and the sampling interval T and is given by

$$f_k = Q_k\, I_{k-1} - I_k\, Q_{k-1} \,. \qquad \text{(B-8)}$$

The recursive digital loop filter equations for a general 2nd order AFC loop are given by

$$\dot{\omega}_{k+1} = \dot{\omega}_k + T\ a'\ AK^2\ (f_k/T)$$

$$\omega_{k+1} = \omega_k + T\ \dot{\omega}_{+1} + T\ AK\ (f_k/T)$$

$$\theta_{k+1} = \theta_k + T\ \omega_{k+1} \qquad \text{(B-9)}$$

where θ_k , ω_k , and $\dot{\omega}_k$ are the phase, frequency, and rate estimates of the received signal, respectively, and the other terms are defined as above.

B.2.3 PSK Demodulation With Differential Decoding.

Although not readily apparent, the digital implementation of CPSK demodulation with the differential decoding is remarkably similar to that of DPSK demodulation. A block diagram showing the essential operations to demodulate the differentially encoded PSK data from the inphase and quadrature baseband signal samples is given in Figure B-3. The timing of each unit is synchronized with the bit synchronization circiut.

CPSK demodulation is accomplished with the use of a modified Costas loop which accurately tracks the received signal phase. The phase modulated digital data is contained in the sign of the inphase baseband signal samples. Coherent demodulation is achieved by averaging these inphase samples over each bit period to minimize variations due to noise. These bit period averaged inphase samples, I, are differentially decoded by comparing the signs of the successive averaged samples. The binary decision rule for decoding the Nth differentially encoded bit is given by

MARK (1), if $D_k = \bar{I}_N \cdot \bar{I}_{N-1} < 0$ (opposite signs)

SPACE(0), if $D_k = \bar{I}_N \cdot \bar{I}_{N-1} \geq 0$ (same signs).

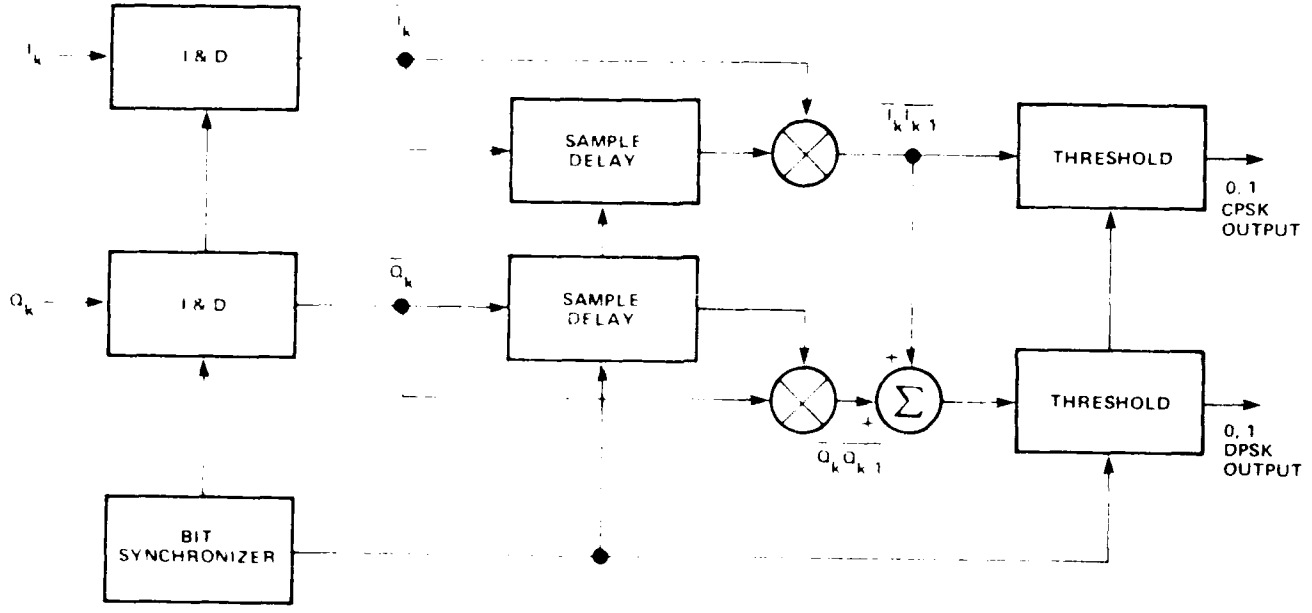

Figure B-1. DECPSK and DPSK demodulation

Digital DPSK demodulation does not require that the carrier phase be tracked for zero phase error, but does require that the phase error remain relatively constant (zero frequency error) between successive data bits. Either a Costas phase tracking loop or an AFC frequency tracking loop may be used for this purpose. The differentially coherent phase demodulation process is achieved by comparing the relative phase, $\bar{\phi} = \tan^{-1}(\bar{Q}/\bar{I})$, of the signal between successive bits using the average (over a full bit period) inphase ($\bar{I}$) and quadrature ($\bar{Q}$) samples of the baseband signal. The Nth decision variable is given by

$$D_N = \bar{I}_N \cdot \bar{I}_{N-1} + \bar{Q}_N \cdot \bar{Q}_{N-1}$$

which represents the dot product between the current and previous signal vectors. The decision rule, like that for DECPSK is given by

$$\text{MARK(1), if } D_k < 0 \quad (\Delta\phi > 90°)$$
$$\text{SPACE(0), if } D_k \geq 0 \quad (\Delta\phi \leq 90°)$$

B.2.4 FSK Demodulator Model.

The FSK demodulator model is a noncoherent matched filter frequency detector as shown in Figure B-4. The received signal r(t) is correlated with orthogonal complex conjugate replicas of the transmitted signal waveforms. The complex correlation bit integrations are sampled at the end of each bit period and the correlator with the larger envelope determines the demodulated bit. The correlations of this digital simulation are performed using digital Fourier transform (DFT) techniques and the complex M-sample correlations are given by

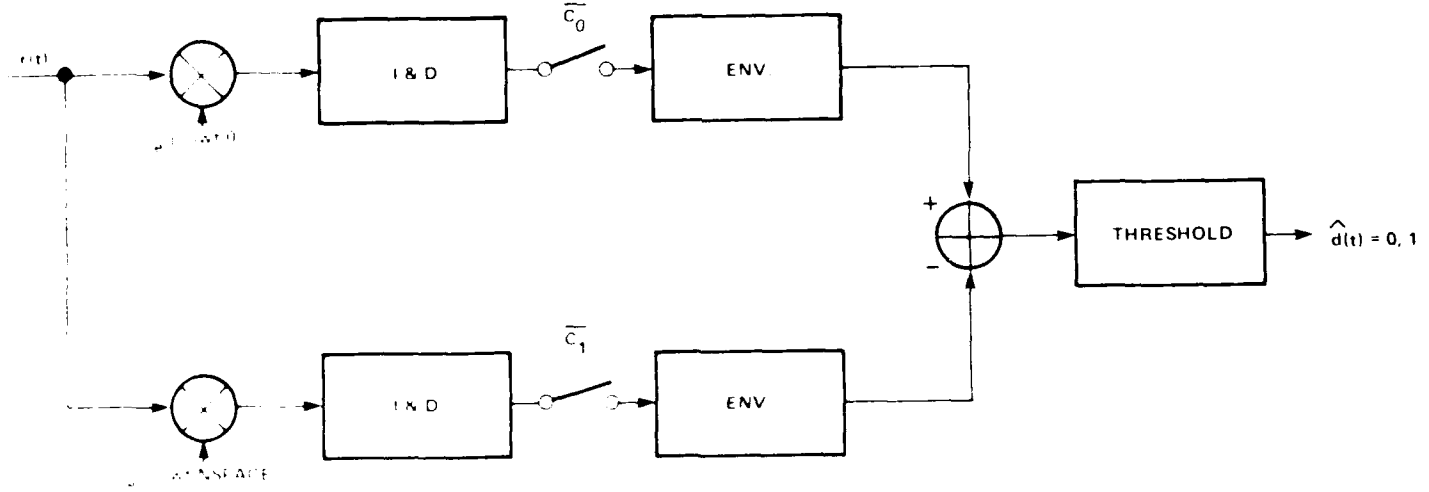

Figure 5-4. Noncoherent FSK demodulator

$$\bar{C}_o = \sum_{k=0}^{M-1} r(k\Delta t)\, e^{-j\Delta w \Delta t\, k \cdot 0}$$

$$\bar{C}_1 = \sum_{k=0}^{M-1} r(k\Delta t)\, e^{-j\Delta w \Delta t\, k \cdot NSPACE} \quad .$$

The binary bit decisions are based on the magnitude of the correlation envelope according to the following decision rule,

$$D_N = \begin{cases} 0 & \text{if} \quad C_o > C_1 \\ 1 & \text{if} \quad C_o < C_1 \end{cases}$$

APPENDIX C
PHASE AND AMPLITUDE FLUCTUATIONS

Both amplitude and phase of communication signals are affected as they propagate through a nuclear fading channel. In this appendix simulation results are presented which isolate the relative effects of time dependent amplitude and phase fluctuations on DECPSK, DPSK, and NCFSK demodulators for different fading environments.

C.1 FADING FOR A DECPSK DEMODULATOR.

Figure C-1 shows bit error rate perfcrmance for a 150 bps data link with a second-order modified Costas loop demodulator at bit energy-to-noise density ratio of 10 and 20 dB, plotted as a function of fading environment decorrelation time. Three curves are shown at each value of E_b/N_o ; the top curve shows performance degradation which results for increasing fade rate when the fading channel is modeled with both amplitude and phase fluctuations while the lower pair shows performance improvement when the fading channel consists of amplitude fluctuations alone and phase held constant.

The lowest of the three curves is that of an ideal phase reference (IPR) demodulator which is assumed to perfectly track the mean channel phase. The IPR demodulator is modeled by removing the phase tracking loop (B_L = 0 Hz) and the phase fluctuations of the fading channel. The next curve above shows the additional degradation which results for a non-ideal (B_L = 53.3 Hz) phase tracking loop in the noisy amplitude alone fading environment. These curves show that with only amplitude variations present the bit error rate decreases as the fading decorrelation time becomes shorter. It is believed that this improvement in BER performance is a

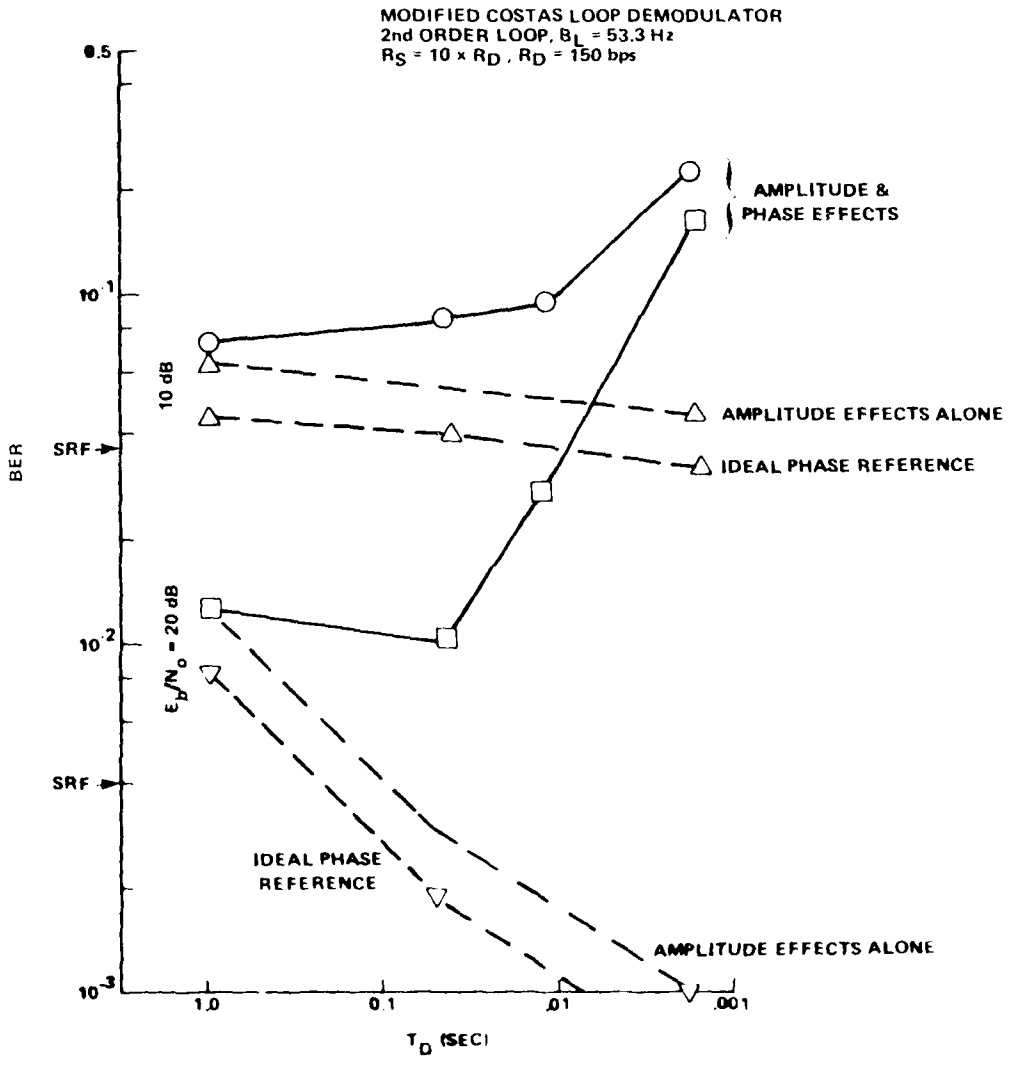

Figure C-1. DECPSK performance with and without phase fluctuations

result of time diversity which lower bounds the minimum E_b/N_o ratio on which decisions are based. For very slow fading ($T_D/T_S >> 1$) the E_b/N_o over that period is equal to that reduced constant E_b/N_o level due to amplitude fading. As fade rate increases, however, the average E_b/N_o over the bit period is always greater than the minimum E_b/N_o level reached during a fade (when most errors occur) since the instantaneous E_b/N_o does not remain at its minimum value for the entire bit period. Thus, increasing amplitude diversity (shorter decorrelation times) over the integration bit period increases the minimum effective E_b/N_o on which bit decisions are based and result in improved performance.

The effect of including the phase fluctuations of the fading channel is also shown by the top curves in these figures. At longer decorrelation times, the 53.3 Hz Costas loop tracks the phase fluctuations and the error performance is about the same as that observed for amplitude fading only. However, at smaller decorrelation times the loop begins to slip cycles as it is no longer able to track the more rapid fluctuations of the received channel phase and this becomes the dominant source of bit errors.

In order to estimate the fade rate at which phase fluctuations become a significant source of performance degradation for DECPSK demodulation, Figure C-2 was prepared which shows BER performance curves as a function of the T_D/T_S ratio for two representative loop designs (B_L/R_D = .044 and .355) and E_b/N_o values of 10, 20, and 30 dB. Although these curves were obtained by simulating 150 and 1200 bps data rate links, these results are applicable to other data rates since performance scales with the T_D/T_S ratio as discussed in Appendix E. These curves plotted on log-log scales show approximately linear performance degradation at moderate T_D/T_S ratios until asymptoting toward a 0.5 error rate at very low

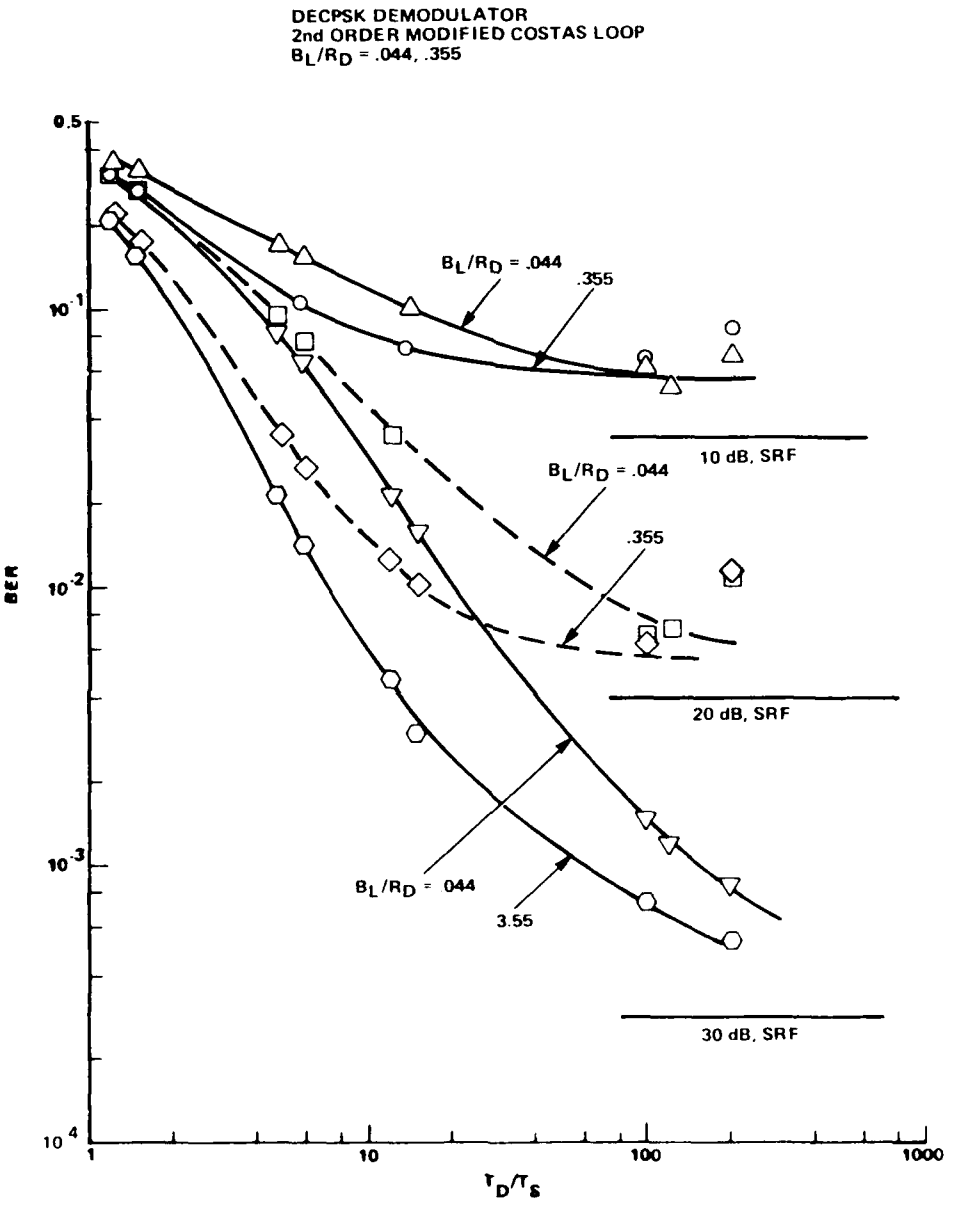

Figure C-2. DECPSK performance versus T_D/T_S

T_D/T_S ratios. At the other extreme the curves asymptote toward the slow Rayleigh fading limit at each E_b/N_o value for large T_D/T_S ratio. The T_D/T_S ratio at which phase fluctuations become significant is higher for larger E_b/N_o ratios since as noise degradation increases it takes increasingly faster fading before phase degradation becomes noticeable. The curves also show that the higher B_L/R_D ratio links are better in faster fading although they are worse in noise alone and slower fading.

C.2 FADING FOR A DPSK DEMODULATOR.

Figure C-3 shows bit error rate performance for a 150 bps data link with a first-order modified Costas loop demodulator at a bit energy-to-noise density ratio of 10 and 20 dB plotted as a function of fading environment decorrelation time. Three curves are presented at each value of E_b/N_o . The top curve shows the performance degradation which results in a fading channel containing both amplitude and phase fluctuations, while the bottom two curves show the improved performance when the fading environment contains only ampltiude fluctuations. The lowest of the three curves is that of an IPR demodulator which tracks the mean phase perfectly, while the next curve above shows results for a non-ideal (B_L = 80 Hz) phase tracking loop in a noisy amplitude only fading environment. It is believed that bit error rate improvement at shorter decorrelation times for amplitude variations only is a result of the diversity gain discussed in the previous section. The top curves for bit error ratios of energy-to-noise ratios of 10 dB and 20 dB show the point at which phase fluctuations become the dominant source of bit errors. At longer decorrelation times, the 80 Hz loop bandwidth Costas loop tracks the phase fluctuations and the error performance is about the same as that observed for amplitude fluctuations only. At smaller decorrelation times the tracking loop begins to slip cycles, because it no longer can track the rapid phase fluctuations.

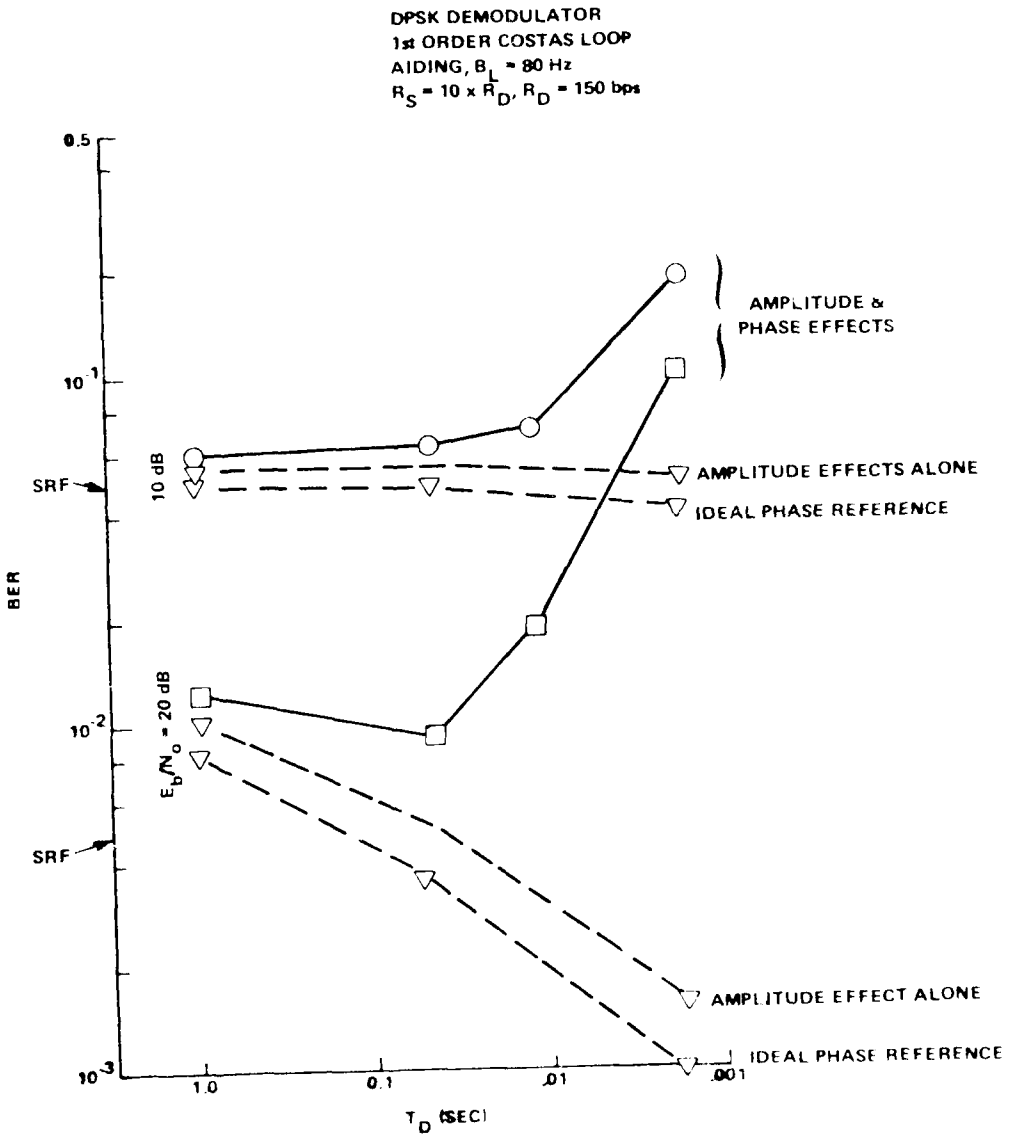

Figure C-3. DPSK performance with and without phase fluctuations

AD-A088 364 ESL INC SUNNYVALE CA F/G 9/5
CPSK, DPSK, AND FSK DEMODULATOR PERFORMANCE UNDER NUCLEAR STRES--ETC(U)
MAR 79 R IBARAKI, R HECKMAN, L KEARNEY DNA001-78-C-0189
UNCLASSIFIED ESL-TM10A3 DNA-5006F NL

2 OF 2
AD A088364

END
DATE FILMED
9-80
DTIC

Figure C-4 shows BER performance curves as a function of the T_D/T_S ratio for two representative loop designs (B_L/R_D = .067 and .533) at 10, 20, and 30 dB. These results were obtained at data rates of 150 and 1200 bps, but are applicable to other data rates since performance scales with the T_D/T_S ratio as discussed in Appendix B. These curves are plotted on log-log scales and much like Figure C-2 for DECPSK show approximately linear performance degradation at moderate T_D/T_S ratios, while at lower values of T_D/T_S the curves asumptote towards a 0.5 error rate and the aymptote toward the slow Rayleigh fading limit for large T_D/T_S ratios for all E_b/N_o . Also like DECPSK these DPSK curves show the T_D/T_S ratio at which phase fluctuations become significant is higher for larger E_b/N_o ratios, however, the B_L/R_D ratio of the doppler tracking loop has much less effect on DPSK performance.

C.3 FADING FOR A NCFSK DEMODULATOR.

Figure C-5 shows bit error rate performance at E_b/N_o=20 dB for an NCFSK receiver operating at data rates of 150 and 1200 bps with tone separation at one data rate ($\Delta f/R_D$=1), plotted as a function of the fading channel decorrelation time. When the fade rate is slow relative to the data rate (T_D/T_S>>1) amplitude variations are the dominant source of performance degradation and BER performance asymptotes toward the SRF limit. Also like PSK demodulation, FSK demodulation shows improved performance due to amplitude diversity at shorter decorrelation times with an amplitude effects alone (phase constant) fading model. When both phase and amplitude effects are included, performance degrades with decreasing decorrelation times since the phase fluctuations cause significant amounts of intersymbol interference through spectral spreading. This figure also verifies to a limited extent that FSK performance can be characterized by the T_D/T_S ratio rather than with T_D and R_D independently. (The 1200 bps (8 x 150 bps) curve appears to be shifted to the right by about a factor of 8.)

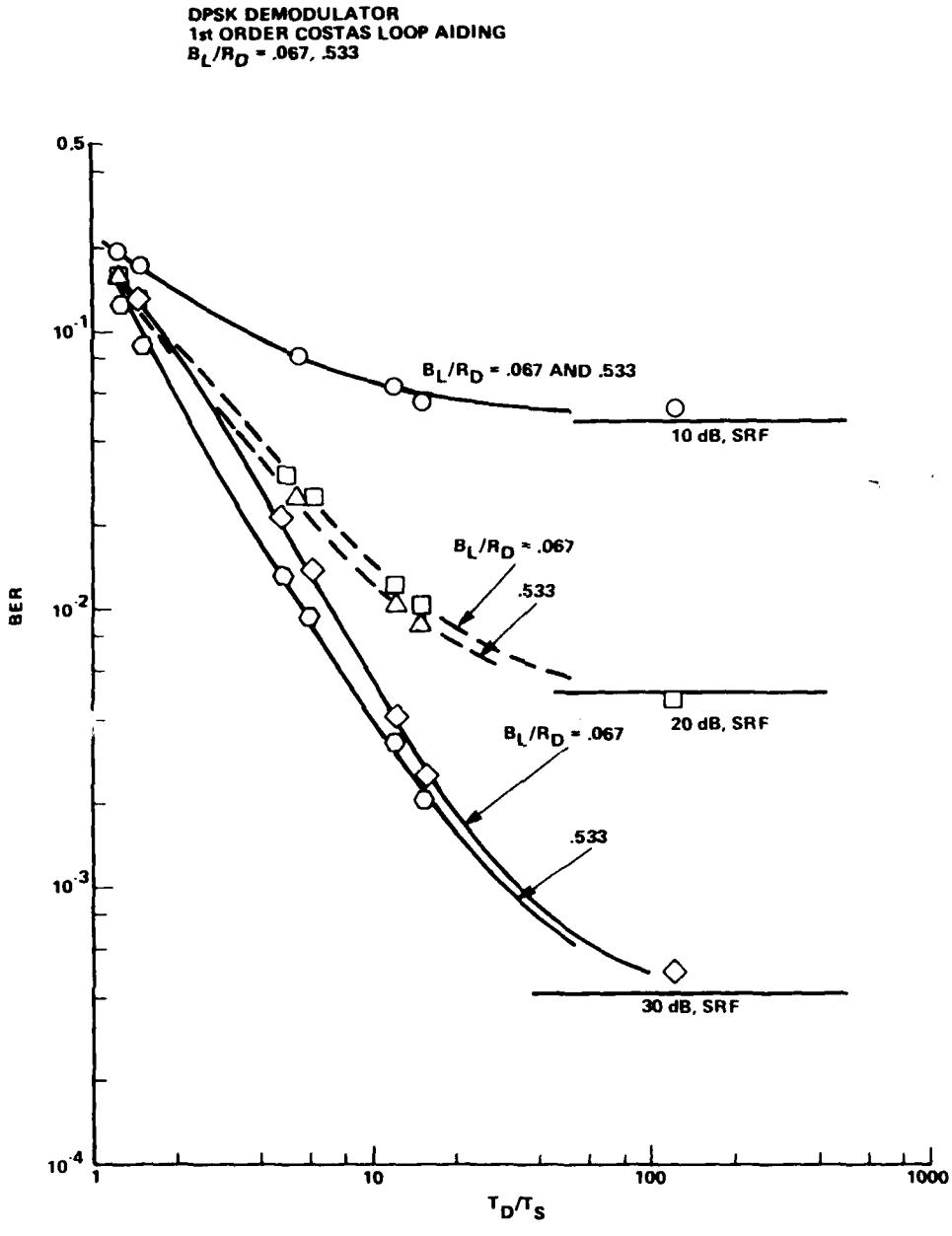

Figure C-4. *DPSK performance* versus T_D/T_S

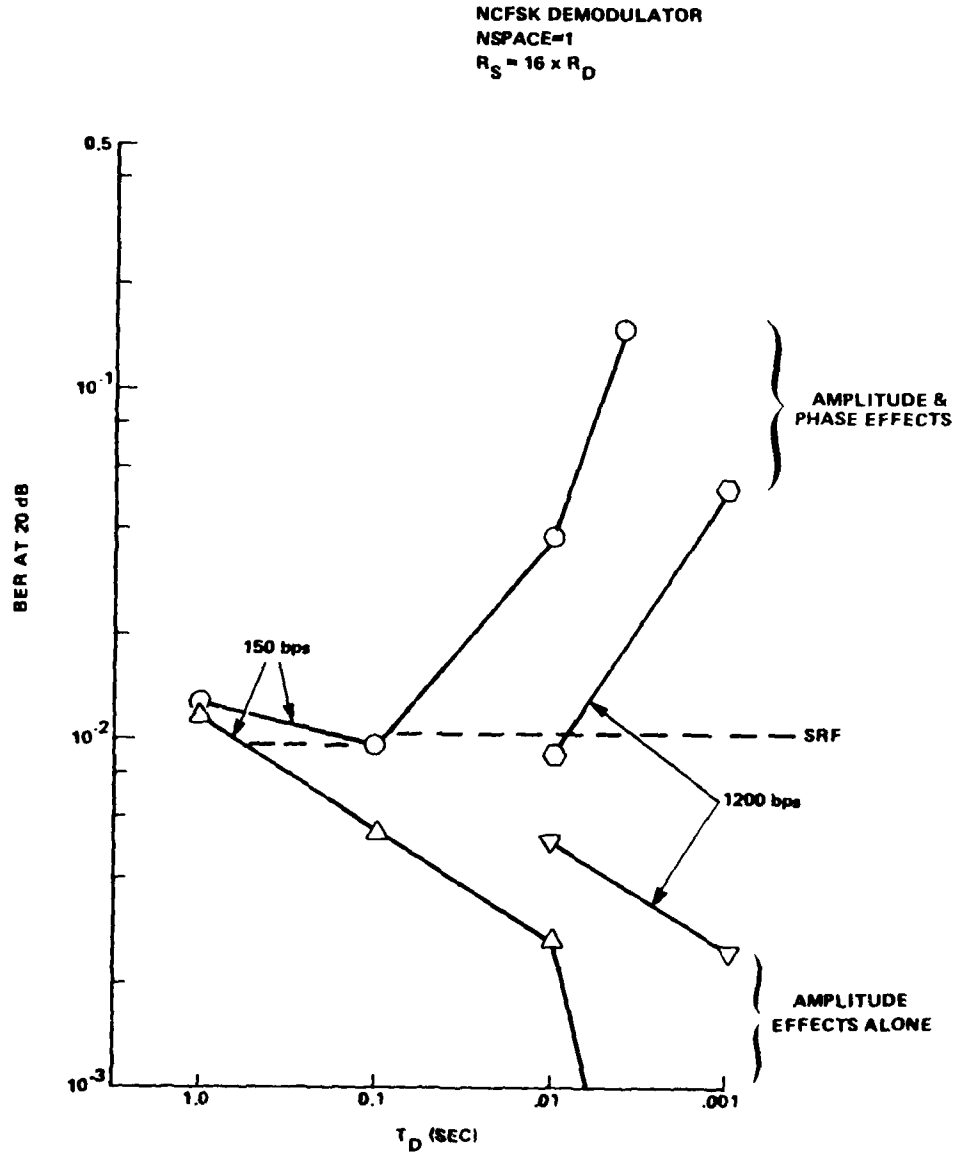

Figure C-5. NCFSK performance with and without phase fluctuations

Again to estimate the fade rate at which phase effects become the dominant source of performance degradation Figure C-6 is presented which shows BER as a function of the T_S/T_S ratio for three values of E_b/N_o . Besides the result for $\Delta f/R_D=1$, BER curves for tone spacings up to 8 times the data rate ($\Delta f/R_D=8$) are shown. Curves for all tone separations approach the SRF limit at large T_D/T_S ratio and degrade in performance for decreasing decorrelation times. The curves for wider tone separations do not degrade as rapidly since although the signal spectrum may be spread outside the transmitted tone detection bandwidth, the wider tone separation reduces the likelihood that the energy will appear in the detection bandwidth of the other tone. As compared with PSK demodulation, however, phase fluctuations do not appear to become a significant degrading factor for FSK until much faster fade rates.

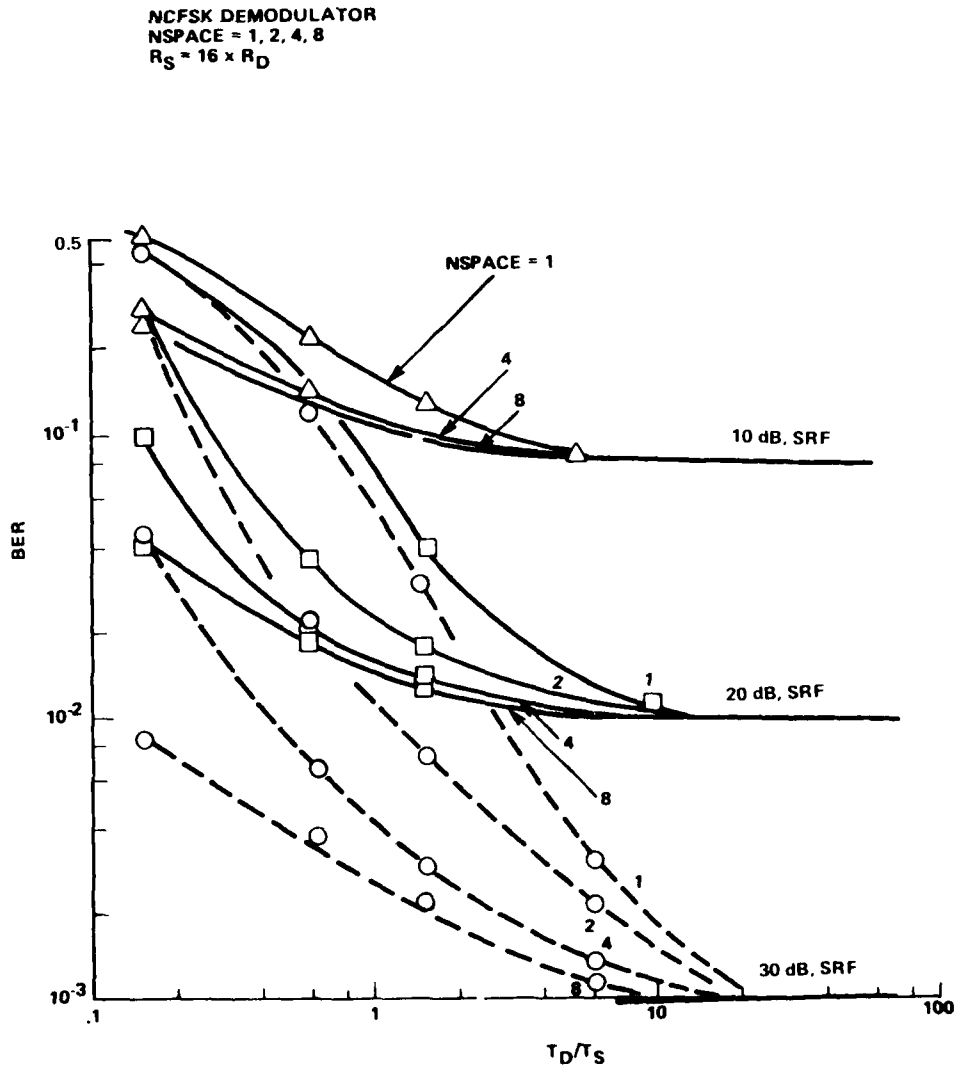

Figure C-6. NCFSK performance versus T_D/T_S

APPENDIX D
GLOSSARY

AFC	Automatic frequency control, frequency tracking loop
AGC	Automatic gain control
AK	Closed loop gain
α	Greek symbol alpha, indicates proportionality
a', b'	Normalized second and third order integrator gains $a' = \frac{a}{AK}$, $b' = \frac{b}{AK^2}$ where a and b are the actual integrator gains.
AWGN	Additive white Gaussian noise
B_L	One-side equivalent loop noise bandwidth (Hz)
BER	Bit error rate
bps	bits per second
C/N_o	Carrier power-to-noise density ratio
CPSK	Coherent phase shift keying; sometimes used interchangeably with DECPSK
DECPSK	CPSK with differential encoding/decoding to remove phase ambiguity at demodulator
Δf	FSK tone separation (Hz)
DPSK	Differentially coherent phase shift keying
E_b/N_o	Bit energy-to-noise density ratio
f	frequency (Hz)
IPR	Ideal Phase Reference
MODCOS	Modified Costas loop
NCFSK	Noncoherent frequency shift keying
NSPACE	Normalized FSK tone separation NSPACE = $\Delta f/R_D$

GLOSSARY (Continued)

PATS	Propagation analysis through structure-computer code
R_D	Data rate = $\frac{1}{T_s}$
R_s	Sampling rate
σ	RMS phase deviation (fading channel)
σ_ϕ^2	Phase error variance (phase locked loops)
SRF	Slow Rayleigh fading
T_D	Envelope decorrelation time (fading channel), inversely related to spectral bandwidth B_{SP}
T_s	Bit period = $\frac{1}{R_D}$
v	Cloud velocity relative to communication link
VCO	Voltage controlled oscillator

DISTRIBUTION LIST

DEPARTMENT OF DEFENSE

Assistant to the Secretary of Defense
Atomic Energy
ATTN: Executive Assistant

Defense Advanced Rsch. Proj. Agency
ATTN: TIO

Defense Communications Engineer Center
ATTN: Code R123
ATTN: Code R720, J. Worthington
ATTN: Code R410, J. McLean
ATTN: Code R410, R. Craighill
ATTN: Code R410, N. Jones

Defense Nuclear Agency
ATTN: STVL
3 cy ATTN: RAAE
4 cy ATTN: TITL

Defense Technical Information Center
12 cy ATTN: DD

Field Command
Defense Nuclear Agency
ATTN: FCPR

Field Command
Defense Nuclear Agency
Livermore Division
ATTN: FCPRL

Interservice Nuclear Weapons School
ATTN: TTV

Undersecretary of Defense for Rsch. & Engrg.
ATTN: Strategic & Space Systems (OS)

WWMCCS System Engineering Org.
ATTN: R. Crawford

DEPARTMENT OF THE ARMY

BMD Advanced Technology Center
Department of the Army
ATTN: ATC-O, W. Davies
ATTN: ATC-T, M. Capps
ATTN: ATC-R, D. Russ

Harry Diamond Laboratories
Department of the Army
ATTN: DELHD-N-P

U.S. Army Communications Command
ATTN: CC-OPS-W
ATTN: CC-OPS-WR, H. Wilson

U.S. Army Communications R&D Command
ATTN: DRDCO-COM-RY, W. Kesselman

U.S. Army Nuclear & Chemical Agency
ATTN: Library

U.S. Army Satellite Comm. Agency
ATTN: Document Control

DEPARTMENT OF THE NAVY

Joint Cruise Missiles Project
Department of the Navy
ATTN: JCMG-707

Naval Electronic Systems Command
ATTN: PME 117-20
ATTN: PME 106-4, S. Kearney
ATTN: PME 117-211, [illegible] Kruger
ATTN: PME 106-13, T. Griffin
ATTN: Code 3101, T. Hughes
ATTN: Code 501A
ATTN: PME 117-2013, G. Burnhart

Naval Ocean Systems Center
ATTN: Code 532, M. Paulson
ATTN: Code 532, J. Bickel
3 cy ATTN: Code 5324, W. Moler

Naval Research Laboratory
ATTN: Code 4700, T. Coffey
ATTN: Code 7500, B. Wald
ATTN: Code 7550, J. Davis
ATTN: Code 4780, S. Ossakow

Naval Surface Weapons Center
ATTN: Code F31

Office of Naval Research
ATTN: Code 465
ATTN: Code 421
ATTN: Code 420

Strategic Systems Project Office
Department of the Navy
ATTN: NSP-43

DEPARTMENT OF THE AIR FORCE

Air Force Geophysics Laboratory
ATTN: OPR-1, J. Ulwick
ATTN: PHP, J. Aarons
ATTN: OPR, H. Gardiner
ATTN: PHI, J. Buchau
ATTN: PHP, J. Mullen

Air Force Weapons Laboratory
Air Force Systems Command
ATTN: SUL
ATTN: DYC

Air Force Wright Aeronautical Laboratories
ATTN: AAD, W. Hunt
ATTN: A. Johnson

Assistant Chief of Staff
Studies & Analyses
Department of the Air Force
ATTN: AF/SASC, W. Kaufman
ATTN: AF/SASC, W. Adams

Ballistic Missile Office
Air Force Systems Command
ATTN: MNNH, M. Baran
ATTN: MNNL, S. Kennedy
ATTN: MNNH

DEPARTMENT OF THE AIR FORCE (Continued)

Deputy Chief of Staff
Research, Development, & Acq.
Department of the Air Force
ATTN: AFRDSP
ATTN: AFRDSS
ATTN: AFRDS
ATTN: AFRDQ

Electronic Systems Division
Department of the Air Force
ATTN: DCKC, J. Clark

Electronic Systems Division
Department of the Air Force
ATTN: XRW, J. Deas

Electronic Systems Division
Department of the Air Force
ATTN: YSM, J. Kobelski
ATTN: YSEA

Headquarters Space Division
Air Force Systems Command
ATTN: YKA, C. Rightmyer
ATTN: YKA, M. Clavin

Headquarters Space Division
Air Force Systems Command
ATTN: YZJ
ATTN: YZJ, W. Mercer
ATTN: YZJ, L. Doan

Strategic Air Command
Department of the Air Force
ATTN: OOKSN
ATTN: DCX
ATTN: XPFS
ATTN: DCXF
ATTN: NRT
ATTN: DCXT
ATTN: DCXT, T. Jorgensen

DEPARTMENT OF ENERGY CONTRACTORS

Lawrence Livermore National Laboratory
ATTN: L-31, R. Hager
ATTN: Technical Information Dept. Library
ATTN: L-389, R. Ott

Los Alamos National Scientific Laboratory
ATTN: D. Simons

Sandia National Laboratories
ATTN: Org. 1250, W. Brown

DEPARTMENT OF DEFENSE CONTRACTORS

Aerospace Corp.
ATTN: S. Bower
ATTN: D. Olsen
ATTN: V. Josephson

BDM Corp.
ATTN: T. Neighbors
ATTN: L. Jacobs

Berkeley Research Associates, Inc.
ATTN: J. Workman

DEPARTMENT OF DEFENSE CONTRACTORS (Continued)

Electrospace Systems, Inc.
ATTN: H. Logston

ESL, Inc.
ATTN: J. Marshall

General Electric Co.
ATTN: A. Harcar

General Electric Company—TEMPO
ATTN: W. Knapp
ATTN: DASIAC

General Research Corp.
ATTN: J. Garbarino
ATTN: J. Ise, Jr.

GTE Sylvania, Inc.
ATTN: M. Cross

IBM Corp.
ATTN: F. Ricci

University of Illinois
ATTN: K. Yeh

Institute for Defense Analyses
ATTN: E. Bauer
ATTN: J. Bengston
ATTN: J. Aein
ATTN: H. Wolfhard

JAYCOR
ATTN: S. Goldman

Linkabit Corp.
ATTN: I. Jacobs

M.I.T. Lincoln Lab.
ATTN: D. Towle
ATTN: L. Loughlin

Mission Research Corp.
ATTN: D. Sowle
ATTN: R. Bogusch

Mitre Corp.
ATTN: C. Callahan
ATTN: G. Harding
ATTN: A. Kymmel
ATTN: B. Adams

Mitre Corp.
ATTN: M. Horrocks
ATTN: W. Hall
ATTN: W. Foster
ATTN: J. Wheeler

Physical Dynamics, Inc.
ATTN: E. Fremouw

R & D Associates
ATTN: B. Gabbard
ATTN: R. Lelevier
ATTN: M. Gantsweg
ATTN: P. Haas
ATTN: C. MacDonald

DEPARTMENT OF DEFENSE CONTRACTORS (Continued)

R & D Associates
ATTN: B. Yoon
ATTN: L. Delaney

Rand Corp.
ATTN: C. Crain
ATTN: E. Bedrozian

Science Applications, Inc.
ATTN: J. McDougall
ATTN: D. Sachs

DEPARTMENT OF DEFENSE CONTRACTORS (Continued)

Science Applications, Inc.
ATTN: D. Divis
ATTN: R. Deliberis

SRI International
ATTN: W. Chesnut
ATTN: A. Burns
ATTN: C. Rino